Dissertation

submitted to the

Combined Faculties for Natural Sciences and Mathematics

of the Ruperto Carola University of Heidelberg, Germany

for the degree of

Doctor of Natural Sciences

Presented by

M.Sc. Chiara Morelli

Born in: Bagno a Ripoli (Florence), Italy

Oral examination: 25th June 2019

Identification of a new population of TrkC^{+} sensory neurons that regulates blood pressure

Referees:

Dr. Hiroki Asari

Jun.-Prof. Dr. Daniela Mauceri

Abstract

Blood pressure is one of the vital signs and its regulation is crucial for survival. Several mechanisms contribute to maintain it in a physiological range: renin-angiotensin-aldosterone system, the autonomous nervous system and specialized baroreceptors neurons. In this study, we demonstrate the existence of a new population of sensory neurons marked by TrkC and TH that innervate blood vessels and are important in the control of blood pressure, blood flow and heart rate. Using an inducible Cre line driven from the *TrkC* locus, we show that TrkC is expressed in 30% of DRG neurons and that a fourth of these neurons are TH^+ and project to blood vessels. Activation of $TrkC^+$ TH^+ neurons leads to high blood pressure, decreased blood flow and increased heart rate variability. Loss of function experiments revealed that $TrkC^+$ TH^+ sensory neurons are crucial for life. Ablation of $TrkC^+$ neurons results in low blood pressure, alteration of blood flow and increased heart rate variability. All these cardiovascular alterations lead ablate mice to death within 48 hours. We also demonstrate that $TrkC^+$ neurons do not act directly on blood vessels, but they exert their functions through a circuit with the sympathetic nervous system. We thus identified a new population of sensory neurons involved in the regulation of blood pressure, blood flow and heart rate and we hope that this can lead to the development of new therapeutic strategies in the near future.

Abstrakt

Der Blutdruck ist eines der Vitalzeichen und seine Regulation ist für das Überleben von entscheidender Bedeutung. Mehrere Mechanismen tragen dazu bei, es in einem physiologischen Bereich zu halten: Renin-Angiotensin-Aldosteron-System, das autonome Nervensystem und spezialisierte Barorezeptor-Neuronen. In dieser Studie zeigen wir die Existenz einer neuen Population von sensorischen Neuronen, die durch TrkC und TH markiert sind und die Blutgefäße innervieren und für die Kontrolle des Blutdrucks, des Blutflusses und der Herzfrequenz wichtig sind. Mit einer induzierbaren Cre-Linie, die vom *TrkC*-Locus gesteuert wird, zeigen wir, dass TrkC in 30% der DRG-Neuronen exprimiert wird und ein Viertel dieser Neuronen TH^+ sind und in Blutgefäße projizieren. Die Aktivierung von $TrkC^+$ TH^+-Neuronen führt zu hohem Blutdruck, vermindertem Blutfluss und erhöhter Herzfrequenzvariabilität. Experimente zum Funktionsverlust ergaben, dass die $TrkC^+$ TH^+-Sinnesneuronen lebenswichtig sind. Die Ablation von $TrkC^+$-Neuronen führt zu niedrigem Blutdruck, Blutflussänderung und erhöhter Herzfrequenzvariabilität. Alle diese kardiovaskulären Veränderungen führen dazu, dass Mäuse innerhalb von 48 Stunden zum Tode gebracht werden. Wir zeigen auch, dass $TrkC^+$-Neuronen nicht direkt auf Blutgefäße wirken, sondern ihre Funktionen über einen Kreislauf mit dem sympathischen Nervensystem ausüben. Wir haben daher eine neue Population von sensorischen Neuronen identifiziert, die an der Regulation des Blutdrucks, des Blutflusses und der Herzfrequenz beteiligt sind, und wir hoffen, dass dies in naher Zukunft zur Entwicklung neuer Therapiestrategien führen kann.

Acknowledgements

I would like to first express my deep gratitude to Paul for giving me the opportunity to work in his lab and on these projects. Your mentorship and guidance throughout this work has been of immense help. Thanks for your constant constructive advice and for always having time for me. I could not have asked for a better PI.

Special thanks should be given to Dr. Laura Castaldi who worked with me on the TrkC project. Thanks for your constant support and enthusiastic encouragement. The results we obtained would not have been achieved without you. In the past four years, you have been much more than a colleague and sharing good and bad times together helped me a lot. I am sure our relationship will not end even if hundreds of km will separate us.

I am grateful to Dr. Mariano Maffei for trusting me to work on his postdoctoral project, for his valuable advice and constant support. Thank you very much also for your humor and laughs. Sometimes bad periods can be overcome more easily with a positive attitude and you helped me a lot.

Next, I would like to thank the students I have had the luck to supervise: Paola, Alex, Sam, Tessa, Blanka and Alessandro. You made me realize how much I love teaching and each one of you contributed to the success of this project.

My special thanks are extended to all the members of the Heppenstall lab and of EMBL Rome who I have had the luck to meet during the past four years. Your inputs and constant support have helped me shape my PhD project and I will never thank you enough. You have been my second family and you have been the reason why I decided to spend my PhD in Monterotondo, when I was sure I had already decided to go abroad. I will never forget the family feeling I experienced from the very first time I met you during the PhD

interviews. It felt like home and this has never changed during the past four years. I could not have asked for better lab members to spend four years of my life with.

My sincere thanks to the facilities at EMBL Monterotondo, the collaborators who are part of this work and my TAC committee for their constant help and advice throughout these years.

Finally, I would like to thank my parents, my brother and my whole family, my boyfriend and my friends for their constant support during these years. A heartfelt thank you is due to my grandmother Grazia, who gave me my first microscope when I was 7 years old. I performed my first experiments with her and I am sure that if I love science as much as I do, it is also thanks to her. I wish she were here with me to celebrate the end of this journey.

Completing a PhD can be very challenging and sometimes you just need to run away from the lab to alleviate stress. I am sure I would not have managed without Dynamo Camp and without music and concerts, where so often I have sheltered. My deep gratitude goes to friends who have shared with me these indescribable experiences and to all the kids of Dynamo Camp, who taught me that nothing is impossible if you truly believe in your dreams.

This work would not have been possible without each one of You.

Thank you from the bottom of my heart.

Table of contents

Table of figures

Table of abbreviations

4-OH T	4-hydroxytamoxifen
α-SMA	α-Smooth Muscle Actin
ACE	Angiotensin-Converting Enzyme
Ach	Acetylcholine
ADH	Antidiuretic Hormone
ANS	Autonomic Nervous System
ASIC2	Acid-Sensing Ion Channel 2
ATP	Adenosine Triphosphate
Avil	Advillin
BAC	Bacterial Artificial Chromosome
BDNF	Brain-Derived Neurotrophic Factor
BP	Blood Pressure
BPM	Beats Per Minute
C21	DREADD agonist Compound 21 dihydrochloride
cGMP	Cyclic Guanosine Monophosphate
CGRP	Calcitonin Gene-Related Peptide
ChR2	Channel Rhodopsin 2
CNO	Clozapine-N-Oxide
CNS	Central Nervous System
CO	Cardiac Output
DREADD	Designer Receptors Exclusively Activated by Designer Drugs
DRG	Dorsal Root Ganglia
DTR	Diphtheria Toxin Receptor
DTX	Diphtheria Toxin
EB	Evan's Blue
ECG	Electrocardiogram
ECM	Extracellular Matrix
ENS	Enteric Nervous System
GFP	Green Fluorescent Protein
hM3Dq	Human Muscarinic 3 receptor couplet with Gq
HR	Heart Rate
HRV	Heart Rate Variability
IB4	Isolectin B4
I.P.	Intraperitoneal
I.T.	Intrathecal
LSCI	Laser Speckle Contrast Imaging
LTMRs	Low-Threshold Mechanoreceptors

M2	Muscarinic receptor 2
M3	Muscarinic receptor 3
MRGPR	Mas-Related G-Protein like Receptor
NE	Norepinephrine
NG2	Neural/Glial antigen 2
NGF	Nerve Growth Factor
NIBP	Non-Invasive Blood Pressure
NN	Normal-to-normal
NO	Nitric Oxide
NPJ	Nodose-Petrosal-Jugular ganglion complex
NPY	Neuropeptide Y
NT-3	Neurotrophin-3
NT-4	Neurotrophin-4
PBS	Phosphate Buffer Saline
PDGFR-β	Platelet-Derived Growth Factor Receptor β
PFA	Paraformaldehyde
PNS	Peripheral Nervous System
PV	Parvalbumin
RAAS	Renin-Angiotensin-Aldosterone System
RBC	Red Blood Cell
RE	Response Element
RT	Room Temperature
SCG	Superior Cervical Ganglion
SD	Standard Deviation
SDNN	Standard Deviation of the NN intervals
SNS	Somatic Nervous System
SP	Substance P
SRA	Small Resistance Arteries
SVR	Systemic Vascular Resistance
TH	Tyrosine Hydroxylase
TINN	Triangular Interpolation of NN interval histogram
TRKC	Tropomyosin Receptor Kinase C
TRPV1	Transient Receptor Potential Vanilloid 1
VEGF-A	Vascular Endothelial Growth Factor A
VGLUT3	Vesicular Glutamate Transporter 3
vSMCs	Vascular Smooth Muscle Cells
YFP	Yellow Fluorescent Protein

1. Introduction

During my PhD I focused my attention on TrkC$^+$ neurons. While neurons expressing other members of the tropomyosin receptor kinases (Trk) family are fairly well characterised, TrkC$^+$ neurons are the least studied. For this reason, we decided to investigate their role in the context of somatosensation, expecting to further characterise their role in proprioception and mechanosensation, as already reported in literature. Surprisingly, we found that a class of TrkC$^+$ neurons projects to blood vessels and we demonstrated that these neurons are sensory. Gain and loss of function experiments revealed their importance in the regulation of blood flow and blood pressure and we proved that they exert their function thanks to a circuit with the sympathetic nervous system.

In the following pages, I will provide an introduction to the different systems involved in blood pressure control so that our findings can be easily placed in the context of the state-of-the-art knowledge.

1.1 The peripheral nervous system

The interaction with the environment and the ability to detect and react to different stimuli are fundamental for survival. The Peripheral Nervous System (PNS) allows the brain and spinal cord to receive information from both the external and internal environment and to send information to all areas of the body.

It was first described by Ancient Greek philosophers and physicians during the 5th Century BC (Lloyd, 1975) and only a century later Herophilus realised that motor nerves were joined to muscles and sensory nerves to organs of sensation (Staden, 1989). The knowledge of the PNS as we know it nowadays was mostly discovered during the

Renaissance and the following centuries, when the different branches of the PNS started to be described.

1.1.1 The autonomic nervous system

The PNS can be divided into three parts: the autonomic nervous system (ANS), the somatic nervous system (SNS) and the enteric nervous system (ENS). The ANS regulates involuntary body functions like digestion, blood flow or breathing. This system can be further divided into two branches:

1. The parasympathetic system helps to keep the body in a "rest and digest" state. Using acetylcholine (Ach) as a neurotransmitter, parasympathetic neurons decrease heart rate, slow breathing and reduce blood flow to muscles, keeping the organism at a resting state.

2. The sympathetic system regulates the so-called "fight or flight" responses. In case of danger or mental stress, heart rate and blood flow to certain areas of the body, like muscles, increase thanks to the action of neurotransmitters like epinephrine and norepinephrine (NE) (vonEuler, 1946). This allows the body to respond quickly to situations that require an immediate action.

1.1.1.1 Tyrosine Hydroxylase

Tyrosine Hydroxylase (TH) is considered a classical marker for sympathetic neurons. It is the rate-limiting enzyme of catecholamines synthesis and it converts tyrosine to L-DOPA (Molinoff and Axelrod, 1971). This step is fundamental in the biosynthesis of dopamine, epinephrine and norepinephrine and a deficit of TH can give rise to several pathological conditions such as addiction, bipolar disorders and high blood pressure (Cousins et al., 2009; Grobecker H, 1978; Koob and Volkow, 2010). Given the importance

of TH role, this enzyme is very tightly regulated by transcriptional mechanisms, phosphorylation (Bobrovskaya et al., 2004; Dunkley et al., 2004; Saraf et al., 2010), negative feedbacks by catecholamines (Gordon et al., 2008; Gordon et al., 2009; Ramsey and Fitzpatrick, 1998) and degradation in the proteasome (Doskeland and Flatmark, 2002).

Apart from its role in the sympathetic nervous system, TH is expressed also in a class of sensory neurons that act as mechanoreceptors (Li et al., 2011) that will be discussed with further details in the next sections of the thesis.

1.1.2 The somatic nervous system

The SNS has the fundamental function of carrying sensory and motor information to and from the central nervous system (CNS). Sensory neurons have the cell bodies located within the Dorsal Root Ganglia (DRG) and are pseudounipolar: their axons branch and one part innervates the target organs (skin, muscles, blood vessels etc.), while the other terminates at the level of the spinal cord that acts as the integration port for the signals (Fig. 1).

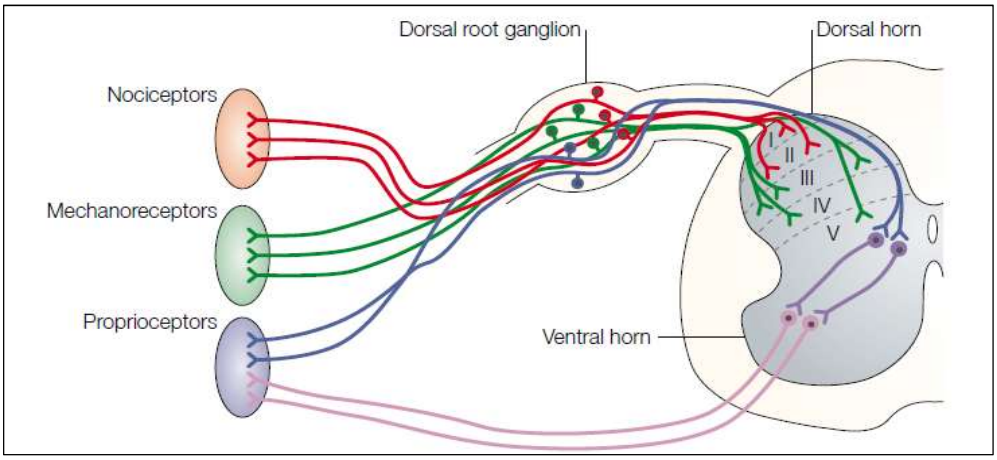

Figure 1. Schematic of sensory neurons.
Sensory neurons are pseudounipolar: on one side their axons innervate target organs, on the other they reach the spinal cord. Each DRG contains a heterogeneous group of sensory neurons that are able to detect different kinds of stimuli and transduce them in different laminae of the spinal cord. Image taken from Caspary & Anderson (Caspary and Anderson, 2003).

Sensory neurons can detect several distinct sensory modalities thanks to the heterogeneity of fibre types and can be broadly categorized as mechanoreceptors, nociceptors, proprioceptors, thermoreceptors and pruriceptors. During development, their specialization is controlled by several transcription factors (neurogenin1 and 2, Runx1 and Runx3) (Ma et al., 1999), neurotrophic growth factors such as Nerve Growth Factor (NGF), Brain-Derived Neurotrophic Factor (BDNF), Neurotrophin 3 (NT-3) and 4 (NT-4) (Ernsberger, 2009) and by some tyrosine kinase receptors (Ret, TrkA, TrkB and TrkC) (Huang et al., 1999; Mu et al., 1993).

1.1.2.1 Sensory neurons classification

At the level of the SNS, the expression of specific tyrosine kinase receptors determines the development of definite neuronal populations (Mu et al., 1993). However, Ret, TrkA, TrkB, TrkC and their ligands have also been used as molecular markers to distinguish different sets of sensory neurons. Recently, Linnarsson's group confirmed this by using single cell RNA sequencing to classify neurons in an unbiased way (Usoskin et al., 2015; Zeisel et al., 2018). Concerning sensory neurons, five main classes emerged from their analysis (Fig. 2): myelinated Low-Threshold Mechanoreceptors (LTMRs), proprioceptors, non-peptidergic and peptidergic nociceptors and unmyelinated C-LTMRs. All these neuronal populations express a combination of different markers that have been validated with immunohistochemical analysis.

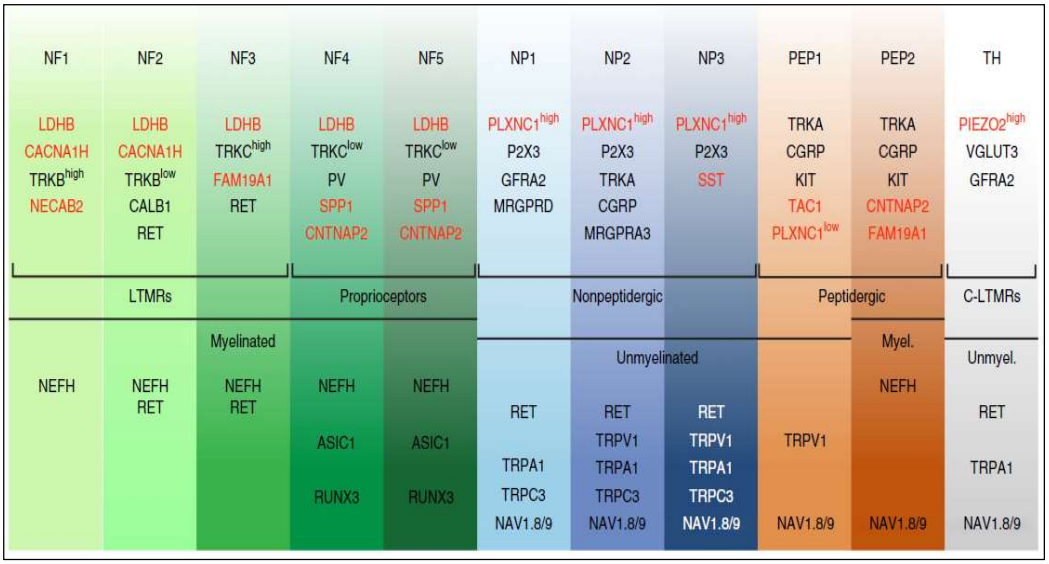

Figure 2. Classification of sensory neurons subtypes.
Unbiased classification of sensory neurons based on single cell RNAseq data. Five main classes can be identified with different subclasses (columns). For each subclass, the characterizing genes are indicated. Image taken from Usoskin et al. (Usoskin et al., 2015).

As briefly mentioned previously, TH is a marker for a subset of mechanosensitive sensory neurons. In particular, it is expressed in a class of C-LTMRs, the most abundant mechanoreceptors in hairy skin. C-LTMRs can be divided into MrgprB4$^+$ and Vglut3$^+$ neurons. Vglut3$^+$ neurons can be further classified as TH$^-$ and TH$^+$ (Liu et al., 2007; Lou et al., 2013). The first form free nerve-endings in the epidermis of the skin, while the latter, also characterized by the expression of Ret, form longitudinal lanceolate endings around most hairs and they are activated by skin indentation and slow movements across the skin (Li et al., 2011; Vrontou et al., 2013).

1.1.2.2 TrkC role in sensory neurons

As depicted in Fig. 2, TrkC (Tropomyosin receptor kinase C) is expressed in some classes of myelinated mechanoreceptors, giving rise to lanceolate endings, that respond to hair deflection, as well as Merkel cells, essential to perceive fine textures (Funfschilling et al., 2004; Hasegawa and Wang, 2008). Recently a new type of TrkC$^+$ mechanoreceptor has

been discovered. These myelinated neurons, defined as Aβ field-LTMRs, are characterized by the concomitant expression of Ret. A single neuron can form more than 150 circumferential endings surrounding the majority of hair follicles and is important to detect gentle stroking over a large area of skin. Its receptive field can be 3-4 mm^2. Aβ field mechanoreceptors are insensitive to hair deflection or light indentation (Bai et al., 2015).

In addition to its role in mechanoreceptors, the NT-3/TrkC axis is fundamental for proprioceptive neuron development and survival (Patapoutian and Reichardt, 2001). NT-3 acts as a chemoattractant for proprioceptive axons during the final phase of their target-directed pathfinding (Genc et al., 2004). Without this neurotrophin, $TrkC^+$ neurons extend their axons arriving close to their targets, but fail to innervate them.

As for all Trk receptors, also TrkC expression in DRG is broader at early stages of development, short after neurogenesis. Genetic tracing of $TrkC^+$ neurons, using a $TrkC^{Cre}$::reporter line, revealed the expression of the reporter not only in $TrkC^+$ neurons, but also in most $TrkB^+$ and some $TrkA^+$ (Funfschilling et al., 2004).

Despite the broader expression of TrkC during early life, mice deficient for NT-3, TrkC, or $TrkC^+$ neuron-specific transcription factor Runx3 display a very well-defined phenotype with severe ataxia, associated with the absence of muscle spindles, and loss of proprioceptive neurons in DRG or their axons (Ernfors et al., 1994; Inoue et al., 2002; Klein et al., 1994; Levanon et al., 2002; Tessarollo et al., 1994).

In particular, in mice lacking Runx3, $TrkC^+$ DRG neurons do not develop, resulting in a loss of connectivity between sensory afferents and motor neurons at the level of the spinal cord. Furthermore, also muscle spindles, the muscles stretch sensors that are important to provide spatial information about the position of the limbs, do not develop. Most homozygous *Runx3* knockout mice die before 2 weeks of age (Levanon et al., 2002).

Homozygous mice lacking TrkC or NT-3 display a similar phenotype. The disruption of the NT-3/TrkC axis results in a decreased number of large myelinated neurons in DRG and in locomotor problems and ataxia due to the loss of proprioceptive afferents and their peripheral sense organs (Klein et al., 1994). Interestingly, mice heterozygous for a mutant inactive form of NT-3 presented half of the number of muscle spindles compared to controls, demonstrating that the concentration of the neurotrophin is crucial during development (Ernfors et al., 1994). It is well known, in fact, that target areas produce restricted amounts of neurotrophins, giving rise to a competition between afferent neurons (Levi-Montalcini, 1987; Oppenheim, 1991) and this appears to be the case also for proprioceptive TrkC$^+$ neurons. NT-3 is the only crucial neurotrophin for TrkC$^+$ neurons development, as muscle spindles and proprioceptive neurons are rescued by the transgenic expression of NT-3 in mice deficient for this neurotrophin (Wright et al., 1997).

Remarkably, homozygous mutant mice for TrkC or NT-3 exhibit a high mortality rate, dying mostly by postnatal day 21 (P21) (Ernfors et al., 1994; Klein et al., 1994). The cause of death remains uncertain, but it is highly probable that it is linked to a non-neuronal function of NT-3. The TrkC/NT-3 axis, in fact, is fundamental for cardiac development (Donovan et al., 1996; Werner et al., 2014) and thus its role in the cardiovascular system may explain the low survival rate.

1.2 Vascular smooth muscle cells

Vascular Smooth Muscle Cells (vSMCs) are a crucial structural component of blood vessels. They contribute to the wall integrity and are fundamental to regulate the vessels diameter in response to different physiological stimuli (Bakker et al., 2005; Hayward et al., 1995; Martinez-Lemus et al., 2009). Together with pericytes, they are considered mural cells and they have a very different morphology according to the type of

blood vessel they are wrapping around (Fig. 3) (Armulik et al., 2011). In arterioles and precapillary arterioles, vSMCs completely encircles the vessels, even if with a slightly different cyto-architecture: in the former ones, they have a spindle-shaped appearance and a very compact aspect, while in the latter ones the cell bodies are more visible and they extend more cytoplasmic processes. At the level of capillaries and venules, instead, vSMCs are not present and are replaced by pericytes.

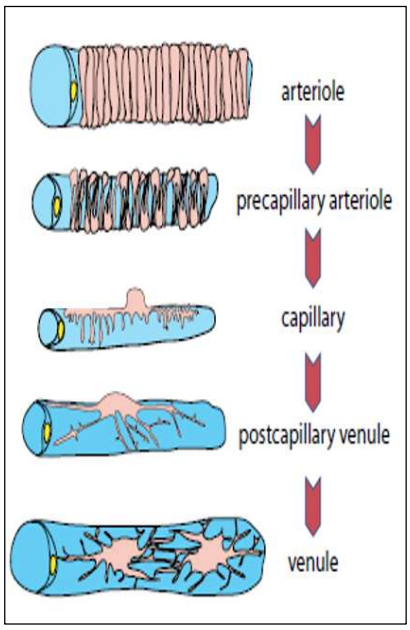

Figure 3. **Mural cells cyto-architecture.**
Mural cells have a very different morphology according to the vessel type they are wrapping around. vSMCs are found around arterioles and precapillary arterioles, pericytes lie on the walls of capillaries, postcapillary venules and venules. Image adapted from Armulik et al. (Armulik et al., 2011).

During development, vSMCs originate from heterogeneous precursors (Majesky, 2007; Tian et al., 2014). In particular, vSMCs of the kidneys, lungs and abdominal aorta arise from various mesodermal lineages (Wasteson et al., 2008), while vSMCs of the aortic arch and branchial arch arteries derive from the neural crest (Jiang et al., 2000; Xie et al., 2013).

vSMCs oscillate between two distinct phenotypes: a quiescent one where vSMCs are differentiated and express contractile proteins like α-smooth muscle actine (α-SMA), fundamental for the contraction of blood vessels wall, and a dedifferentiated phenotype (Salmon et al., 2012). In this latter state, vSMCs contractile proteins are not present anymore, but the cells express a series of markers fundamental for proliferation, migration and extracellular matrix (ECM) protein synthesis (Yoshida et al., 2008). This phenotypic switch is crucial when repairing a vascular injury and also during some pathological conditions like atherosclerosis (Ross, 1993).

vSMCs of small arteries play a crucial role in the control of blood flow and arterial pressure, acting on blood vessels diameter. In particular, the myogenic response is the contraction of small arteries in response to the increased intraluminal pressure and the relaxation following a pressure decrease (Bayliss, 1902; Davis, 1993). vSMCs depend on Ca^{2+} influx to start contraction (Knot and Nelson, 1998), but the mechanosensors component still remains elusive. Probably the myogenic mechanosensor is at the level of the cell membrane and the deformation induced by the increased intraluminal pressure determines a conformational change that initiates signal transduction events. Putative myogenic mechanosensors interact with the ECM, cytoskeleton or intercellular junctions (Hill et al., 2007). vSMCs contraction is controlled by feedback mechanisms mediated by the endothelium. Thanks to the presence of gap junctions, Ca^{2+} passes from vSMCs to endothelial cells hyperpolarizing them. This in turn leads to a hyperpolarization of vSMCs and as a consequence to the vasodilation with a feedback mechanism (Garland et al., 2017).

Because of their crucial functions, vSMCs are involved in the pathogenesis of several cardiovascular diseases like atherosclerosis, restenosis or hypertension (Allahverdian et al., 2012; Bauters and Isner, 1997; Hill et al., 2015; Luo et al., 2012;

Thyberg, 1998) and diabetes (Yamazaki et al., 2018) and they are starting to be addressed as potential therapeutic targets (Guan et al., 2012; Han et al., 2015; Liu et al., 2015; Liu et al., 2017).

Even if their functions are fairly well established, there is still a lack of specific markers to identify vSMCs unambiguously. Most markers used nowadays (α-SMA, NG2, desmin, PDGFR-β) detect the entire set of mural cells, namely pericytes and vSMCs (Nehls et al., 1992; Smyth et al., 2018).

1.3 Blood vessels innervation

Apart from vSMCs, another crucial component for blood flow and blood pressure control is blood vessels innervation. Blood vessels are innervated by sensory, sympathetic and parasympathetic fibres at the same time. While sensory and parasympathetic nerves travel along the vessels, sympathetic neurons form a mesh-like network around the vessel wall. Electron microscopy experiments revealed a similar number of sympathetic and parasympathetic fibres associated with the same vessel and showed that autonomic fibres are more closely associated with endothelial or smooth muscle cells compared to sensory fibres (Ruocco et al., 2002).

The close association of peripheral nerves and blood vessels is defined as "neurovascular congruence". Two opposite mechanisms have been proposed for its development: nerves follow specific factors secreted by blood vessels to reach their targets (Glebova and Ginty, 2005) or, in contrast, peripheral nerves grow first, guiding the development of arteries and arterioles (Mukouyama et al., 2005; Mukouyama et al., 2002). The latter hypothesis is supported by studies where mice lacking cutaneous nerves do not develop proper skin arteriogenesis (Mukouyama et al., 2002). Cutaneous nerves secrete the Cxcl12 factor that is essential for vascular remodelling (Li et al., 2013) and at a later stage

vascular endothelial growth factor A (VEGF-A) to trigger arterial differentiation (Mukouyama et al., 2005). This mechanism is crucial for peripheral arteries and arterioles innervating the skin, but it has still to be demonstrated for major arteries and veins throughout the body.

All components of vascular innervation are crucial to regulate blood flow and blood pressure and act together to ensure tissue and organ homeostasis. Their functions will be discussed more in detail in the next sections of the thesis.

1.4 Blood pressure and heart rate control

Blood pressure (BP) is one of the vital signs, along with respiratory rate, heart rate, oxygen saturation, and body temperature. Normal resting blood pressure in humans is approximately 120 millimetres of mercury (mm Hg) systolic and 80 mm Hg diastolic and it is very important keeping it in this range. Low blood pressure (hypotension) or high blood pressure (hypertension) are risk factors for many diseases and affect more than 20% of the global population (Kearney et al., 2004).

BP is related to cardiac output (CO) and systemic vascular resistance (SVR), according to the equation:

$$BP = CO \times SVR$$

Because of the steep inverse relationship between vessel radius and vascular resistance (r^4), as described in Poiseuille's law, pressure and flow are mainly regulated at the level of small resistance arteries (SRAs) that have a diameter of 50-300 μm. In these vessels, vSMCs play a pivotal role.

Because of its vital importance, BP is very tightly regulated and several different mechanisms contribute to maintain it in a physiological range.

1.4.1 Autonomous nervous system regulation

The autonomic nervous system (ANS) is one of the key players in keeping BP homeostasis. Sympathetic and parasympathetic perivascular nerves release several neurotransmitters that act on endothelial cells or vSMCs to regulate vascular tone and contractility. In turn, endothelial cells produce different factors that influence the ANS effects.

Norepinephrine

Norepinephrine (NE) is the most abundant neurotransmitter released by sympathetic fibres. It acts on different adrenergic receptors that can give rise to opposite effects (Furchgott, 1959; Insel, 1996; Molinoff, 1984). α1 receptor, expressed on vSMCs, mediates the increase of Ca^{2+} levels leading to contraction (Colucci and Alexander, 1986; Colucci et al., 1984), while activation of the endothelial α2 receptor results in vasodilation (Tesfamariam et al., 1992; Vanhoutte and Miller, 1989). The same effect is obtained stimulating β2-adrenergic receptors on vSMCs (O'Donnell and Wanstall, 1984). NE acts also on β1-adrenergic receptors at the level of the heart, increasing heart rate and contractility and thus cardiac output.

ATP

Adenosine triphosphate (ATP) is stored in the same synaptic vesicles as NE (Burnstock and Kennedy, 1986) and its release leads to vasoconstriction, acting on purinergic receptors expressed on vSMCs and endothelial cells (Draid et al., 2005; Rummery et al., 2007).

Neuropeptide Y

Neuropeptide Y (NPY) is a sympathetic neurotransmitter that is often released with NE (Ekblad et al., 1984; Hakanson et al., 1986). It induces vasoconstriction acting on vSMCs and endothelial cells and may also lead to vSMCs proliferation (Edvinsson, 1985).

Acetylcholine

Acetylcholine (ACh) is released from parasympathetic fibres that innervate both endothelial and vSMCs. Through the activation of muscarinic receptors 2 and 3 (M2 and M3) on vSMCs, Ach induces vascular contraction inhibiting the production of nitric oxide (NO), an endothelial-derived relaxing factor. Acting on the endothelium, instead, Ach has the opposite effect, regulating the release of NO and thus mediating vasodilation (Bolton and Lim, 1991; van Zwieten et al., 1995).

As described before, several neurotransmitters can act on different components of blood vessels, but also endothelial cells can influence the ANS through the synthesis of factors like NO and endothelin.

NO is produced by the endothelium in response to shear stress. It diffuses into vSMCs and increases cGMP concentration, resulting in vessels dilation. This mechanism can inhibit NE-induced vasoconstriction (Tesfamariam and Cohen, 1988; Thorin and Atkinson, 1994).

Endothelin is a peptide mainly produced by endothelial cells that has a key role in vascular homeostasis. High levels induce vasoconstriction, enhancing vSMCs sensitivity to NE, while low concentrations inhibit sympathetic activity, resulting in vasodilation (Nakamaru et al., 1989; Tabuchi et al., 1990).

While historically the relationship between the ANS and blood vessels has often been investigated, less is known about the interaction of blood vessels and sensory neurons.

Perivascular sensory nerves can be identified with immunostaining for calcitonin gene-related peptide (CGRP) and substance P (SP) (Grasby et al., 1999; Ruocco et al., 2002). CGRP is the main neurotransmitter of these fibres. It causes vasodilation targeting CGRP1 receptors on the endothelium (Hagner et al., 2001) and stimulating the synthesis of NO. It also acts on vSMCs leading to the opening of K^+ channels and thus to vascular dilatation (Nelson et al., 1990; Standen et al., 1989). SP seems to exert the same effect, increasing NO synthesis (Bolton and Clapp, 1986), but its functions remain more controversial, as several studies suggest that its concentration may not be sufficient to affect vessels diameter (Brain, 1997; Kawasaki et al., 1988).

Although several groups are trying to unravel the complex interaction between sensory neurons and blood vessels, much remains to be elucidated.

1.4.2 Baroreceptors

Responding to changes in BP is crucial for normal vital functions. Some mechanisms, that will be described in the next section, control long-term BP regulation by changing blood volume. To counteract BP changes within seconds and minutes, instead, baroreceptors are the key players. They are stretch-sensitive neurons with cell bodies located in nodose and petrosal ganglia that extend their peripheral projections primarily in the wall of the aortic arch and in each of the carotid sinuses (Kirchheim, 1976; Wehrwein and Joyner, 2013). The vagus and glossopharyngeal nerves convey information from the baroreceptors of the aortic arch and carotid sinuses respectively, to the nucleus of the solitary tract and from there further projections reach the medulla oblongata. Sympathetic and parasympathetic motor neurons from the medulla oblongata innervate heart and vasculature to execute the cardiovascular response initiated by the baroreceptors (Critchley and Harrison, 2013; Thayer et al., 2009) (Fig. 4).

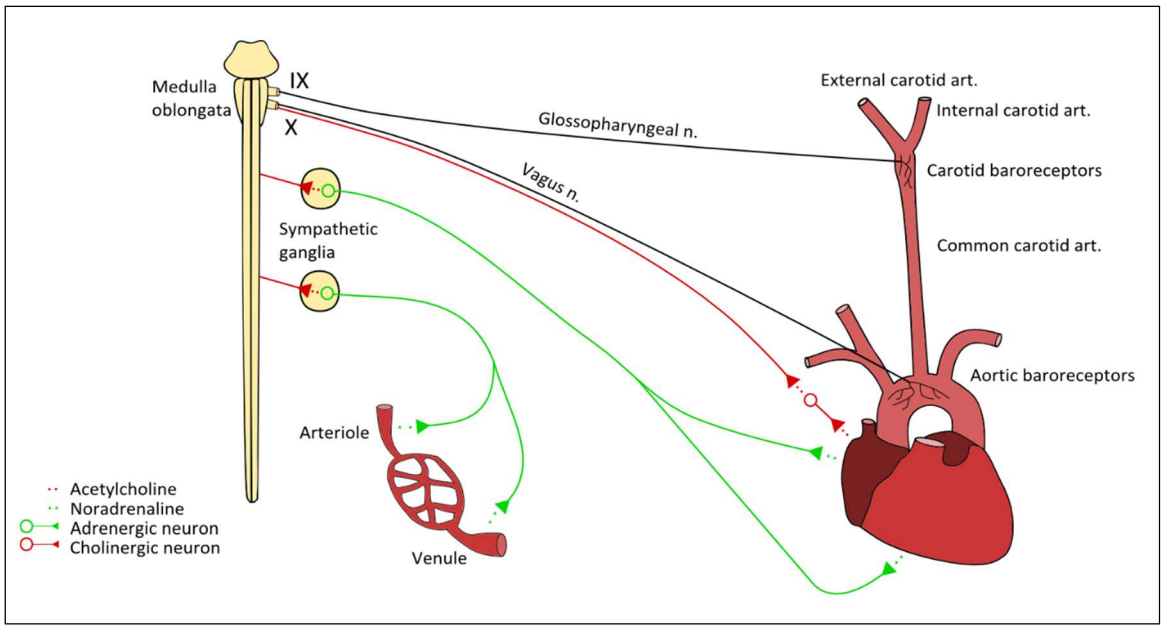

Figure 4. Schematic of baroreceptors circuit.
Baroreceptors located in the aortic arch and the carotid sinuses transmit information to the CNS through the vagus nerve and the glossopharyngeal nerve. From there, sympathetic and parasympathetic motor neurons arise to act on heart and vasculature to respond to baroreceptors signals. Image taken from nataliescasebook.com.

If BP increases, baroreceptors nerve endings are stretched and thus baroreceptors increase their firing rate. The cardioinhibitory centre in the central nervous system is stimulated and this results in an increased vagal tone that leads to a reduced heart rate (HR). At the same time, the vasomotor centre is inhibited and so a reduced sympathetic tone results in vasodilation. Reduced HR and reduced vascular resistance lead to BP reduction within minutes from the initial increase. In case of low BP, baroreceptors decrease their firing rate causing vasoconstriction and increased heart rate that will lead to a restoration of physiological BP (Duschek et al., 2007; Duschek et al., 2009).

From a molecular point of view, several ion channels have been proposed as the baroreceptors mechanosensors (Drummond et al., 1998; Lau et al., 2016; Lu et al., 2009; Sun et al., 2009).

ASIC2, an acid sensing ion channel required for mechanosensation in some cutaneous and gastrointestinal fibres (Garcia-Anoveros et al., 2001; Page et al., 2005; Price et al., 2000), seems implicated in baroreceptor sensitivity. ASIC2 null mice develop hypertension and exhibit a disrupted regulation of the circulation by the autonomic nervous system (Lu et al., 2009), thus supporting the hypothesis of a role in baroreceptors sensing.

Transient receptor potential (TRP) channels are other putative baroreceptor mechanosensors. They play this role in several cell types and are expressed in nerve terminals at the level of the aortic arch (Glazebrook et al., 2005). Mice lacking TRP Vanilloid 1 (TRPV1) display an impaired inhibition of the sympathetic nerve activity following an increase in BP (Sun et al., 2009). Similarly, TRPC5 knockout mice present an attenuated baroreflex response and BP instability, with severe fluctuations during the day (Lau et al., 2016).

However, in all the previous studies a residual baroreflex was always observed, implicating the presence of other mechanosensors. Recently, Zeng et al. demonstrated that the ion channels Piezo1 and Piezo2 are the crucial elements for baroreceptors function (Zeng et al., 2018). Selective knockout of both channels in nodose and petrosal ganglia abolished the baroreflex, i.e. a BP increase did not result in a HR decrease. Strikingly, mice knockout for a single channel did not display any change in baroreceptors functionality. Double knockout mice displayed also higher HR and BP during active times and increased BP variability.

A further evidence of Piezo channels importance in baroreceptors function is the decrease in HR and BP following Piezo2 optogenetic stimulation in Piezo2^{Cre+}::ChR2-eYFP mice. The light-induced activation of Piezo2^{+} afferents in the aortic arch and carotid sinuses causes a sudden decrease in both BP and HR. These effects are attenuated by the

administration of a β-adrenergic blocker, proving the involvement of the sympathetic nervous system (Zeng et al., 2018).

1.4.2.1 Piezo channels

Piezo1 and Piezo2 belong to an evolutionarily conserved ion channel family. They are mechanically activated non-selective cation channels and their opening results in Na^+ and Ca^{2+} influx (Gnanasambandam et al., 2015; Zhao et al., 2016). Piezo1 and Piezo2 have a 50% identity at the amino acid level and both are arranged as homotrimers to form a pore (Ge et al., 2015). Membrane tension activates the channel altering the lipid-protein interactions and thus opening the pore (Syeda et al., 2016).

Piezo1 is mainly expressed in non-neuronal cells, while sensory neurons and some specialized mechanosensory structures express Piezo2.

Piezo1

Piezo1 is crucial for cardiovascular mechanotransduction. Lack of this channel is incompatible with life: mice develop until mid-gestation, when blood flow should start. In the absence of Piezo1, endothelial cells are not able to reorganize to form new blood vessels, causing embryo death (Li et al., 2014; Ranade et al., 2014a).

Being expressed on the endothelium, Piezo1 provokes Ca^{2+} influx in response to shear stress. This in turn leads to ATP release that results in NO synthesis, causing vasodilation (Wang et al., 2016).

Piezo1 is also expressed on vSMCs. In these cells, the stretching-induced Ca^{2+} influx activates the enzyme transglutaminase that is important for vascular remodelling: vessel diameter decreases and the wall thickness increases in response to Piezo1 activation (Retailleau et al., 2015).

A recent study suggested that Piezo1 is fundamental to keep high BP during physical activity, but not inactivity and that it has a different effect according to the specific vascular bed (Rode et al., 2017). During whole body physical activity, mesenteric resistance arteries shrink to redirect blood flow towards skeletal muscles (Joyner and Casey, 2015) and far from the gastrointestinal tract (Qamar and Read, 1987). In mesenteric arteries the activation of Piezo1 on vSMCs leads to vasoconstriction, while in saphenous and carotid arteries Piezo1 activation do not cause any effect, allowing the vessels to increase blood flow to improve physical performance (Rode et al., 2017).

Piezo1 activity is fundamental also to regulate red blood cells (RBCs) volume. In this case, Ca^{2+} causes the activation of a potassium channel resulting in the efflux of K^{+} and water. The dehydration and volume decrease counteract the stretch-induced activation of Piezo1 channels (Cahalan et al., 2015).

Apart from the cardiovascular system, Piezo1 role is crucial also for epithelial homeostasis. Knockdown studies in zebrafish showed epithelial mass formation (Eisenhoffer et al., 2012) and attenuated cell division in the absence of Piezo1 (Gudipaty et al., 2017). These pathways could be conserved across species and could be involved in tumorigenesis, as some mutations of the channel were identified in patients with colorectal adenomatous polyposis (Spier et al., 2016).

Recently, Piezo1 has also been implicated in the differentiation of neural stem cells. Lack of this channel drives the differentiation towards astrocytes, inhibiting the ability to differentiate into neurons (Pathak et al., 2014).

Piezo2

Unlike Piezo1, Piezo2 is mainly expressed in neuronal cells, where it is crucial to detect light touch and proprioception.

Piezo2 is expressed in low-threshold mechanoreceptors, fundamental for the sensation of innocuous touch, and in Merkel cells, specialized epithelial cells essential to perceive fine textures (Ranade et al., 2014b; Woo et al., 2014).

Piezo2 is also the main mechanotransduction channel for proprioception, the ability to sense body position, body orientation and body and limb motion. Lack of these channels results in severe locomotor deficits with abnormal limb position and loss of coordination. In the absence of Piezo2, proprioceptive neurons decrease their stretch-induced activity, giving rise to this phenotype (Florez-Paz et al., 2016; Woo et al., 2015).

Piezo2 is expressed also in sensory neurons innervating the lungs, where it is crucial for an efficient respiration. Mice lacking these channels display a severe decrease of stretch-induced firing of lungs sensory neurons and develop respiratory distress (Nonomura et al., 2016). Specific activation of Piezo2$^+$ vagal sensory neurons, instead, causes apnoea. This mechanism is conserved through evolution, as some gain of function mutations cause a restrictive lung disease in humans (Coste et al., 2013; Okubo et al., 2015).

1.4.3 Renin-angiotensin-aldosterone system

Another key player in BP regulation is the renin-angiotensin-aldosterone system (RAAS). Among its various functions, it regulates the extracellular fluid volume, thus acting on water, blood, lymph and interstitial fluid (Navar, 2014).

Low BP, low plasma concentration of NaCl and sympathetic nervous system activity, especially through β1-adrenoreceptros, lead to the expression of renin (Drenjancevic-Peric et al., 2011). Renin is produced by the kidney granular cells (Kopp and DiBona, 1993) as a precursor and then it is proteolitically cleaved in the kidney by cathepsin B. Once activated, renin hydrolyses angiotensinogen, produced by the liver in

response to corticosteroids, estrogen or thyroid hormones (Verdecchia et al., 2008), to angiotensin I. Angiotensin I is then further processed into angiotensin II by the endothelial angiotensin-converting enzyme (ACE) (Crisan and Carr, 2000). Angiotensin II has several crucial functions (Peach and Dostal, 1990):

- it causes vasoconstriction acting on vSMCs. Binding the G-protein-coupled receptor AT1, it activates phospholipase C leading to increased concentration of Ca^{2+} and so to vessels shrinkage and increased BP (Feener et al., 1995).
- It influences the release of prostaglandins by the kidney, influencing renal vasoconstriction and renal water retention and K^+ excretion (Cao et al., 2012).
- It stimulates the secretion of aldosterone by the cortex of the adrenal gland (Yatabe et al., 2011). Aldosterone increases Na^+ reabsorption at the level of the kidney proximal tubules, leading to water retention.
- It also stimulates the posterior lobe of the pituitary gland to secrete the antidiuretic hormone (ADH) to reabsorb water (Sands and Layton, 2009).

All the angiotensin II-mediated effects lead to water retention and so to an increase in blood volume that counteract the initial low BP.

The RAAS is regulated also by some hormones. Thyroid hormones activate the system by binding to thyroid hormone response elements (REs) that increase the level of renin mRNA (Kobori et al., 2001). Similarly, estrogen binds to other REs regulating the expression of renin (Lu et al., 2016).

1.4.4 Exercise pressor reflex

BP needs to adjust to several different situations during everyday life. One of the most common activities that leads to BP regulation is muscle exercise (Alam and Smirk, 1937; Coote et al., 1971). All kinds of persistent exercise result in increased heart rate, BP

and ventilation. This is due to a reflex originating from skeletal muscles, known as "the exercise pressor reflex". During muscle contraction, several receptors are activated by mechanical forces or metabolic products. From a molecular point of view not much is known about the receptors: ATP purinergic receptors (Hanna and Kaufman, 2003), TRPV1 or ASIC channels have been proposed as putative metabolic receptors (Li et al., 2004), but their molecular identity still needs to be elucidated. Despite the poorly understood characterization, it is known that these receptors are found on both thinly myelinated (group III) and unmyelinated (group IV) nerve fibres in skeletal muscles that are the afferent fibres responsible for the exercise pressor reflex (Kaufman et al., 1982; Tibes, 1977). While group III fibres are mainly mechanically sensitive, group IV predominately sense metabolic products (Kaufman et al., 1983). Signals from both groups of fibres reach the nucleus tractus solitarii and the ventrolateral medulla where they activate the sympathetic nervous system, resulting in increased BP and HR (Hill et al., 1996; Kaufman, 2012; Matsukawa et al., 1994).

The exercise pressor reflex behaves differently in different types of muscles. Some muscles contain slow twitch fibres that express oxidative enzymes, are highly vascularized and resistant to fatigue. Others are made of fast twitch fibres expressing glycolytic enzymes, are less vascularized and susceptible to fatigue. The exercise pressor reflex gives rise to a robust BP increase mainly in fast twitch muscles, whereas slow twitch fibres respond to exercise to a smaller extent (Iwamoto and Botterman, 1985). This is due to afferent sensory neurons that respond differently to metabolic stimuli in slow-twitch or fast-twitch fibres (Xing et al., 2008).

1.5 General aims

In this study we have:

- characterized TrkC expression in the different classes of peripheral neurons.
- Focused our attention in particular to $TrkC^+$ sensory neurons innervating blood vessels.
- Performed gain and loss of function experiments to understand their role and contribution in the control of blood pressure.
- Understood the mechanism by which they exert their functions, i.e. if they directly act on blood vessels or if they need a circuit with other neurons.

2. Materials and methods

2.1 Generation of TrkC^{CreERT2} mice

A bacterial artificial chromosome (BAC) containing the *TrkC* mouse locus was obtained from SourceBioscience (RP23-38E14) and a modified CreERT2-pA-Frt-Ampicillin-Frt cassette was inserted into the ATG of *TrkC*. The positive clones were confirmed by PCR and a full-length sequencing of the inserted cassette was performed. The ampicillin cassette was then removed using bacterial Flp and the accomplished removal was confirmed by sequencing analysis. Purified BAC DNA was then dissolved into endotoxin-free TE and prepared for intracytoplasmic sperm injection (ICSI). The method successfully produced offspring and the mice genotype was determined by performing PCR using the following primers: gcactgatttcgaccaggtt (fwd) and gagtcatccttagcgccgta (rev), yielding products of 408 bp.

(Note: the above-mentioned mouse line was generated by the Heppenstall laboratory before my arrival at EMBL Rome).

2.2 Avil$^{hM3Dq\text{-}mCherry}$ mice

For gain of function studies, Avil$^{hM3Dq\text{-}mCherry}$ mice as described previously (Dhandapani et al., 2018) were crossed to TrkC^{CreERT2} to generate TrkC^{CreERT2}::Avil$^{hM3Dq\text{-}mCherry}$ heterozygous mice. Thanks to the knock-in of hM3Dq-mCherry in the sensory neurons-specific *Advillin* locus, only TrkC^{+} sensory neurons will express the hM3Dq DREADD receptor. For all the experiments, littermates lacking Cre were used as controls.

2.3 Rosa26$^{ChR2\text{-}YFP}$ mice

For optogenetic experiments, TrkC^{CreERT2} mice were crossed to Rosa26$^{ChR2\text{-}YFP}$ mice (The Jackson Laboratory, 024109) to generate TrkC^{CreERT2}::Rosa26$^{ChR2\text{-}YFP}$ mouse line. In these mice, the tamoxifen-inducible Cre drives the expression of Channelrhodopsin2-Yellow Fluorescent Protein fusion protein (ChR2-YFP), permitting the activation of TrkC^{+} cells with blue light and also their visualization thanks to the endogenous expression of YFP. For this reason, TrkC^{CreERT2}:: Rosa26$^{ChR2\text{-}YFP}$ mice have also been used as a reporter line for histological characterization.

2.4 Avil^{iDTR} mice

For diphtheria toxin-mediated ablation, Avil^{iDTR} mice, as described in (Stantcheva et al., 2016), were crossed to TrkC^{CreERT2} to generate TrkC^{CreERT2}::Avil^{iDTR} heterozygous mice. As in the case of TrkC^{CreERT2}::Avil$^{hM3Dq\text{-}mCherry}$ mice, the inducible diphtheria toxin receptor (iDTR) is under the *Advillin* promoter and so only TrkC^{+} sensory neurons will express it upon Cre recombination.

Triple transgenic mice were also generated by crossing TrkC^{CreERT2}::Avil^{iDTR} to Rosa26$^{ChR2\text{-}YFP}$ mice. The obtained TrkC^{CreERT2}::Avil^{iDTR}::Rosa26$^{ChR2\text{-}YFP}$ mice were used as a reporter line in ablation experiments, thanks to the endogenous expression of YFP in TrkC^{+} cells.

All mice were housed in the EMBL Epigenetics and Neurobiology Unit, Rome, according to the Italian legislation (Art. 9, 27 Jan 1992, no 116) under licence from the Italian Ministry of Health and in compliance with the ARRIVE guidelines.

2.5 Tamoxifen treatment

To induce the expression of Cre, adult mice (older than 8 weeks of age) were treated intraperitoneally (i.p.) with 75 mg/kg of body weight of tamoxifen (Sigma Aldrich, T5648) dissolved in sunflower seed oil (Sigma Aldrich, S5007) for 3 consecutive days. Mice were then used for experiments at least one week after the last injection.

In some cases, to restrict the expression of Cre to DRG neurons, $TrkC^{CreERT2}$::$Rosa26^{ChR2\text{-}YFP}$ mice were treated with a single intrathecal (i.t.) injection of 90 ng of 4-hydroxytamoxifen (4-OH Tamoxifen, Sigma Aldrich, H7904). Experiments were performed at least one week after the treatment.

2.6 Immunofluorescence

DRG were dissected and fixed in 4% PFA overnight at 4°C. Ganglia were then embedded in 2% agarose (Sigma Aldrich, A9539) and cut in 50 μm sections using a vibratome (Leica, VT1000S). After an incubation of 30 minutes with a blocking solution containing 5% goat serum and 0.01% Tween-20 in PBS, the sections were incubated with one or more primary antibodies (Table 1) in blocking solution overnight at 4°C. The next morning, secondary antibodies in blocking solution were added and the sections were incubated for 1 hour and 30 minutes at room temperature (RT). After some washes with PBS, slides were mounted with prolong gold (Invitrogen, P36930).

To examine $TrkC^+$ peripheral afferents, mice were injected intravenously (i.v.) with a solution of 2% Evan's Blue (Sigma Aldrich, E2129) in PBS. After 30 minutes, the skin of the hind limb was carefully dissected and fixed in 4% PFA overnight at 4°C. After a permeabilization step with PBS-T (0.3% TritonX in PBS) of 30 minutes at RT, the tissue was incubated in a blocking solution (10% goat serum in PBS-T) for 2 hours at RT and then with one or more primary antibodies (Table 1) in blocking solution overnight at

4°C. Secondary antibodies were added in blocking solution for 1 hour and 30 minutes at RT and then the tissue was whole-mounted using prolong gold.

For immunofluorescence experiments, the following primary antibodies were used:

Antibody	Concentration	Supplier/catalog number
Rabbit anti-TH	1:1000	Millipore, AB152
Mouse anti-CGRP	1:500	Rockland, 200-301-D15
Rabbit anti-PV	1:1000	Swant, PV27
Isolectin GS-B4-biotin XX-conjugate	1:100	Invitrogen, I21414
Rabbit anti-desmin	1:200	Abcam, Ab32362

Table 1. List of primary antibodies used for immunohistochemical experiments.

All secondary antibodies were Alexa-conjugated and were used at a concentration of 1:1000. Streptavidin-conjugated secondary antibodies were used at a concentration of 1:500.

All images were acquired using a Leica SP5 confocal microscope and analysed using ImageJ.

2.7 *Ex-vivo* live imaging

Mice were injected i.v. with a solution of 2% Evan's Blue. After 30 minutes, the skin of the hind limb was carefully dissected and placed in a bath chamber where physiological conditions were maintained (32°C, 5% CO_2, synthetic interstitial fluid: 108

mM NaCl, 3.5 mM KCl, 0.7 mM $MgSO_4$, 26 mM $NaHCO_3$, 1.7 mM NaH_2PO_4, 1.5 mM $Cacl_2$, 9.5 mM sodium gluconate, 5.5 mM glucose and 7.5 mM sucrose at a pH of 7.4).

In the case of $TrkC^{CreERT2}$::$Avil^{hM3Dq\text{-}mCherry}$ mice, 50 μM of Clozapine-N-oxide (CNO, Tocris, 4936) were added in the chamber. As a positive control, L-norepinephrine hydrochloride (Sigma Aldrich, 74480) was used at a concentration of 10 mM.

For $TrkC^{CreERT2}$::$Rosa26^{ChR2\text{-}YFP}$ mice, the skin was stimulated for 40 seconds every minute for 15 minutes with the built-in 488 nm laser of the microscope we used.

All tissues were imaged using a Nikon Ti Eclipse spinning disk microscope. Images were acquired every minute for 15 minutes and analysed using ImageJ. For each blood vessel, the change in diameter was measured by randomly selecting three areas and comparing the initial diameter with the diameter at the end of the acquisition. Averaging the results, we obtained the mean diameter change for each vessel that was expressed as the percentage of the initial diameter.

2.8 Administration of DREADD ligands

In order to have a systemic activation of $TrkC^{+}$ neurons, $TrkC^{CreERT2}$::$Avil^{hM3Dq\text{-}mCherry}$ mice were injected i.p. with 2.5 mg/kg of body weight of the DREADD agonist compound 21 dihydrochloride (C21, Hello Bio, HB6124).

For a local activation, instead, 2.5 mg/kg of CNO were injected subcutaneously in the hind paw.

2.9 Propranolol administration

The nonselective β-blocker propranolol hydrochloride (Sigma Aldrich, P0884) was injected i.p. at a concentration of 5 mg/kg of body weight or locally with a subcutaneous

injection in the hind paw at a dosage of 2.5 mg/kg. Both administrations were always performed immediately after the administration of the DREADD ligand.

2.10 Diphtheria toxin injection

$TrkC^{CreERT2}$::$Avil^{iDTR}$ mice were injected i.p. with 40 ng/g of body weight of diphtheria toxin (DTX, Sigma Aldrich, D0564). All mice were monitored during the injection period and blood pressure, heart rate and blood flow were measured before the injection of DTX and 16, 24 and 32 hours after.

2.11 Blood pressure measurements

Mice were anesthetized with a 2% isoflurane and medical air mixture through a nose cone and placed on a heat pad at 37°C. Blood pressure (BP) was measured using a Non-Invasive Blood Pressure (NIBP) system (AD Instruments) paired with a PowerLab 4/20 ML840 (AD Instruments) and LabChart 4 software to acquire and analyze data. For each measurement, BP was registered four times per mouse with a 1-minute interval and the mean value was recorded. To calculate BP variation, the baseline mean value was subtracted to each time point measurement.

2.12 Heart rate measurements

Mice were anesthetized with 2% isoflurane and kept at 37°C using a heat pad. Their heart rate was monitored for 30 or 60 minutes using a PhysioSuite MouseSTAT (Kent Scientific) and Free Serial Port Terminal 1.0.0.710 software that detected the beats per minute (BPM) every half a second. All data were analysed with gHRV 1.6 software (Rodriguez-Linares et al., 2014).

To measure the heart rate trend, we averaged the BPM acquired every 2 minutes and for each time point we subtracted the baseline BPM acquired in the 2 minutes before the treatment. We thus obtained a measure of the HR variation.

The HR variability was assessed measuring the standard deviation of the NN intervals (SDNN; Normal-to-normal (NN) intervals are the time gaps between consecutive QRS complexes in a continuous ECG recording) (1996). HR variability was measured also by plotting the beats per minute in a Poincaré plot. The output of this analysis are two standard deviation (SD) parameters that indicate how stable or variable are the beat-to-beat events. SDNN and Poincaré plots parameters were calculated using the gHRV 1.6 software.

2.13 Laser Speckle Contrast Imaging

To analyse blood flow, recordings were performed using a 780 nm, 100mW laser (LaserLands) at a working distance of 5 cm and a Leica Z16 Apo microscope with a high resolution camera (AxioCam MRM, Carl Zeiss) with 5 ms exposure time at maximum speed for 100 cycles. Data were then analyzed using ImageJ as previously described (Briers and Webster, 1996). Briefly, speckle contrast is defined as:

$$\text{speckle contrast } K = \sigma_s / I$$

where σ_s is the standard deviation of the spatial intensity variations measured in the speckle pattern and I is the average intensity. To obtain the speckle contrast, raw images were analyzed in order to get σ_s and I and their ratio was calculated.

The output images were then subjected to a densitometry analysis using ImageJ. For each image, two areas containing a blood vessel were randomly selected. The mean grey value of the pixels was calculated and the background of the nearby area where the blood vessel was not present was subtracted. The obtained values were averaged in order

to get one speckle contrast value (K) per image. Then, the ratio between K before treatment and K at each time point was calculated.

For gain of function experiments, mice were anesthetized with an i.p. injection of 90 mg/kg ketamine (Lobotor, Acme) and 0.5 mg/kg medetomidine (Domitor, Orion Pharma) and their hind paw was attached using double-sided tape to a plastic platform for better imaging. Images were acquired before the treatment with CNO to get a baseline and after its administration every 2 minutes for 30 minutes.

For ablation experiments, mice were anesthetized with 2% isoflurane and their ear was attached to a plastic platform with the external side up, facing the camera. Images were acquired before the injection of DTX and 16, 24 and 32 hours after.

2.14 Behavioural testing

All behaviour experiments were performed on adult male mice (>8 weeks of age). Littermates not expressing Cre were used as controls. Unless otherwise specified, all tests were performed 1 hour after local injection of CNO.

2.14.1 Von Frey test

Mice were placed on an elevated platform with a mesh floor and habituated for 30 minutes. The hind paw was poked with calibrated von Frey filaments (North coast medical, NC12775-99) and the 50% withdrawal thresholds were calculated using the Up-Down method previously described (Chaplan et al., 1994). Briefly, the plantar side of the paw was stimulated by a certain filament. If mice were sensitive to that filament, the test continued stimulating the paw using a lower filament, while if mice did not respond a filament corresponding to a higher force was used.

To measure the sensitivity to mechanical pain over time, the hind paw of $TrkC^{CreERT2}$::$Avil^{hM3Dq\text{-}mCherry}$ mice was stimulated with a 0.02 g filament five times, 10 minutes, 25 minutes and 40 minutes after the local injection of CNO. The percentage of withdrawals was calculated per each time point.

2.14.2 Acetone drop test

Mice were habituated on an elevated platform with a mesh floor for 30 minutes. A single drop of acetone was sprayed on the hind paw with a blunt syringe making sure not to touch the paw. The test was repeated 5 times per mouse and the behavioural responses were scored as follows:

0 = no response

1 = paw withdrawal or single flick

2 = repeated flicking

3 = licking of the paw

2.14.3 Paintbrush test

After a habituation of 30 minutes as described before, the hind paw of mice was stimulated with a paintbrush in the heel-to-toe direction. The responses were scored according to Duan et al. (Duan et al., 2014):

0 = no response

1 = paw withdrawal

2 = flicking of the paw

3 = licking of the paw

2.15 Statistical analysis

All statistical data are represented as standard error of the mean (SEM). Student's t-test and/or 2-way repeated measures ANOVA were used and $p<0.05$ was considered statistically significant.

3. Results

3.1 Molecular characterisation of TrkC^{+} neurons

3.1.1 TrkC expression in DRG

In order to characterize TrkC expression pattern in the DRG, we used TrkC^{CreERT2}::Rosa26$^{ChR2\text{-}YFP}$ mice, exploiting the fact that upon administration of tamoxifen only TrkC^{+} cells will express the Yellow Fluorescent Protein (YFP) reporter. We found that TrkC is expressed in around 30% of all DRG neurons, marking neurons of both big and small size (Fig. 5A).

We next co-labelled DRG neurons with well-known markers of different populations of sensory neurons and, as expected, we found a strong co-localization of TrkC and parvalbumin (PV), marker for proprioceptors (Fig. 5B). 9.6% of all DRG neurons expressed both TrkC and PV. Instead, TrkC^{+} neurons were only minimally overlapping with nociceptors markers like CGRP (marker of peptidergic nociceptors; 1.8% overlap) and IB4 (marker of non-peptidergic nociceptors; 0.7% overlap) (Fig 5C-D).

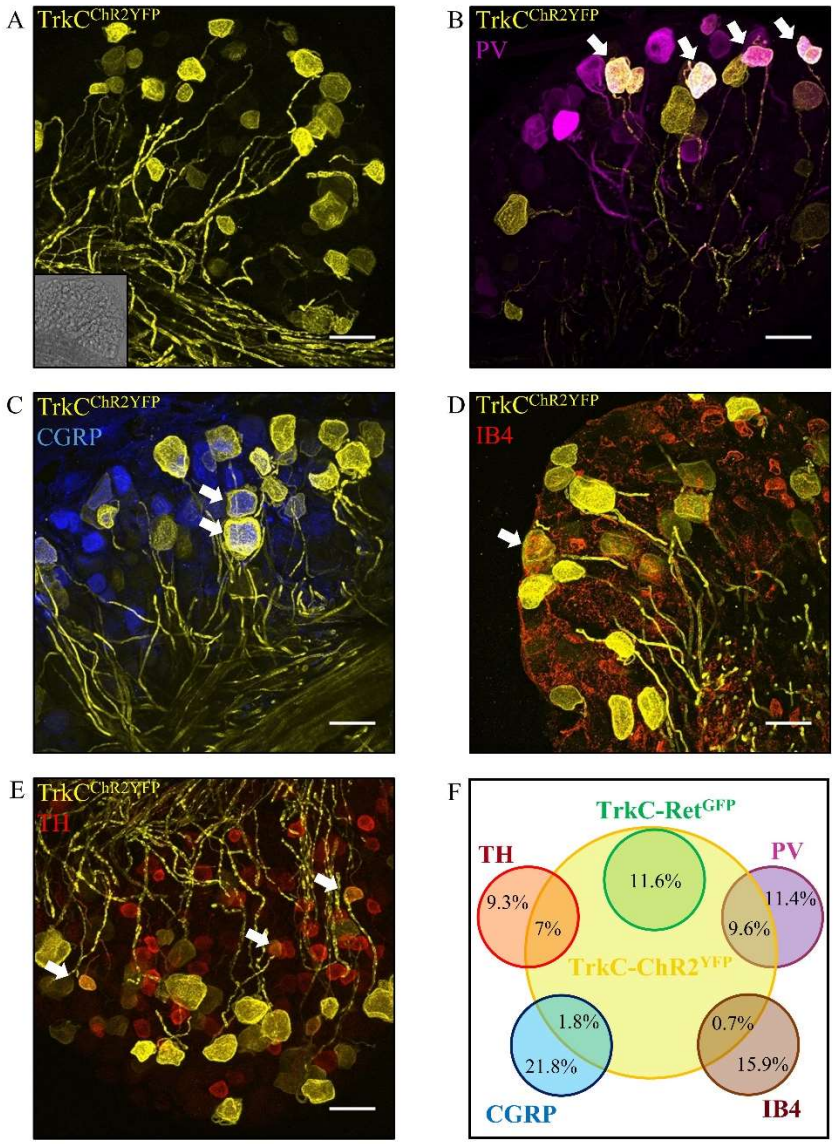

Figure 5. Expression of TrkC in DRG neurons.
TrkC expression was investigated using TrkC^{CreERT2}::Rosa26$^{ChR2\text{-}YFP}$ reporter mouse line. **(A)** TrkC expression in DRG sections showing that 30% of all DRG neurons are TrkC^{+}. The brightfield image is shown in the inset. **(B-E)** Immunofluorescence of DRG sections with markers of different neuronal populations: PV **(B)**, CGRP **(C)**, IB4 **(D)** and TH **(E)**. Double positive neurons are indicated by arrows. Scale bar is 50 µm. **(F)** Quantification of TrkC co-localization with different markers, expressed as percentage of the total number of DRG neurons.

Surprisingly, we found that around 7% of all DRG neurons were expressing both TrkC and TH (Fig. 5E). TH is a marker for a subset of mechanoreceptors that are known to express Ret as well. To understand if TrkC^{+} TH^{+} neurons were belonging to the same

population, we used TrkC^{CreERT2}::Ret^{GFP} mice, where the Green Fluorescent Protein is expressed only in TrkC^{+} Ret^{+} cells. Labelling of DRG neurons from TrkC^{CreERT2}::Ret^{GFP} mice showed no overlap at all between TH^{+} and TrkC^{+} Ret^{+} neurons (Fig. 6A), demonstrating that TrkC^{+} TH^{+} and TrkC^{+} Ret^{+} neurons are two different populations. As expected, TrkC^{+} Ret^{+} neurons do not express PV either (Fig. 6B).

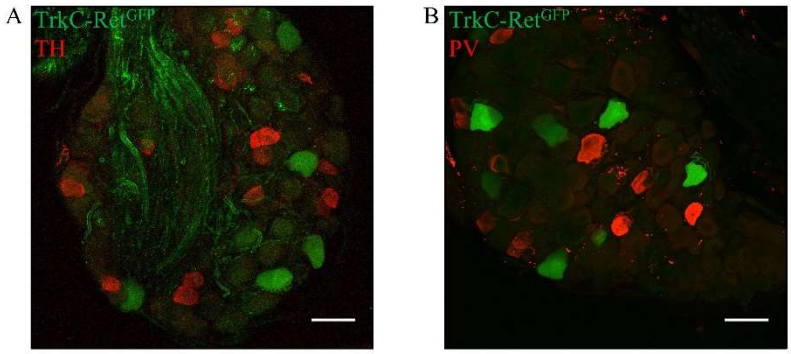

Figure 6. TrkC marks three mutually exclusive DRG populations.
Immunofluorescence of DRG sections from TrkC^{CreERT2}::Ret^{GFP} mice. Labelling with anti-TH antibodies **(A)** and anti-PV antibodies **(B)** revealed 0% overlap between these neuronal populations. Scale bar 50 μm.

Taken together, these results suggest that TrkC is expressed in three different populations of DRG neurons: TrkC^{+} PV^{+} neurons, known to be proprioceptors, TrkC^{+} Ret^{+} neurons, that are a class of mechanoreceptors, and TrkC^{+} TH^{+} neurons, small neurons that were never described before and whose role I will try to clarify in the course of this thesis. These three TrkC populations are mutually exclusive: there is 0% overlap between neurons belonging to one population and neurons belonging to the others.

TrkC^{+} TH^{+} neurons are significantly smaller than TrkC+ TH- neurons and slightly bigger than TrkC- TH+ (Fig. 7).

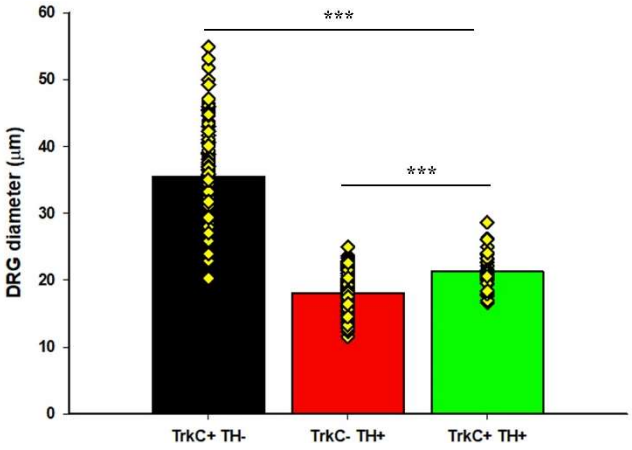

Figure 7. TrkC$^+$ TH$^+$ DRG neurons are medium-sized.
TrkC$^+$ TH$^+$ DRG neurons have a diameter of 21.28 ± 0.52 μm that is significantly bigger than TrkC$^-$ TH$^+$ neurons (18.03 ± 0.24 μm) and smaller than TrkC$^+$ TH$^-$ neurons (35.43 ± 0.62 μm). (n=129 for TrkC$^+$ TH$^-$ neurons, n=139 for TrkC$^-$ TH$^+$ neurons, n=30 for TrkC$^+$ TH$^+$ neurons; ***p<0.001).

Additional characterization showed that TrkC$^+$ TH$^+$ neurons are more prevalent in lumbar DRG (5.9% of all neurons) than thoracic (1.2%) or cervical (0.7%) (Fig 8).

We also further analyzed a published dataset of DRG neurons single cell RNAseq data (Zeisel et al., 2018). We confirmed the presence of a population of TrkC$^+$ TH$^+$ DRG neurons that are unmyelinated and do not express PV or peptidergic genes. Interestingly, they express Piezo2, a mechanically activated channel required for light touch and proprioception, and Asic2, fundamental for baroreceptive function (Supplementary Fig. 1).

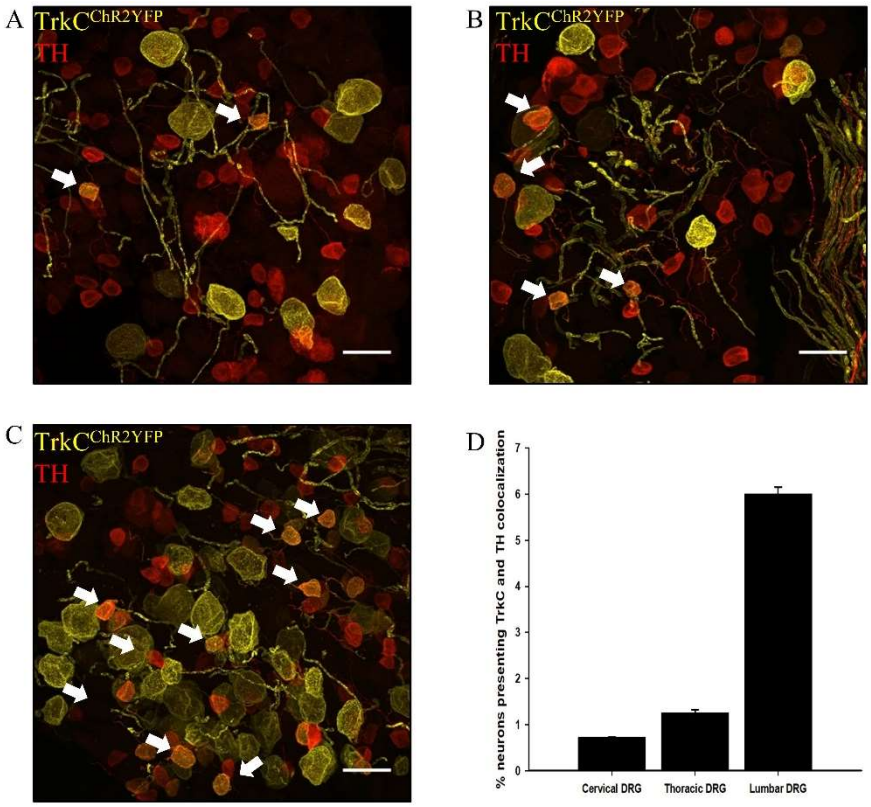

Figure 8. Differential expression of TrkC along the spinal cord.
(A-C) Immunofluorescence of DRG sections from TrkC^{CreERT2}::Rosa26$^{ChR2\text{-}YFP}$ mice labelled with anti-TH antibodies. TrkC expression was investigated in cervical DRG **(A)**, thoracic DRG **(B)** and lumbar DRG **(C)**. Double positive neurons are indicated by arrows. Scale bar is 50 μm. **(D)** Quantification of the number of neurons co-expressing TrkC and TH in the different segments of the spinal cord, expressed as percentage of the total number of DRG neurons.

3.1.2 TrkC expression in the sympathetic chain

Since TH is a classical marker for sympathetic neurons, we decided to investigate TrkC expression also in this branch of the nervous system. Using TrkC^{CreERT2}::Rosa26$^{ChR2\text{-}YFP}$ mouse line, we examined the presence of TrkC in the Superior Cervical Ganglion (SCG) and in the Nodose-Petrosal-Jugular ganglion (NPJ) complex. No TrkC expression was detected in the SCG, nor in the NPJ complex, while almost all neurons were TH$^+$ (Fig. 9).

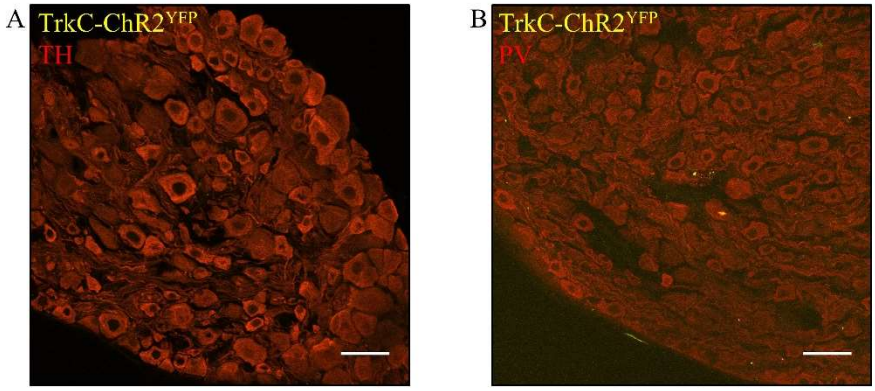

Figure 9. TrkC expression in sympathetic neurons.
Immunofluorescence of sections of ganglia from TrkC^{CreERT2}::Rosa26$^{ChR2\text{-}YFP}$ mice. Labelling with anti-TH antibodies revealed a high expression of TH, but no expression of TrkC, neither in the superior cervical ganglion **(A)**, nor in the NPJ complex **(B)**. Scale bar 50 μm.

3.1.3 TrkC expression in the skin

We next investigated TrkC expression in the skin using TrkC^{CreERT2}::Rosa26$^{ChR2\text{-}YFP}$ mouse line. As expected, TrkC marked some mechanoreceptive structures, in particular circumferential endings surrounding the majority of hair follicles (Fig. 10A, arrows), that are important to detect stroking over a large area of skin.

Surprisingly, we found that TrkC is also expressed in vascular Smooth Muscle Cells (vSMCs) wrapping around blood vessels (Fig. 10A, arrowheads). The presence of TrkC in vSMCs is consistent throughout the body, not only in skin blood vessels (Fig. 10B), but also in vSMCs surrounding the aorta (Fig. 10C) or other arteries like the saphenous one (Fig. 10D). Interestingly, immunohistochemical analysis with anti-desmin antibodies, marking all mural cells, revealed that TrkC does not mark all mural cells, but only vSMCs. Pericytes are TrkC^{-} (Fig. 10E).

Apart from being expressed in vSMCs, TrkC marks also some nerves innervating blood vessels (Fig. 10F).

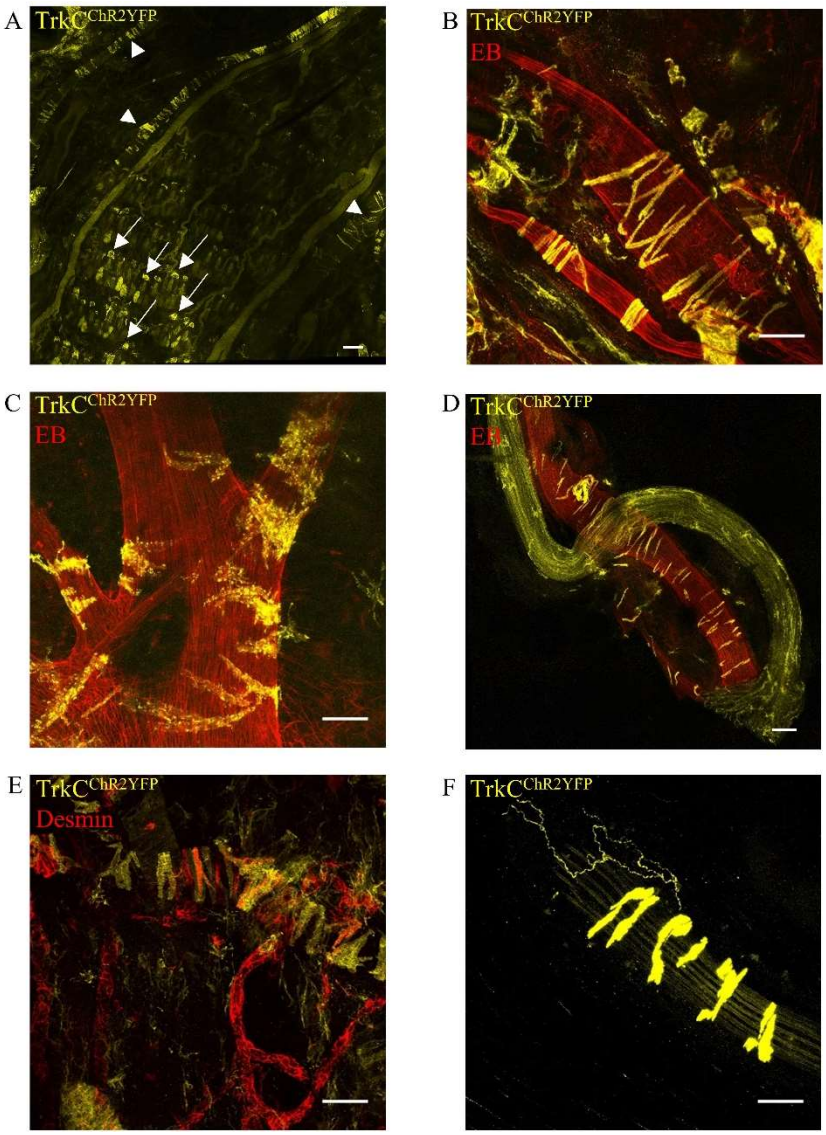

Figure 10. TrkC is expressed in vSMCs and nerves projecting to blood vessels.
All images were acquired using TrkC^{CreERT2}::Rosa26$^{ChR2\text{-}YFP}$ reporter mouse line. **(A)** Whole-mount skin showing TrkC expression in circumferential endings (arrows), and vSMCs (arrowheads). Scale bar 100 mm. **(B-D)** TrkC is expressed in vSMCs throughout the body: skin **(B)**, aorta **(C)**, saphenous artery **(D)**. Mice were injected with EB i.v. to visualize blood vessels. Scale bar 50 mm **(B-C)** or 100 mm **(D)**. **(E)** TrkC marks only vSMCs, but not pericytes. Both vSMCs and pericytes are desmin^{+}. **(F)** TrkC is expressed in some perivascular nerves.

All the results mentioned so far were achieved using TrkC^{CreERT2}::Rosa26$^{ChR2\text{-}YFP}$ mice treated with tamoxifen i.p. Upon systemic administration of tamoxifen, all TrkC^{+} cells throughout the body express the Cre recombinase and thus the YFP reporter.

Since we were more interested in TrkC^{+} neurons than in vSMCs, we decided to administer tamoxifen intrathecally (i.t.) to restrict Cre expression to DRG neurons. As a result of such treatment, only TrkC^{+} neurons express YFP, while vSMCs do not express the reporter anymore. At the level of DRG, TrkC expression remains unaltered (Supplementary fig. 2).

Using TrkC^{CreERT2}::Rosa26$^{ChR2\text{-}YFP}$ mice treated with tamoxifen i.t., we demonstrated that all TrkC^{+} perivascular nerves express also TH. Some TrkC^{-} TH^{+} nerves were also present around blood vessels, indicating a sympathetic innervation (Fig 11).

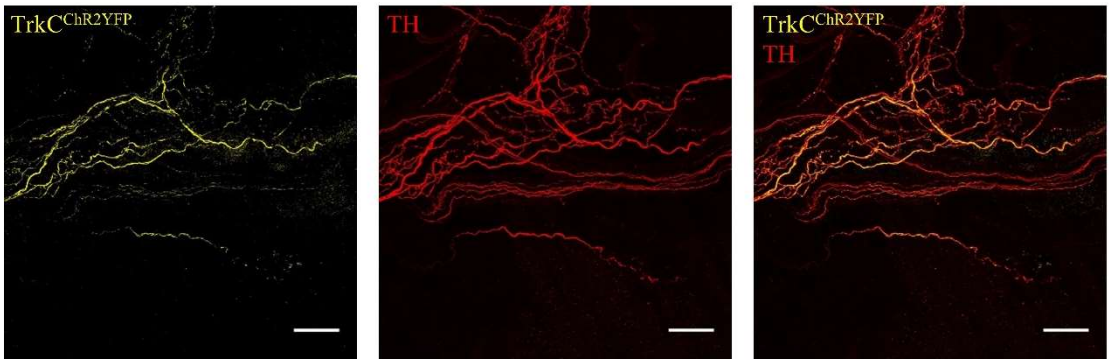

Figure 11. TrkC^{+} perivascular nerves are marked by TH.
Whole-mount skin of TrkC^{CreERT2}::Rosa26$^{ChR2\text{-}YFP}$ mice treated with tamoxifen i.t. All TrkC^{+} fibres express also TH. Some nerves are TrkC^{-} TH^{+} and represent sympathetic innervation.

3.2 Functional characterization of TrkC^{+} neurons

3.2.1 Activation of TrkC^{+} neurons

To understand the role of TrkC^{+} neurons, we first performed some gain of function experiments using TrkC^{CreERT2}::Avil$^{hM3Dq\text{-}mCherry}$ mouse line. In these mice, the Cre-dependent expression of the hM3Dq DREADD is driven from the sensory neuron-specific *Advillin* promoter and so only TrkC^{+} sensory neurons express the modified muscarinic

receptor. Upon administration of specific DREADD ligands, only $TrkC^{+}$ sensory neurons are activated.

For *ex-vivo* live imaging experiments, we also used $TrkC^{CreERT2}$::$Rosa26^{ChR2\text{-}YFP}$ mice, activating TrkC-expressing cells with optogenetic.

3.2.1.1 $TrkC^{+}$ neurons do not act directly on blood vessels

To understand if $TrkC^{+}$ neurons have a direct action on blood vessels, we conducted some *ex-vivo* live imaging experiments. The hind limb skin from $TrkC^{CreERT2}$::$Avil^{hM3Dq\text{-}mCherry}$ mice was dissected and kept under physiological conditions. Adding CNO to the imaging chamber to activate $TrkC^{+}$ neurons, we monitored what happened at the level of blood vessels. No statistically significant changes in vessels diameter were observed. Using norepinephrine (NE) as a positive control, instead, we observed a significant vessel shrinkage (Fig. 12A).

The same experiment was repeated using $TrkC^{CreERT2}$::$Rosa26^{ChR2\text{-}YFP}$ mouse line. Mice treated with tamoxifen i.p. expressed the light-gated ion channel channelrhodopsin (ChR2) in $TrkC^{+}$ neurons and vascular Smooth Muscle Cells (vSMCs). Photostimulation of their skin with blue light (488 nm) resulted in a statistically significant shrinkage of blood vessels (Fig. 12B). $TrkC^{CreERT2}$::$Rosa26^{ChR2\text{-}YFP}$ mice injected with tamoxifen i.t., instead, expressing ChR2 only in $TrkC^{+}$ neurons, upon stimulation with blue light did not display any change in blood vessels diameter (Fig. 12C).

These results suggest that $TrkC^{+}$ neurons do not act directly on blood vessels and that the shrinkage we observed was due to the action of vSMCs.

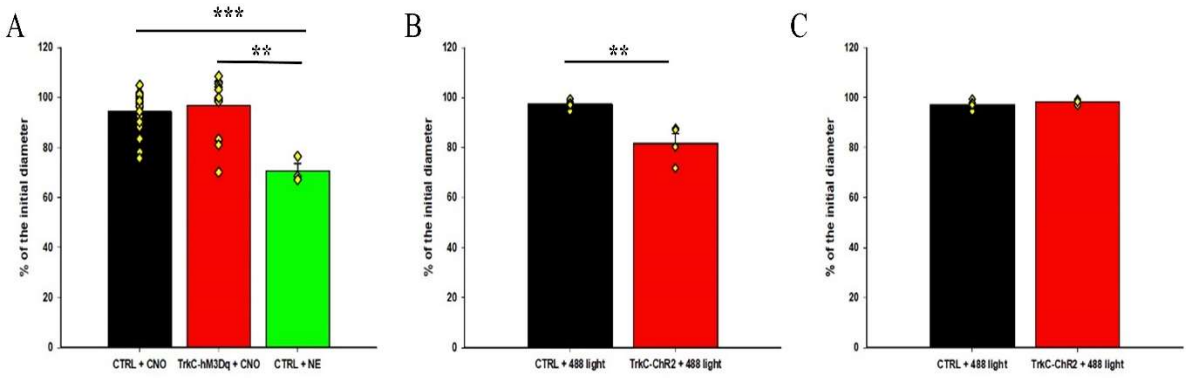

Figure 12. TrkC^{+} neurons do not act directly on blood vessels.
Ex-vivo live imaging of hind limb skin prep. **(A)** Stimulation of TrkC^{+} neurons in TrkC^{CreERT2}::Avil$^{hM3Dq\text{-}mCherry}$ mice (red bar, n=19) do not result in blood vessels diameter changes compared to controls (black bar, n=22) ($p>0.05$). As a positive control, treating the skin prep with NE caused a statistically significant reduction in vessels diameter (green bar, n=3, **$p<0.01$, ***$p<0.001$). **(B-C)** Activation of TrkC^{+} cells with 488 light in TrkC^{CreERT2}::Rosa26$^{ChR2\text{-}YFP}$ mice treated with tamoxifen i.p. **(B)** or i.t. **(C)**. The statistically significant diameter change in panel **B** ($p<0.01$) is due to the contribution of vSMCs. Removing them **(C)** no change is detected anymore ($p>0.05$). For both TrkC^{CreERT2}::Rosa26$^{ChR2\text{-}YFP}$ experiments, n=4.

3.2.1.2 Systemic activation leads to increased blood pressure

TrkC^{CreERT2}::Avil$^{hM3Dq\text{-}mCherry}$ mice were injected systemically with Compound 21 (C21) to specifically activate TrkC^{+} sensory neurons. Mice were monitored for 40 minutes after the injection. Already after 10 minutes, blood pressure increased by around 40 mm Hg compared to the baseline before C21 administration and remained high for the whole time course measurements. Control mice injected with C21 did not show any statistically significant increase or decrease of blood pressure over time (Fig. 13).

When we repeated the experiment injecting, together with C21, 5 mg/kg of propranolol, a nonselective β-adrenoreceptor blocker, we did not observe any statistically significant change in blood pressure values (Fig. 13).

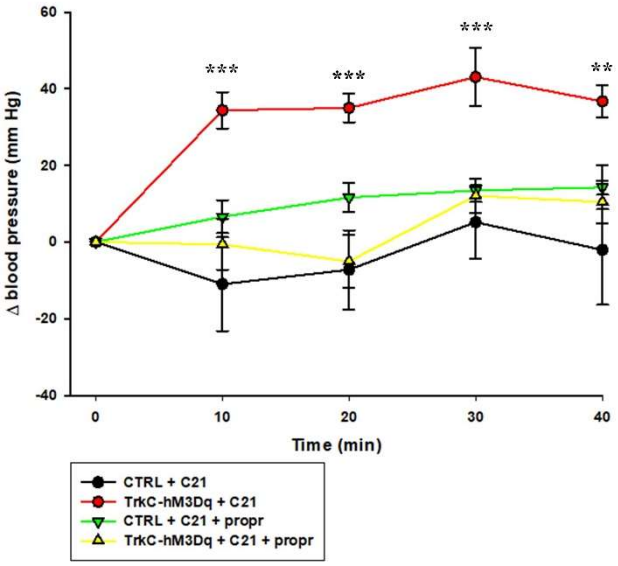

Figure 13. Activation of TrkC^{+} neurons results in increased BP.
Stimulation of TrkC^{+} neurons in TrkC^{CreERT2}::Avil$^{hM3Dq\text{-}mCherry}$ mice causes a BP increase by around 40 mm Hg (red line) compared to control mice (black line) (n=6). This result is reverted by the administration of propranolol (yellow line) (n=6). **p<0.01, ***p<0.001.

3.2.1.3 Systemic activation leads to increased heart rate variability

The heart rate (HR) of TrkC^{CreERT2}::Avil$^{hM3Dq\text{-}mCherry}$ mice, treated with C21 as described before, was also monitored for 1 hour after the DREADD ligand administration. On average, the HR of TrkC^{CreERT2}::Avil$^{hM3Dq\text{-}mCherry}$ mice increased compared to controls, becoming statistically significant between 32 and 46 minutes after the treatment with C21 (Fig. 14A). Additionally, most TrkC^{CreERT2}::Avil$^{hM3Dq\text{-}mCherry}$ mice exhibited an increase or decrease of around 100 beats per minute (BPM) several times during the experimental time course (Fig 14B), while the HR of control mice was stable.

The variability, and so the presence of oscillations in an electrocardiogram (ECG), can be assessed using different parameters, like the standard deviation of the NN intervals (SDNN). Normal-to-normal (NN) intervals are the time gaps between consecutive QRS complexes in a continuous ECG recording and their variability is an index of the overall HR variability. TrkC^{CreERT2}::Avil$^{hM3Dq\text{-}mCherry}$ mice SDNN almost doubled after C21

administration, while it did not change if TrkC^{CreERT2}::Avil$^{hM3Dq\text{-}mCherry}$ mice were treated with both C21 and propranolol (Fig. 14C).

Another indication of heart rate variability can be obtained by plotting the measured beats per minute in a Poincaré plot. The output of this analysis are two standard deviation (SD) parameters that indicate how stable or variable are the beat-to-beat events. As displayed in Fig. 14D, the scattergram of control mice is very different from the one of TrkC^{CreERT2}::Avil$^{hM3Dq\text{-}mCherry}$ mice and the SD2 is statistically higher in the latter ones, indicating that their heart rate is much more variable over time (Fig. 14D).

These results can be reverted by the administration of propranolol. Mice injected i.p. with both C21 and the β-blocker do not display any heart rate variability (Fig. 14 C-D).

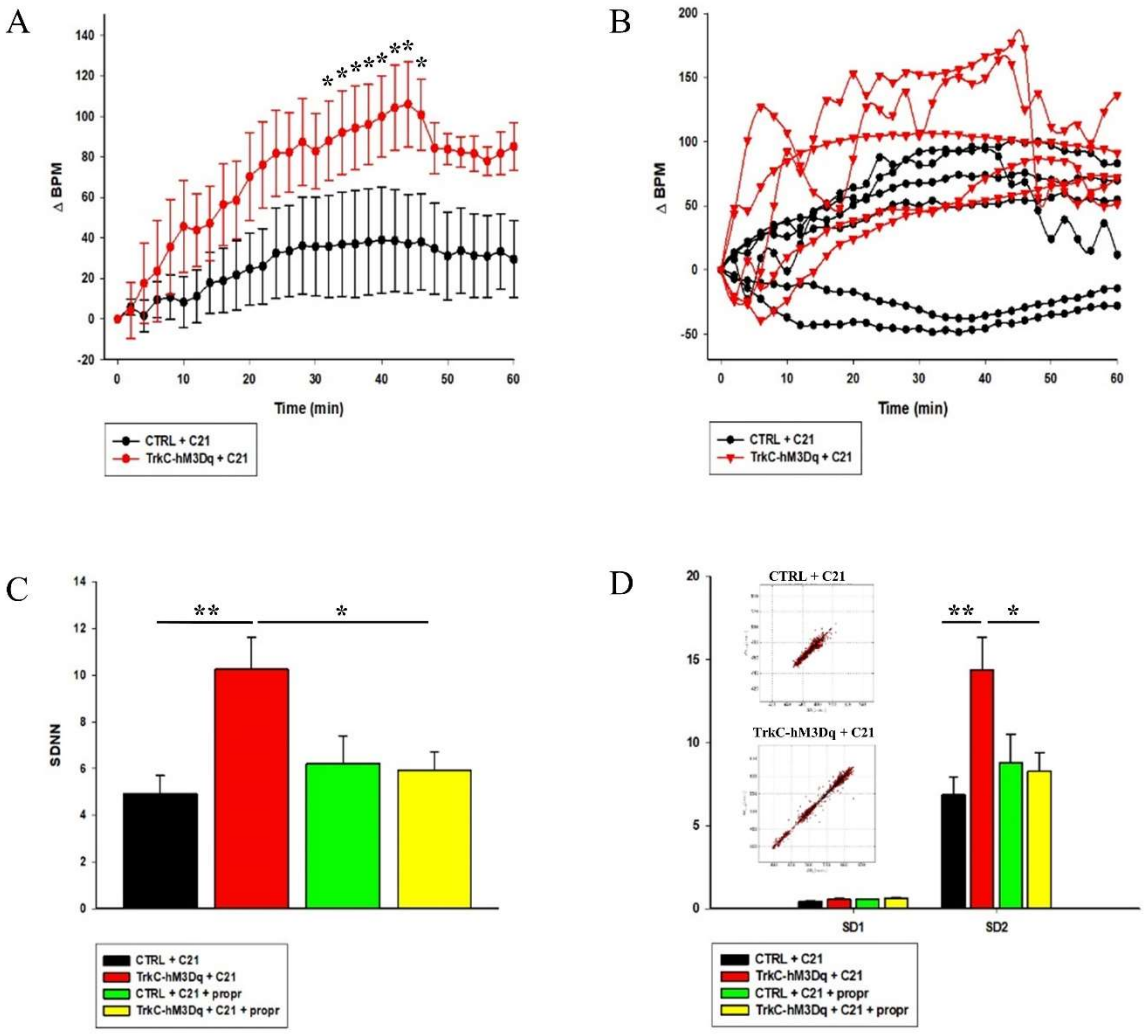

Figure 14. Activation of TrkC^{+} neurons causes heart rate variability.
(A) TrkC^{CreERT2}::Avil$^{hM3Dq\text{-}mCherry}$ mice treated systemically with C21 display an increased average HR (n=6, $p<0.05$) between 32 and 46 minutes after the treatment. **(B)** Most mice show sudden increases and decreases of around 100 BPM (red lines), while control mice are stable (black lines). Each mouse is represented by one line. **(C-D)** HR variability increases in TrkC^{CreERT2}::Avil$^{hM3Dq\text{-}mCherry}$ mice after C21 treatment (red bar) compared to controls (black bar) (n=6, $p<0.01$) and it is reverted by administration of propranolol (green bar) ($p<0.05$), **(C)** Standard deviation of NN intervals. **(D)** SD1 and SD2 derived from Poincaré plot analysis. The upper inset shows a representative Poincaré plot of a control mouse treated with C21. The lower inset displays a representative Poincaré plot of a TrkC^{CreERT2}::Avil$^{hM3Dq\text{-}mCherry}$ mouse treated with C21.

3.2.1.4 Local activation leads to decreased blood flow

Apart from the systemic activation, we also activated TrkC^{+} sensory neurons locally using an injection of clozapine-N-oxide (CNO) in the palm of the hind paw. In this case,

we monitored the local blood flow using Laser Speckle Contrast Imaging (LSCI). This technique allows the visualization of blood vessels with a high spatial and temporal resolution. Starting from 10 minutes after CNO injection, TrkC^{CreERT2}::Avil$^{hM3Dq\text{-}mCherry}$ mice displayed a massive blood flow reduction in the fingers and palm of the hind paw (Fig. 15). Controls treated with CNO, instead, did not show any change in local blood flow.

As in the case of systemic activation, local administration of propranolol impaired blood flow changes. No differences were observed in the 30 minutes following the injection compared to the blood flow baseline at time 0.

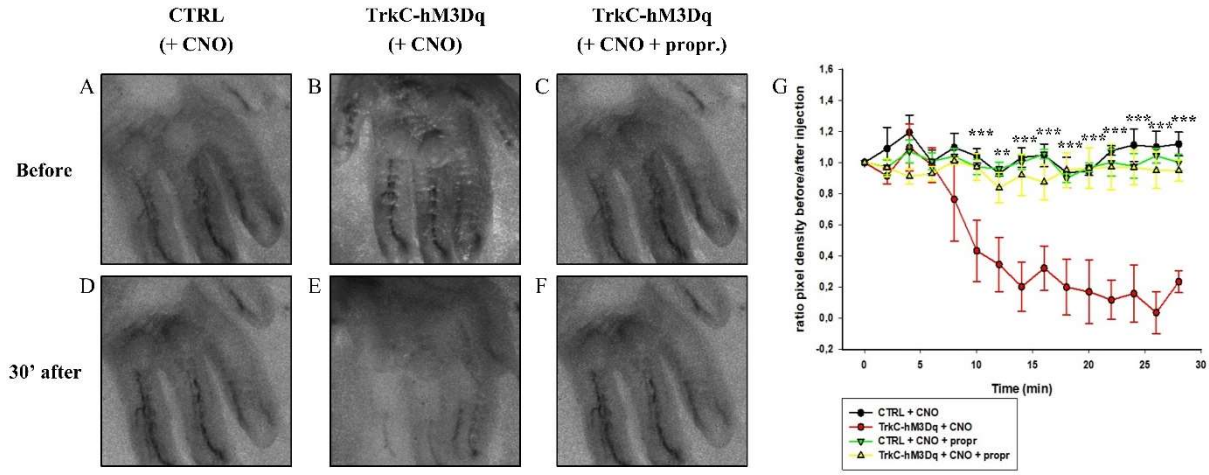

Figure 15. TrkC+ neurons activation causes decreased blood flow.
(A-F) Representative LSCI images depicting blood vessels in the hind paw of TrkC^{CreERT2}::Avil$^{hM3Dq\text{-}mCherry}$ **(B-C; E-F)** and control mice **(A; D)** treated with local CNO **(A-B; D-E)** or CNO + propranolol **(C; F)**. The upper panels **(A-C)** show blood flow before the treatment, the lower panels show blood flow after 30 minutes from local injections. **(G)** Densitometry analysis of LSCI images (n=3, ***p<0.001, **p<0.01).

Taken together, these results suggest that TrkC^{+} neurons are important in the control of blood pressure, heart rate and blood flow and that they act through a circuit with the sympathetic nervous system.

3.2.1.5 Local activation leads to increased sensitivity to mechanical pain

Upon local activation of TrkC^{+} sensory neurons, TrkC^{CreERT2}::Avil$^{hM3Dq\text{-}mCherry}$ mice were subjected to a series of behavioural tests to examine if TrkC^{+} neurons play a role in different sensory modalities. One hour after CNO injection, mice showed normal responses to evaporative cooling of the hind paw evoked by acetone (Fig. 16A) as well as to dynamic mechanical stimulation of the skin achieved by brushing the plantar surface of the paw with a paintbrush (Fig. 16B).

Instead, a striking increase in sensitivity to mechanical pain was observed with the Von Frey test (Fig. 16C). Most TrkC^{CreERT2}::Avil$^{hM3Dq\text{-}mCherry}$ mice perceived as painful the lightest Von Frey filament, corresponding to a force of 0.02 g. None of the controls did.

For this reason, we decided to measure the sensitivity to this calibrated Von Frey filament over time. Already 10 minutes after CNO injection in the paw, TrkC^{CreERT2}::Avil$^{hM3Dq\text{-}mCherry}$ mice became hypersensitive and the hypersensitivity persisted for the whole time course of the experiment (Fig. 16D). None of the controls displayed a statistically significant increase in sensitivity.

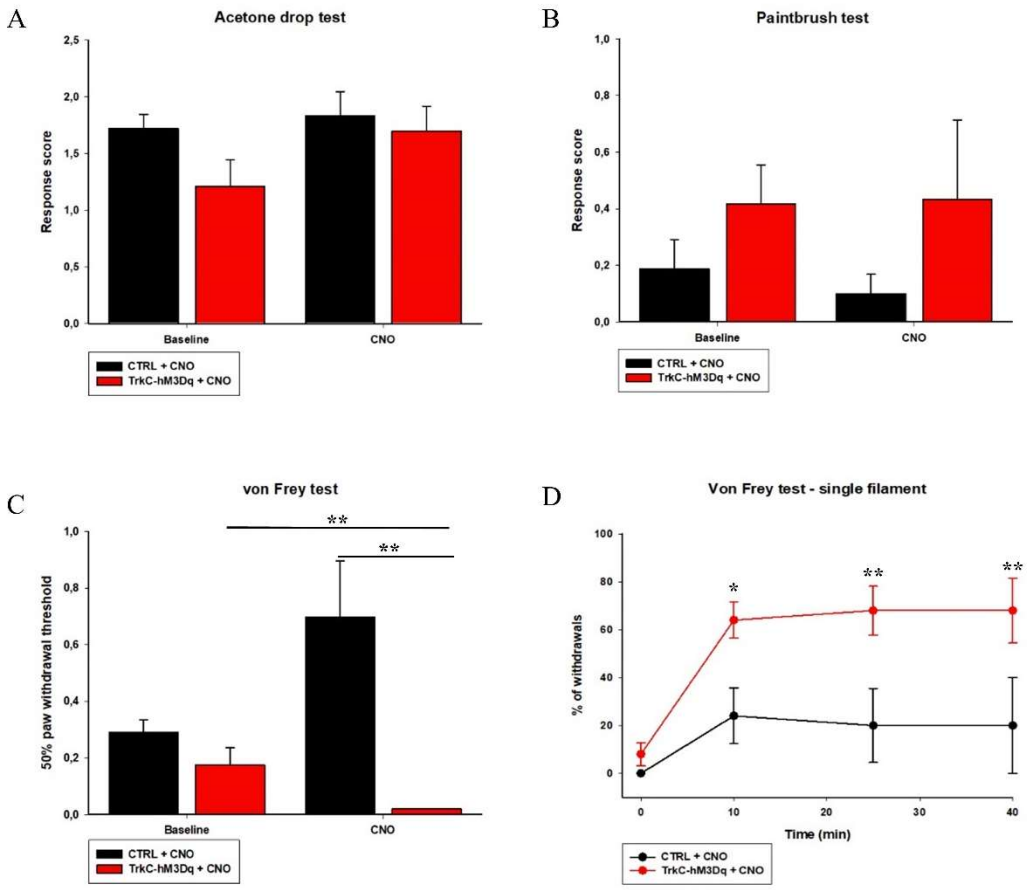

Figure 16. TrkC^{+} neurons activation causes increased sensitivity to mechanical pain. Behavioural tests following local CNO injection showed no differences between TrkC^{CreERT2}::Avil$^{hM3Dq\text{-}mCherry}$ (red bars) and control mice (black bars) in acetone drop test (n=6, p>0.05) **(A)** and paintbrush test (p>0.05) **(B)**. TrkC^{CreERT2}::Avil$^{hM3Dq\text{-}mCherry}$ mice developed hypersensitivity to mechanical pain (p<0.01) **(C)** that started 10 minutes after CNO treatment and persisted for more than 40 minutes (*p<0.05, **p<0.01) **(D)**.

3.2.2 Ablation of TrkC^{+} neurons

Next, to clarify the function of TrkC^{+} neurons, we performed some loss of function experiments, genetically ablating them. We used a Cre-dependent diphtheria toxin receptor (iDTR) knocked-in to the sensory neuron-specific *Advillin* locus to precisely ablate only TrkC^{+} neurons in the peripheral nervous system.

3.2.2.1 TrkC^{+} neurons are fundamental for life

As expected, upon systemic administration of diphtheria toxin (DTX) TrkC^{CreERT2}::Avil^{iDTR} mice displayed severe locomotor deficits (Supplementary fig. 3), due to the fact that with this method all TrkC^{+} peripheral neurons are removed, including proprioceptors. However, surprisingly, all TrkC^{CreERT2}::Avil^{iDTR} mice died within 48 hours from the injection (Fig. 17A). None of the controls was affected by DTX treatment.

Using triple transgenic TrkC^{CreERT2}::Avil^{iDTR}::Rosa26$^{ChR2\text{-}YFP}$ mice, we confirmed the complete ablation of TrkC^{+} neurons at the level of DRG (Fig. 17C). We also noticed a marked reduction of TrkC^{+} TH^{+} fibres innervating blood vessels in ablated mice (Fig. 17E).

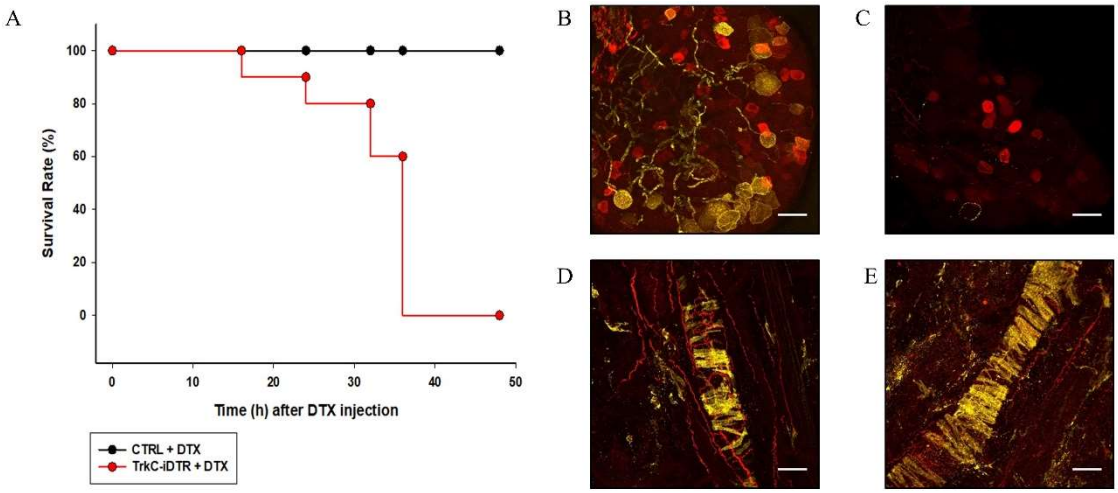

Figure 17. DTX-mediated ablation of TrkC^{+} neurons.
(A) Survival rate of TrkC^{CreERT2}::Avil^{iDTR} (red line) and control mice (black line) upon administration of DTX (n=9). **(B-E)** Immunofluorescence of DRG sections **(B-C)** and whole-mount skin **(D-E)** from TrkC^{CreERT2}::Avil^{iDTR}::Rosa26$^{ChR2\text{-}YFP}$ mice with anti-TH antibodies in untreated mice **(B; D)** and after ablation **(C; E)**. Scale bars 50 μm.

3.2.2.2 Blood pressure decreases upon ablation

Already 16 hours after DTX administration, TrkC^{CreERT2}::Avil^{iDTR} mice displayed a statistically lower blood pressure compared to the baseline values recorded before DTX

injection. This trend was confirmed at 24 hours and 32 hours post-injection (Fig. 18). Control mice treated with DTX showed no changes in blood pressure values over time.

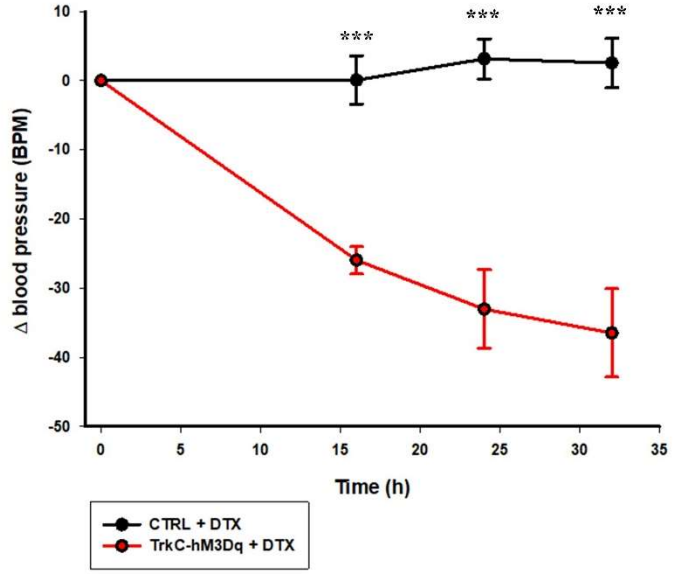

Figure 18. Ablation of TrkC^{+} neurons causes BP decrease.
Upon DTX injection, TrkC^{CreERT2}::Avil^{iDTR} mice display low blood pressure (red line). Control mice are not affected (black line) (n=6, p<0.001).

3.2.2.3 Heart rate variability increases in ablated mice

After DTX treatment, the heart rate of TrkC^{CreERT2}::Avil^{iDTR} mice was monitored for 30 minutes at different time points. While before DTX injection and 16 hours post-injection TrkC^{CreERT2}::Avil^{iDTR} mice showed a stable HR over the 30 monitored minutes, 24 and 32 hours after the injection most TrkC^{CreERT2}::Avil^{iDTR} mice displayed a very variable HR, with sudden increases or decreases of more than 80 BPM (Fig. 19).

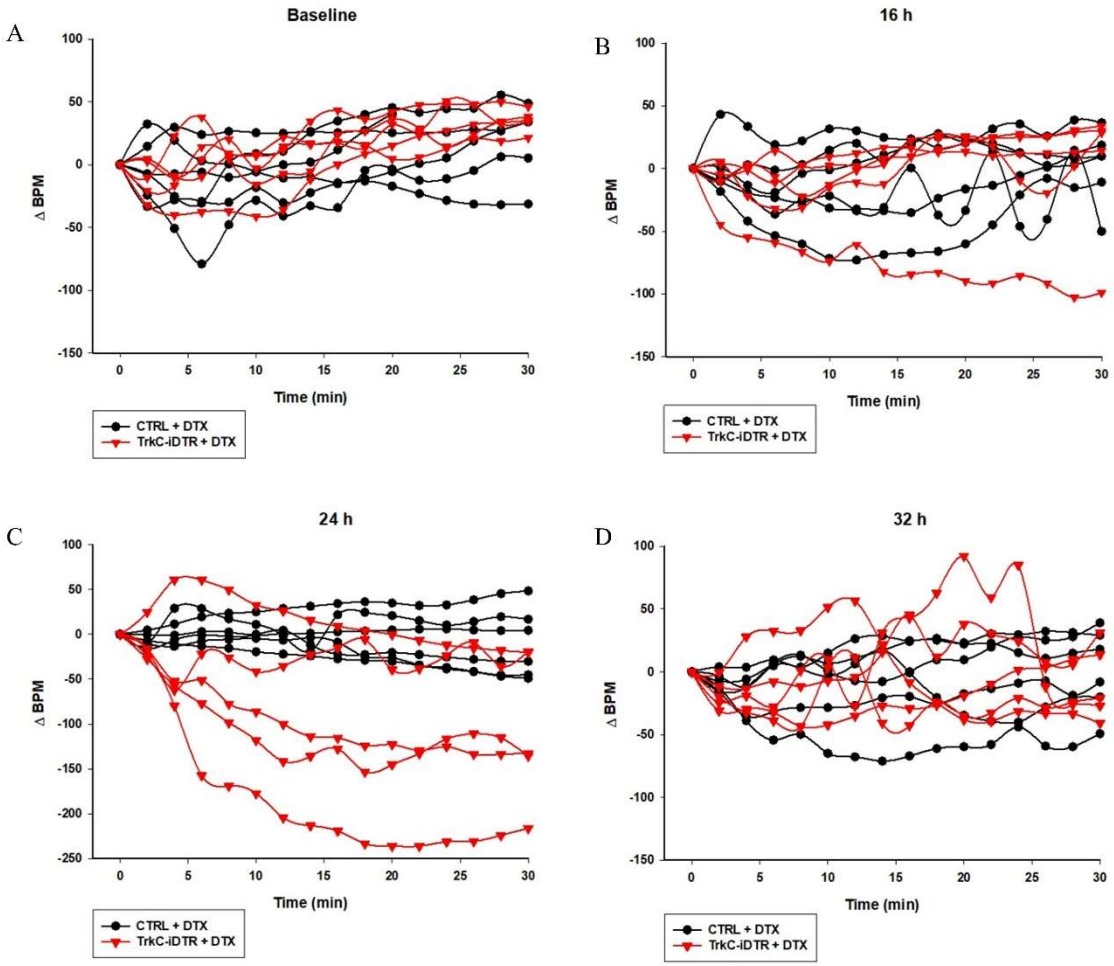

Figure 19. HR oscillations following DTX treatment.
HR fluctuations over 30 minutes before DTX injection **(A)**, 16 hours post-injection **(B)**, 24 hours post-injection **(C)** and 32 hours post-injection **(D)**. Each line represents a single mouse: $TrkC^{CreERT2}$::$Avil^{iDTR}$ mice in red, control mice in black.

As for ablation experiments, HR variability was measured with the standard deviation of NN intervals (SDNN) and the SD extrapolated from Poincaré plots. Twenty-four hours after DTX injection, ablated mice showed a striking increase of the heart rate variability, with a statistically significant increase of SDNN (Fig. 20A). SD2 derived from Poincaré plots showed a statistically significant HR variability at 24 hours post-injection that was maintained also at 32 hours (Fig. 20B). Control mice, instead, had a stable heart rate during the entire monitored period.

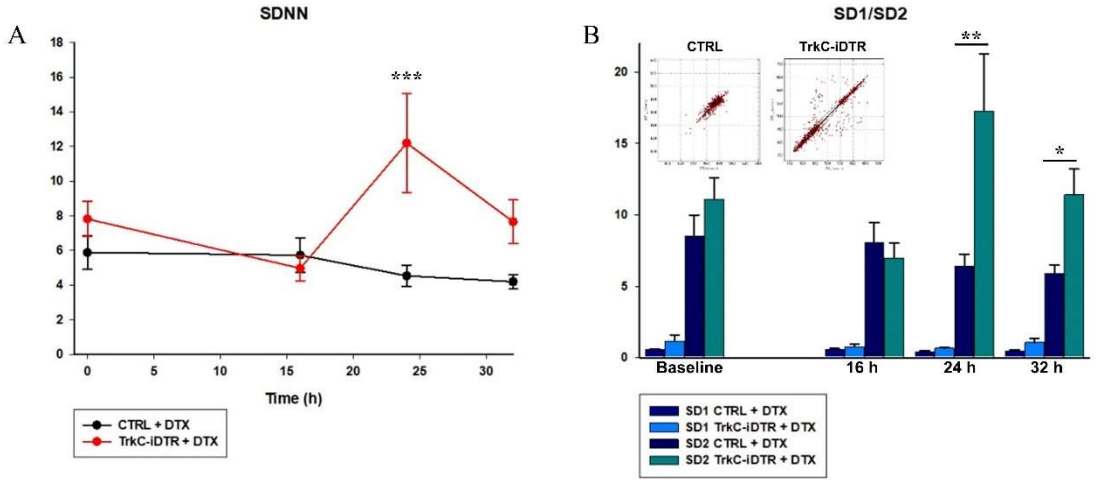

Figure 20. DTX-mediated ablation causes HR variability.
(A) TrkC^{CreERT2}::Avil^{iDTR} mice (red line) display increased HR variability compared to controls (black line) 24 hours after DTX injection (n=6, $p<0.001$). 32 hours post-treatment HR variability is not statistically significant ($p=0.055$). **(B)** SD1 and SD2 derived from Poincaré plot analysis. SD2 values show a statistically significant HR variability at 24 h ($p<0.01$) and 32 hours after DTX treatment ($p<0.05$) in TrkC^{CreERT2}::Avil^{iDTR} mice compared to controls (n=6). The left inset shows a representative Poincaré plot of a control mouse treated with DTX. The right inset displays a representative Poincaré plot of a TrkC^{CreERT2}::Avil^{iDTR} mouse treated with DTX.

3.2.2.4 Alterations of blood flow during ablation

TrkC^{+} neurons ablation influenced also peripheral blood flow. Ear blood vessels were imaged before DTX treatment and 16, 24 and 32 hours after post-injection. At 16 hours, TrkC^{CreERT2}::Avil^{iDTR} mice showed a 20% decrease in blood flow that was reverted 24 hours post-injection. Thirty-two hours after DTX treatment, instead, the blood flow in the ears of ablated mice increased by 20% compared to the baseline condition (Fig. 21).

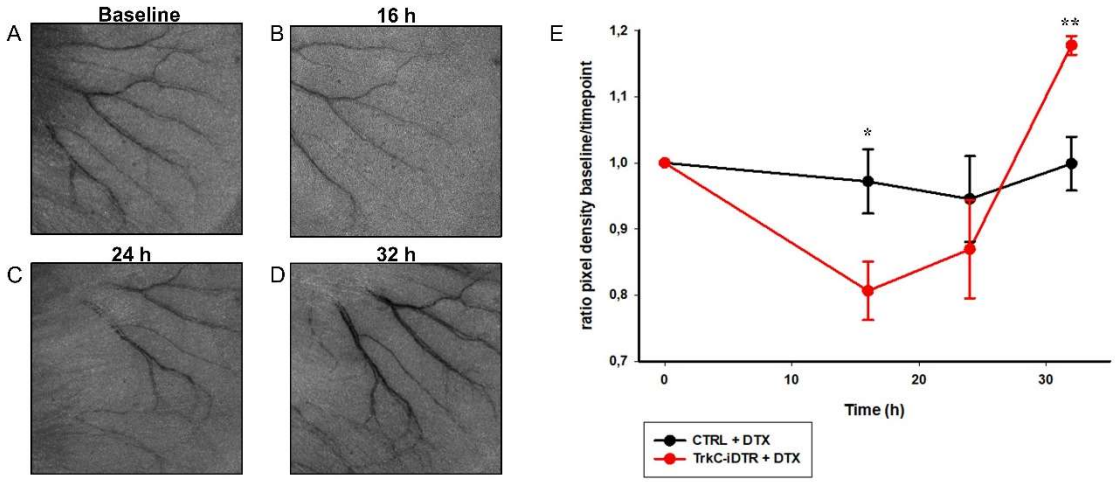

Figure 21. TrkC^{+} neurons ablation causes blood flow alterations.
(A-D) Representative LSCI images of the ear of a TrkC^{CreERT2}::Avil^{iDTR} mouse before DTX treatment **(A)** and 16 h **(B)**, 24 h **(C)** and 32 h post-injection **(D)**. Densitometry analysis of LSCI images (n=6, *p<0.05, **p<0.01).

Taken together, these results prove that the loss of TrkC^{+} neurons has a strong impact on the physiology of the cardiocirculatory system. The ablation of such neurons results in fact in an increase of heart rate variability, a decrease of blood pressure and alterations of peripheral blood flow. The impact on the cardiocirculatory system is lethal, leading to mice death within 48 hours from the treatment with DTX.

4. Discussion

Regulation of blood pressure is essential for whole body homeostasis. Amongst different systems, the innervation of blood vessels plays a crucial role in keeping BP in a physiological range. While the role of the autonomous nervous system is well established, with sympathetic neurons mainly mediating vasoconstriction through the action of NE and parasympathetic neurons causing vasodilation, less is known about sensory neurons. Apart from specialized baroceptors, only sensory peptidergic neurons have been described to innervate blood vessels.

In this study, we identify a new population of sensory neurons marked by TrkC and TH that project to blood vessels. With gain of function and ablation experiments, we demonstrate their importance in regulating BP, blood flow and heart rate and we show that they act through a circuit with the sympathetic nervous system.

4.1 TrkC is expressed in a population of sensory neurons innervating blood vessels

Sensory neurons are essential to detect several kinds of stimuli, both from the external and the internal environment. Their molecular heterogeneity gives rise to different classes of neurons that respond to specific stimuli. During development and adult life, most DRG neurons express one or more tyrosine kinase receptors. While Ret, TrkA and TrkB-expressing neurons are fairly well characterized, less is known about $TrkC^{+}$ neurons. For this reason, the Heppenstall laboratory generated a tamoxifen-inducible mouse line where the expression of Cre is driven by *TrkC* promoter. Crossing $TrkC^{CreERT2}$ mice with a reporter line, we found that in adult mice 30% of all DRG neurons express TrkC. We identified three classes of $TrkC^{+}$ neurons: large proprioceptors neurons co-labelled by PV, a subset of mechanoreceptors that express Ret as well and a new class of medium-sized

neurons identified by the marker TH. While TrkC$^+$ proprioceptors and mechanoceptors have already been described, TrkC$^+$ TH$^+$ neurons have never been identified before. These neurons are medium-sized, unmyelinated and more prevalent in lumbar DRG compared to thoracic or cervical.

We next investigated the presence of TrkC$^+$ TH$^+$ neurons in other peripheral ganglia. While TH is highly expressed in the nodose-petrosal-jugular ganglion complex and in the sympathetic neurons of the superior cervical ganglia, no TrkC expression was detected and this is consistent with previous studies (Funfschilling et al., 2004). This means that TrkC$^+$ TH$^+$ neurons are sensory neurons that are only present in DRG.

Proprioceptive neurons innervate muscle spindles and Golgi tendon organs to send information about the position and orientation of the body in space. Mechanoreceptive afferents innervate different end organs in the skin to detect light touch, vibration and other sensory modalities. To understand the target organs of TrkC$^+$ TH$^+$ sensory neurons we first examined the skin. As expected, we found TrkC$^+$ circumferential endings wrapping around most hair follicles, identifying Aβ-field mechanoreceptors, crucial to detect stroking over a large area.

Surprisingly, we also noticed TrkC$^+$ vascular smooth muscle cells (vSMCs) wrapping around blood vessels. These cells are known to regulate vessels diameter and play a crucial role in the control of blood flow and arterial pressure. Given their important role in physiological and pathological processes, it would be useful to identify them unambiguously. Several markers are known to recognise mural cells, but it is often difficult to mark only vSMCs or only pericytes. TrkC could be used as a univocal marker for vSMCs as it is not expressed in pericytes. The expression of TrkC in vSMCs is consistent

throughout the body, as it has been demonstrated in blood vessels of the skin, in the aorta and also in other peripheral arteries like the saphenous one.

TrkC not only marks vSMCs, but it is also expressed in fibres innervating blood vessels.

While the initial experiments were carried out using $TrkC^{CreERT2}$ mice treated systemically with tamoxifen, to remove vSMCs contribution we injected the active metabolite of tamoxifen intrathecally. Doing so, we obtained a Cre-dependent recombination only in DRG neurons. At the level of the skin, we observed a clear blood vessels innervation by $TrkC^{+}$ neurons, but no more vSMCs. Immunostaining with TH revealed that all $TrkC^{+}$ neurons were TH^{+} as well, while some fibres, presumably sympathetic, were $TrkC^{-}$ TH^{+}.

4.2 $TrkC^{+}$ neurons are involved in the control of blood pressure, heart rate and blood flow

Blood pressure regulation is crucial for survival. If BP values go out of the physiological range, hypotension or hypertension arise and consequently several cardiovascular-related diseases develop. Nowadays around a quarter of the global population is considered hypertense (Kearney et al., 2004) and it has been predicted that if hypertension was controlled in all patients, the incidence of stroke and other ischemic heart diseases would be reduced by more than 30% (He and MacGregor, 2003). Keeping BP in the physiological range is thus fundamental to improve the world health status.

Current treatments for hypertension include inhibitors of the renin-angiotensin-aldosterone system such as angiotensin receptors blockers or ACE inhibitors (Investigators et al., 1991), diuretics (Moser and Feig, 2009), calcium channels blockers (Tamargo and Ruilope, 2016) and α- and β-receptors blockers (Cruickshank, 2017). Currently around

25% of patients require treatment with three or more anti-hypertensive drugs belonging to different classes (Dusing et al., 2017). Despite this combinational treatment, 9-18% of patients develop resistant hypertension, failing to decrease BP with all the proposed anti-hypertensive drugs (Epstein, 2007). The discovery of new regulatory systems could thus help to develop new therapeutic strategies.

To understand the function of $TrkC^+$ neurons we first investigated if they could act directly on blood vessels. Using *ex vivo* live imaging techniques, we demonstrated that activation of $TrkC^+$ neurons has no direct effect on blood vessels diameter and thus we hypothesized a purely sensory role. Up to date, the only sensory neurons known to innervate blood vessels are peptidergic neurons and baroreceptors. With histology analysis we showed that $TrkC^+$ neurons do not belong to these two classes, as they do not express CGRP and they are not present in the NPJ ganglion complex, where baroreceptors cell bodies are known to be found (Kirchheim, 1976). Therefore, $TrkC^+$ neurons seem to be a new class of sensory neurons innervating blood vessels.

Gain of function experiments revealed the importance of $TrkC^+$ neurons in the control of blood pressure, heart rate and blood flow. Activation of $TrkC^+$ sensory neurons with a systemic injection of C21 in $TrkC^{CreERT2}$ mice expressing the DREADD hM3Dq receptor under the sensory-specific promoter *Advillin* (Dhandapani et al., 2018) resulted in a BP increase that persisted for more than 40 minutes. Also the HR was affected by the activation of $TrkC^+$ neurons: the average BPM and the HR variability increased, with oscillations of around 100 BPM.

Local activation of $TrkC^+$ neurons in the paw showed a marked reduction in blood flow starting 10 minutes after CNO administration and lasting around 30 minutes.

Behavioural tests revealed that TrkC^{CreERT2}::Avil$^{hM3Dq\text{-}mCherry}$ mice became hypersensitive to mechanical pain upon local activation of TrkC^{+} sensory neurons in the paw. The hypersensitivity developed already 10 minutes after CNO treatment and persisted for more than 40 minutes. Other sensory modalities, like sensitivity to cold or to dynamic mechanical stimuli, remained unaltered.

Taken together, these findings suggest a role of TrkC^{+} neurons in the control of blood flow, blood pressure and heart rate. Upon activation, TrkC^{+} neurons send signals to the central nervous system that result in blood vessels shrinkage. This in turn leads to diminished blood flow and increased blood pressure because of a higher vascular resistance. Systemically also the heart rate is affected by the stimulation of TrkC^{+} neurons: BPM increase and HR variability becomes evident. Locally, the mechanical pain hypersensitivity may be explained by the reduced blood flow leading to tissue hypoxia. Lack of oxygen starts anaerobic glycolysis, resulting in decreased ATP levels and increased concentration of lactate (Birklein et al., 2000b). Low tissue pH could thus trigger the hypersensitivity with the same mechanism described in complex regional pain syndromes (CRPS) patients where pain has been linked to low tissue pH (Birklein et al., 2000a; Koban et al., 2003). Also in animal studies it has been shown that skin low pH acts on nociceptors exciting them and thus contributing to pain sensitivity (Steen et al., 1995) and in case of TrkC^{CreERT2} mice this could be the result of the hypoxia generated by TrkC^{+} neurons-induced vessels shrinkage.

The importance of TrkC^{+} neurons in the control of blood flow, blood pressure and heart rate has been further demonstrated with ablation experiments. DRG specific ablation of TrkC^{+} neurons using diphtheria toxin receptor driven from the *Advillin* locus (Stantcheva et al., 2016) revealed that these neurons are fundamental for life. TrkC^{CreERT2}::Avil^{iDTR}

mice treated with DTX died within 48 hours. Several studies showed that homozygous mutant mice for TrkC, NT-3 or $TrkC^+$ neurons-specific transcription factor Runx3 exhibit a high mortality rate, probably linked to abnormal cardiac development (Ernfors et al., 1994; Klein et al., 1994; Levanon et al., 2002). With our study, we demonstrated that $TrkC^+$ neurons are crucial not only for development, but also for adult life. In fact, removing $TrkC^+$ neurons in fully developed adult mice caused death. With DTX, we ablate all $TrkC^+$ peripheral neurons: proprioceptors, mechanoceptors and blood vessels-innervating neurons. It is well known that mice lacking crucial components of proprioceptive neurons develop locomotor problems (Woo et al., 2015), but their survival rate is not affected. The same holds true in case of the ablation of some classes of mechanoreceptors: only the sensitivity to different stimuli is impaired, but mice survive (Dhandapani et al., 2018; Shields et al., 2010). Taking into consideration this evidence, we can hypothesize that $TrkC^{CreERT2}$ mice die because they lack the crucial population of $TrkC^+$ TH^+ neurons innervating blood vessels. Histological characterization showed a marked reduction of TH^+ fibres around blood vessels and lack of $TrkC^+$ DRG neurons. Ablated mice displayed decreased blood pressure already after 16 hours from DTX administration and increased heart rate variability starting 24 hours post-injection. Also blood flow was affected by the ablation. While soon after DTX treatment the flow decreased, after 32 hours it became higher than before the ablation. Probably the organism tries to compensate the BP drop with an initial vasoconstriction, but with the ongoing loss of $TrkC^+$ neurons the whole system is altered and by 32 hours the BP decrease cannot be contrasted anymore. We have thus a systemic vasodilation leading to an exacerbation of the overall condition that becomes fatal. Further studies are necessary to elucidate the mechanism leading to the mice death and the interplay between $TrkC^+$ neurons and the different BP regulatory systems.

4.3 TrkC$^+$ neurons act on blood vessels through a circuit with the sympathetic nervous system

Sensory neurons transmit signals from the periphery to the central nervous system. Circuits with the autonomous nervous system are particularly important to regulate whole body homeostasis, affecting blood flow, breathing and heart rate. Sympathetic and parasympathetic perivascular nerves act on endothelial cells or vSMCs regulating vascular tone and contractility. Up to date, only specialized baroreceptors and peptidergic sensory neurons have been described to directly interact with blood vessels. We have demonstrated that a new population of sensory neurons marked by TrkC and TH innervate blood vessels and that they sense the vessels state, without acting directly on vessels, but sending signals to the central nervous system. Gain of function and loss of function experiments showed that these neurons affect the whole cardio-circulatory system. Given the fact that activation led to increased BP and reduced blood flow and that ablation resulted in low BP and vasodilation, we hypothesized that TrkC$^+$ TH$^+$ neurons act through a circuit with the sympathetic nervous system. Sympathetic perivascular nerves release NE, ATP and NPY that mostly cause vasoconstriction acting on endothelial cells and vSMCs. To investigate if TrkC$^+$ neurons play their role interacting with the sympathetic nervous system, we repeated gain of function experiments in presence of propranolol, a nonselective β-blocker that counteracts the sympathetic-mediated effects. Administering propranolol together with the DREADD ligand, TrkC^{CreERT2}::Avil$^{hM3Dq\text{-}mCherry}$ mice did not develop high blood pressure and did not display any heart rate variability. Similarly, propranolol impaired changes at the level of blood flow. These results demonstrate that TrkC$^+$ neurons exert their actions through the sympathetic nervous system. Although further experiments are needed to investigate the molecular mechanisms of this interaction, this is a first important step to

unravel the interplay of these systems. It is not the first time that TrkC is linked to catecholaminergic neurons. At the level of the central nervous system, overexpression of TrkC gives rise to an increased number of TH^+ neurons (Dierssen et al., 2006). The NT-3/TrkC axis is important for the development of catecholaminergic nuclei, but little is known about other central functions. Lack of NT-3 in the central nervous system causes attenuation of functional and behavioral aspects regulated by noradrenergic neurons (Akbarian et al., 2001), but these interplay has never been demonstrated in the peripheral nervous system.

Taken together our findings demonstrate the existence of a new population of sensory neurons innervating blood vessels that are marked by TrkC and TH. These neurons are small, unmyelinated and nonpeptidergic. Gain and loss of function experiments have proven their importance in the control of blood pressure, blood flow and heart rate. $TrkC^+$ TH^+ neurons do not act directly on blood vessels, but they exert their functions through a circuit with the sympathetic nervous system. The activation of these neurons has also been linked to the development of hypersensitivity to mechanical pain. Although the molecular mechanisms need to be further investigated, we hypothesize that tissue hypoxia resulting from decreased blood flow could play an important role, together with sympathetic nervous system stimulation, that is known to be linked to pain and hyperalgesia in some cases (Drummond et al., 2001). $TrkC^+$ neurons have also proven to be fundamental for life. Ablated mice died within 48 hours for cardio-circulatory problems due to low blood pressure and high heart rate variability. Given that $TrkC^+$ TH^+ neurons express Piezo2, we could hypothesize that their function is to sense the vessels state thanks to these mechanically activated channels and then to act through a circuit with the sympathetic nervous system to help keeping whole body homeostasis. Further studies are necessary to

unravel the molecular mechanisms through which $TrkC^+$ TH^+ neurons act, but our findings are a first step in the discovery of a new system to regulate blood pressure. Given the prevalence of hypertension in the world population, we hope that these results one day could help to develop new therapeutic strategies.

5. Conclusion

In this study we identified a new population of sensory neurons projecting to blood vessels that are important in the control of blood pressure, blood flow and heart rate.

In conclusion:

1. TrkC is expressed in 30% of all DRG neurons. $TrkC^+$ neurons can be divided into 3 different populations: proprioceptors, mechanoreceptors and $TrkC^+$ TH^+ neurons that were never described before.
2. The new class of $TrkC^+$ TH^+ neurons innervate blood vessels.
3. *Ex-vivo* live imaging experiments show that $TrkC^+$ neurons do not act directly on blood vessels.
4. Activation of $TrkC^+$ neurons leads to high blood pressure, increased heart rate variability and decreased blood flow. Mice develop also an increased sensitivity to mechanical pain.
5. Ablation of $TrkC^+$ neurons causes reduced blood pressure, increased heart rate variability and oscillations in blood flow. Strikingly, all ablated mice die within 48 hours.
6. $TrkC^+$ neurons exert their functions on blood vessels through a circuit with the sympathetic nervous system.

Further experiments need to be carried out to understand the molecular mechanisms of $TrkC^+$ TH^+ neurons function. Nevertheless, I hope that with this study we made a first step in the characterization of a new blood pressure regulatory system. Hopefully our

findings one day could be translated in the development of new therapeutic strategies to control hypertension, a pathology that affects more than a quarter of the global population.

6. References

(1996). Heart rate variability. Standards of measurement, physiological interpretation, and clinical use. Task Force of the European Society of Cardiology and the North American Society of Pacing and Electrophysiology. Eur Heart J *17*, 354-381.
Akbarian, S., Bates, B., Liu, R.J., Skirboll, S.L., Pejchal, T., Coppola, V., Sun, L.D., Fan, G., Kucera, J., Wilson, M.A.*, et al.* (2001). Neurotrophin-3 modulates noradrenergic neuron function and opiate withdrawal. Mol Psychiatry *6*, 593-604.
Alam, M., and Smirk, F.H. (1937). Observations in man upon a blood pressure raising reflex arising from the voluntary muscles. The Journal of physiology *89*, 372-383.
Allahverdian, S., Pannu, P.S., and Francis, G.A. (2012). Contribution of monocyte-derived macrophages and smooth muscle cells to arterial foam cell formation. Cardiovascular research *95*, 165-172.
Armulik, A., Genove, G., and Betsholtz, C. (2011). Pericytes: developmental, physiological, and pathological perspectives, problems, and promises. Developmental cell *21*, 193-215.
Bai, L., Lehnert, B.P., Liu, J., Neubarth, N.L., Dickendesher, T.L., Nwe, P.H., Cassidy, C., Woodbury, C.J., and Ginty, D.D. (2015). Genetic Identification of an Expansive Mechanoreceptor Sensitive to Skin Stroking. Cell *163*, 1783-1795.
Bakker, E.N., Buus, C.L., Spaan, J.A., Perree, J., Ganga, A., Rolf, T.M., Sorop, O., Bramsen, L.H., Mulvany, M.J., and Vanbavel, E. (2005). Small artery remodeling depends on tissue-type transglutaminase. Circ Res *96*, 119-126.
Bauters, C., and Isner, J.M. (1997). The biology of restenosis. Prog Cardiovasc Dis *40*, 107-116.
Bayliss, W.M. (1902). On the local reactions of the arterial wall to changes of internal pressure. The Journal of physiology *28*, 220-231.
Birklein, F., Weber, M., Ernst, M., Riedl, B., Neundorfer, B., and Handwerker, H.O. (2000a). Experimental tissue acidosis leads to increased pain in complex regional pain syndrome (CRPS). Pain *87*, 227-234.
Birklein, F., Weber, M., and Neundorfer, B. (2000b). Increased skin lactate in complex regional pain syndrome: evidence for tissue hypoxia? Neurology *55*, 1213-1215.
Bobrovskaya, L., Dunkley, P.R., and Dickson, P.W. (2004). Phosphorylation of Ser19 increases both Ser40 phosphorylation and enzyme activity of tyrosine hydroxylase in intact cells. J Neurochem *90*, 857-864.
Bolton, T.B., and Clapp, L.H. (1986). Endothelial-dependent relaxant actions of carbachol and substance P in arterial smooth muscle. Br J Pharmacol *87*, 713-723.
Bolton, T.B., and Lim, S.P. (1991). Action of acetylcholine on smooth muscle. Z Kardiol *80 Suppl 7*, 73-77.
Brain, S.D. (1997). Sensory neuropeptides: their role in inflammation and wound healing. Immunopharmacology *37*, 133-152.
Briers, J.D., and Webster, S. (1996). Laser speckle contrast analysis (LASCA): a nonscanning, full-field technique for monitoring capillary blood flow. J Biomed Opt *1*, 174-179.
Burnstock, G., and Kennedy, C. (1986). A dual function for adenosine 5'-triphosphate in the regulation of vascular tone. Excitatory cotransmitter with noradrenaline from perivascular nerves and locally released inhibitory intravascular agent. Circ Res *58*, 319-330.
Cahalan, S.M., Lukacs, V., Ranade, S.S., Chien, S., Bandell, M., and Patapoutian, A. (2015). Piezo1 links mechanical forces to red blood cell volume. eLife *4*.
Cao, X., Peterson, J.R., Wang, G., Anrather, J., Young, C.N., Guruju, M.R., Burmeister, M.A., Iadecola, C., and Davisson, R.L. (2012). Angiotensin II-dependent hypertension requires cyclooxygenase 1-derived prostaglandin E2 and EP1 receptor signaling in the subfornical organ of the brain. Hypertension *59*, 869-876.
Caspary, T., and Anderson, K.V. (2003). Patterning cell types in the dorsal spinal cord: what the mouse mutants say. Nature reviews. Neuroscience *4*, 289-297.

Chaplan, S.R., Bach, F.W., Pogrel, J.W., Chung, J.M., and Yaksh, T.L. (1994). Quantitative assessment of tactile allodynia in the rat paw. Journal of neuroscience methods *53*, 55-63.
Colucci, W.S., and Alexander, R.W. (1986). Norepinephrine-induced alteration in the coupling of alpha 1-adrenergic receptor occupancy to calcium efflux in rabbit aortic smooth muscle cells. Proceedings of the National Academy of Sciences of the United States of America *83*, 1743-1746.
Colucci, W.S., Brock, T.A., Gimbrone, M.A., Jr., and Alexander, R.W. (1984). Regulation of alpha 1-adrenergic receptor-coupled calcium flux in cultured vascular smooth muscle cells. Hypertension *6*, I19-24.
Coote, J.H., Hilton, S.M., and Perez-Gonzalez, J.F. (1971). The reflex nature of the pressor response to muscular exercise. The Journal of physiology *215*, 789-804.
Coste, B., Houge, G., Murray, M.F., Stitziel, N., Bandell, M., Giovanni, M.A., Philippakis, A., Hoischen, A., Riemer, G., Steen, U.*, et al.* (2013). Gain-of-function mutations in the mechanically activated ion channel PIEZO2 cause a subtype of Distal Arthrogryposis. Proceedings of the National Academy of Sciences of the United States of America *110*, 4667-4672.
Cousins, D.A., Butts, K., and Young, A.H. (2009). The role of dopamine in bipolar disorder. Bipolar Disord *11*, 787-806.
Crisan, D., and Carr, J. (2000). Angiotensin I-converting enzyme: genotype and disease associations. J Mol Diagn *2*, 105-115.
Critchley, H.D., and Harrison, N.A. (2013). Visceral influences on brain and behavior. Neuron *77*, 624-638.
Cruickshank, J.M. (2017). The Role of Beta-Blockers in the Treatment of Hypertension. Advances in experimental medicine and biology *956*, 149-166.
Davis, M.J. (1993). Myogenic response gradient in an arteriolar network. Am J Physiol *264*, H2168-2179.
Dhandapani, R., Arokiaraj, C.M., Taberner, F.J., Pacifico, P., Raja, S., Nocchi, L., Portulano, C., Franciosa, F., Maffei, M., Hussain, A.F.*, et al.* (2018). Control of mechanical pain hypersensitivity in mice through ligand-targeted photoablation of TrkB-positive sensory neurons. Nature communications *9*, 1640.
Dierssen, M., Gratacos, M., Sahun, I., Martin, M., Gallego, X., Amador-Arjona, A., Martinez de Lagran, M., Murtra, P., Marti, E., Pujana, M.A.*, et al.* (2006). Transgenic mice overexpressing the full-length neurotrophin receptor TrkC exhibit increased catecholaminergic neuron density in specific brain areas and increased anxiety-like behavior and panic reaction. Neurobiology of disease *24*, 403-418.
Donovan, M.J., Hahn, R., Tessarollo, L., and Hempstead, B.L. (1996). Identification of an essential nonneuronal function of neurotrophin 3 in mammalian cardiac development. Nature genetics *14*, 210-213.
Doskeland, A.P., and Flatmark, T. (2002). Ubiquitination of soluble and membrane-bound tyrosine hydroxylase and degradation of the soluble form. Eur J Biochem *269*, 1561-1569.
Draid, M., Shiina, T., El-Mahmoudy, A., Boudaka, A., Shimizu, Y., and Takewaki, T. (2005). Neurally released ATP mediates endothelium-dependent hyperpolarization in the circular smooth muscle cells of chicken anterior mesenteric artery. Br J Pharmacol *146*, 983-989.
Drenjancevic-Peric, I., Jelakovic, B., Lombard, J.H., Kunert, M.P., Kibel, A., and Gros, M. (2011). High-salt diet and hypertension: focus on the renin-angiotensin system. Kidney Blood Press Res *34*, 1-11.
Drummond, H.A., Price, M.P., Welsh, M.J., and Abboud, F.M. (1998). A molecular component of the arterial baroreceptor mechanotransducer. Neuron *21*, 1435-1441.
Drummond, P.D., Finch, P.M., Skipworth, S., and Blockey, P. (2001). Pain increases during sympathetic arousal in patients with complex regional pain syndrome. Neurology *57*, 1296-1303.
Duan, B., Cheng, L., Bourane, S., Britz, O., Padilla, C., Garcia-Campmany, L., Krashes, M., Knowlton, W., Velasquez, T., Ren, X.*, et al.* (2014). Identification of spinal circuits transmitting and gating mechanical pain. Cell *159*, 1417-1432.

Dunkley, P.R., Bobrovskaya, L., Graham, M.E., von Nagy-Felsobuki, E.I., and Dickson, P.W. (2004). Tyrosine hydroxylase phosphorylation: regulation and consequences. J Neurochem *91*, 1025-1043.
Duschek, S., Hadjamu, M., and Schandry, R. (2007). Dissociation between cortical activation and cognitive performance under pharmacological blood pressure elevation in chronic hypotension. Biol Psychol *75*, 277-285.
Duschek, S., Heiss, H., Werner, N., and Reyes del Paso, G.A. (2009). Modulations of autonomic cardiovascular control following acute alpha-adrenergic treatment in chronic hypotension. Hypertension research : official journal of the Japanese Society of Hypertension *32*, 938-943.
Dusing, R., Waeber, B., Destro, M., Santos Maia, C., and Brunel, P. (2017). Triple-combination therapy in the treatment of hypertension: a review of the evidence. J Hum Hypertens *31*, 501-510.
Edvinsson, L. (1985). Characterization of the contractile effect of neuropeptide Y in feline cerebral arteries. Acta Physiol Scand *125*, 33-41.
Eisenhoffer, G.T., Loftus, P.D., Yoshigi, M., Otsuna, H., Chien, C.B., Morcos, P.A., and Rosenblatt, J. (2012). Crowding induces live cell extrusion to maintain homeostatic cell numbers in epithelia. Nature *484*, 546-549.
Ekblad, E., Edvinsson, L., Wahlestedt, C., Uddman, R., Hakanson, R., and Sundler, F. (1984). Neuropeptide Y co-exists and co-operates with noradrenaline in perivascular nerve fibers. Regul Pept *8*, 225-235.
Epstein, M. (2007). Resistant hypertension: prevalence and evolving concepts. J Clin Hypertens (Greenwich) *9*, 2-6.
Ernfors, P., Lee, K.F., Kucera, J., and Jaenisch, R. (1994). Lack of neurotrophin-3 leads to deficiencies in the peripheral nervous system and loss of limb proprioceptive afferents. Cell *77*, 503-512.
Ernsberger, U. (2009). Role of neurotrophin signalling in the differentiation of neurons from dorsal root ganglia and sympathetic ganglia. Cell Tissue Res *336*, 349-384.
Feener, E.P., Northrup, J.M., Aiello, L.P., and King, G.L. (1995). Angiotensin II induces plasminogen activator inhibitor-1 and -2 expression in vascular endothelial and smooth muscle cells. J Clin Invest *95*, 1353-1362.
Florez-Paz, D., Bali, K.K., Kuner, R., and Gomis, A. (2016). A critical role for Piezo2 channels in the mechanotransduction of mouse proprioceptive neurons. Scientific reports *6*, 25923.
Funfschilling, U., Ng, Y.G., Zang, K., Miyazaki, J., Reichardt, L.F., and Rice, F.L. (2004). TrkC kinase expression in distinct subsets of cutaneous trigeminal innervation and nonneuronal cells. The Journal of comparative neurology *480*, 392-414.
Furchgott, R.F. (1959). The receptors for epinephrine and norepinephrine (adrenergic receptors). Pharmacological reviews *11*, 429-441; discussion 441-422.
Garcia-Anoveros, J., Samad, T.A., Zuvela-Jelaska, L., Woolf, C.J., and Corey, D.P. (2001). Transport and localization of the DEG/ENaC ion channel BNaC1alpha to peripheral mechanosensory terminals of dorsal root ganglia neurons. The Journal of neuroscience : the official journal of the Society for Neuroscience *21*, 2678-2686.
Garland, C.J., Bagher, P., Powell, C., Ye, X., Lemmey, H.A.L., Borysova, L., and Dora, K.A. (2017). Voltage-dependent Ca2+ entry into smooth muscle during contraction promotes endothelium-mediated feedback vasodilation in arterioles. Science signaling *10*.
Ge, J., Li, W., Zhao, Q., Li, N., Chen, M., Zhi, P., Li, R., Gao, N., Xiao, B., and Yang, M. (2015). Architecture of the mammalian mechanosensitive Piezo1 channel. Nature *527*, 64-69.
Genc, B., Ozdinler, P.H., Mendoza, A.E., and Erzurumlu, R.S. (2004). A chemoattractant role for NT-3 in proprioceptive axon guidance. PLoS Biol *2*, e403.
Glazebrook, P.A., Schilling, W.P., and Kunze, D.L. (2005). TRPC channels as signal transducers. Pflugers Archiv : European journal of physiology *451*, 125-130.
Glebova, N.O., and Ginty, D.D. (2005). Growth and survival signals controlling sympathetic nervous system development. Annu Rev Neurosci *28*, 191-222.
Gnanasambandam, R., Bae, C., Gottlieb, P.A., and Sachs, F. (2015). Ionic Selectivity and Permeation Properties of Human PIEZO1 Channels. PLoS One *10*, e0125503.

Gordon, S.L., Quinsey, N.S., Dunkley, P.R., and Dickson, P.W. (2008). Tyrosine hydroxylase activity is regulated by two distinct dopamine-binding sites. J Neurochem *106*, 1614-1623.
Gordon, S.L., Webb, J.K., Shehadeh, J., Dunkley, P.R., and Dickson, P.W. (2009). The low affinity dopamine binding site on tyrosine hydroxylase: the role of the N-terminus and in situ regulation of enzyme activity. Neurochem Res *34*, 1830-1837.
Grasby, D.J., Morris, J.L., and Segal, S.S. (1999). Heterogeneity of vascular innervation in hamster cheek pouch and retractor muscle. Journal of vascular research *36*, 465-476.
Grobecker H, J.S., R McCarty VK Weise, IJ Kopin (1978). Role of noradrenergic nerves and adrenal medulla during the development of genetic and experimental hypertension in rats. In Catecholamines: Basic and clinical frontiers (New York: Pergamon Press), pp. 906-908.
Guan, H., Zhu, L., Fu, M., Yang, D., Tian, S., Guo, Y., Cui, C., Wang, L., and Jiang, H. (2012). 3,3'Diindolylmethane suppresses vascular smooth muscle cell phenotypic modulation and inhibits neointima formation after carotid injury. PLoS One *7*, e34957.
Gudipaty, S.A., Lindblom, J., Loftus, P.D., Redd, M.J., Edes, K., Davey, C.F., Krishnegowda, V., and Rosenblatt, J. (2017). Mechanical stretch triggers rapid epithelial cell division through Piezo1. Nature *543*, 118-121.
Hagner, S., Haberberger, R., Kummer, W., Springer, J., Fischer, A., Bohm, S., Goke, B., and McGregor, G.P. (2001). Immunohistochemical detection of calcitonin gene-related peptide receptor (CGRPR)-1 in the endothelium of human coronary artery and bronchial blood vessels. Neuropeptides *35*, 58-64.
Hakanson, R., Wahlestedt, C., Ekblad, E., Edvinsson, L., and Sundler, F. (1986). Neuropeptide Y: coexistence with noradrenaline. Functional implications. Prog Brain Res *68*, 279-287.
Han, J.H., Kim, Y., Jung, S.H., Lee, J.J., Park, H.S., Song, G.Y., Cuong, N.M., Kim, Y.H., and Myung, C.S. (2015). Murrayafoline A Induces a G0/G1-Phase Arrest in Platelet-Derived Growth Factor-Stimulated Vascular Smooth Muscle Cells. Korean J Physiol Pharmacol *19*, 421-426.
Hanna, R.L., and Kaufman, M.P. (2003). Role played by purinergic receptors on muscle afferents in evoking the exercise pressor reflex. J Appl Physiol (1985) *94*, 1437-1445.
Hasegawa, H., and Wang, F. (2008). Visualizing mechanosensory endings of TrkC-expressing neurons in HS3ST-2-hPLAP mice. The Journal of comparative neurology *511*, 543-556.
Hayward, I.P., Bridle, K.R., Campbell, G.R., Underwood, P.A., and Campbell, J.H. (1995). Effect of extracellular matrix proteins on vascular smooth muscle cell phenotype. Cell Biol Int *19*, 839-846.
He, F.J., and MacGregor, G.A. (2003). Cost of poor blood pressure control in the UK: 62,000 unnecessary deaths per year. J Hum Hypertens *17*, 455-457.
Hill, J.M., Adreani, C.M., and Kaufman, M.P. (1996). Muscle reflex stimulates sympathetic postganglionic efferents innervating triceps surae muscles of cats. Am J Physiol *271*, H38-43.
Hill, M.A., Sun, Z., Martinez-Lemus, L., and Meininger, G.A. (2007). New technologies for dissecting the arteriolar myogenic response. Trends in pharmacological sciences *28*, 308-315.
Hill, R.A., Tong, L., Yuan, P., Murikinati, S., Gupta, S., and Grutzendler, J. (2015). Regional Blood Flow in the Normal and Ischemic Brain Is Controlled by Arteriolar Smooth Muscle Cell Contractility and Not by Capillary Pericytes. Neuron *87*, 95-110.
Huang, E.J., Wilkinson, G.A., Farinas, I., Backus, C., Zang, K., Wong, S.L., and Reichardt, L.F. (1999). Expression of Trk receptors in the developing mouse trigeminal ganglion: in vivo evidence for NT-3 activation of TrkA and TrkB in addition to TrkC. Development *126*, 2191-2203.
Inoue, K., Ozaki, S., Shiga, T., Ito, K., Masuda, T., Okado, N., Iseda, T., Kawaguchi, S., Ogawa, M., Bae, S.C.*, et al.* (2002). Runx3 controls the axonal projection of proprioceptive dorsal root ganglion neurons. Nature neuroscience *5*, 946-954.
Insel, P.A. (1996). Seminars in medicine of the Beth Israel Hospital, Boston. Adrenergic receptors--evolving concepts and clinical implications. N Engl J Med *334*, 580-585.
Investigators, S., Yusuf, S., Pitt, B., Davis, C.E., Hood, W.B., and Cohn, J.N. (1991). Effect of enalapril on survival in patients with reduced left ventricular ejection fractions and congestive heart failure. N Engl J Med *325*, 293-302.
Iwamoto, G.A., and Botterman, B.R. (1985). Peripheral factors influencing expression of pressor reflex evoked by muscular contraction. J Appl Physiol (1985) *58*, 1676-1682.

Jiang, X., Rowitch, D.H., Soriano, P., McMahon, A.P., and Sucov, H.M. (2000). Fate of the mammalian cardiac neural crest. Development *127*, 1607-1616.
Joyner, M.J., and Casey, D.P. (2015). Regulation of increased blood flow (hyperemia) to muscles during exercise: a hierarchy of competing physiological needs. Physiol Rev *95*, 549-601.
Kaufman, M.P. (2012). The exercise pressor reflex in animals. Exp Physiol *97*, 51-58.
Kaufman, M.P., Iwamoto, G.A., Ashton, J.H., and Cassidy, S.S. (1982). Responses to inflation of vagal afferents with endings in the lung of dogs. Circ Res *51*, 525-531.
Kaufman, M.P., Longhurst, J.C., Rybicki, K.J., Wallach, J.H., and Mitchell, J.H. (1983). Effects of static muscular contraction on impulse activity of groups III and IV afferents in cats. J Appl Physiol Respir Environ Exerc Physiol *55*, 105-112.
Kawasaki, H., Takasaki, K., Saito, A., and Goto, K. (1988). Calcitonin gene-related peptide acts as a novel vasodilator neurotransmitter in mesenteric resistance vessels of the rat. Nature *335*, 164-167.
Kearney, P.M., Whelton, M., Reynolds, K., Whelton, P.K., and He, J. (2004). Worldwide prevalence of hypertension: a systematic review. J Hypertens *22*, 11-19.
Kirchheim, H.R. (1976). Systemic arterial baroreceptor reflexes. Physiol Rev *56*, 100-177.
Klein, R., Silos-Santiago, I., Smeyne, R.J., Lira, S.A., Brambilla, R., Bryant, S., Zhang, L., Snider, W.D., and Barbacid, M. (1994). Disruption of the neurotrophin-3 receptor gene trkC eliminates la muscle afferents and results in abnormal movements. Nature *368*, 249-251.
Knot, H.J., and Nelson, M.T. (1998). Regulation of arterial diameter and wall [Ca2+] in cerebral arteries of rat by membrane potential and intravascular pressure. The Journal of physiology *508 (Pt 1)*, 199-209.
Koban, M., Leis, S., Schultze-Mosgau, S., and Birklein, F. (2003). Tissue hypoxia in complex regional pain syndrome. Pain *104*, 149-157.
Kobori, H., Hayashi, M., and Saruta, T. (2001). Thyroid Hormone Stimulates Renin Gene Expression Through the Thyroid Hormone Response Element. Hypertension *37*, 99-104.
Koob, G.F., and Volkow, N.D. (2010). Neurocircuitry of addiction. Neuropsychopharmacology *35*, 217-238.
Kopp, U.C., and DiBona, G.F. (1993). Neural regulation of renin secretion. Semin Nephrol *13*, 543-551.
Lau, O.C., Shen, B., Wong, C.O., Tjong, Y.W., Lo, C.Y., Wang, H.C., Huang, Y., Yung, W.H., Chen, Y.C., Fung, M.L.*, et al.* (2016). TRPC5 channels participate in pressure-sensing in aortic baroreceptors. Nature communications *7*, 11947.
Levanon, D., Bettoun, D., Harris-Cerruti, C., Woolf, E., Negreanu, V., Eilam, R., Bernstein, Y., Goldenberg, D., Xiao, C., Fliegauf, M.*, et al.* (2002). The Runx3 transcription factor regulates development and survival of TrkC dorsal root ganglia neurons. The EMBO journal *21*, 3454-3463.
Levi-Montalcini, R. (1987). The nerve growth factor 35 years later. Science *237*, 1154-1162.
Li, J., Hou, B., Tumova, S., Muraki, K., Bruns, A., Ludlow, M.J., Sedo, A., Hyman, A.J., McKeown, L., Young, R.S.*, et al.* (2014). Piezo1 integration of vascular architecture with physiological force. Nature *515*, 279-282.
Li, J., Maile, M.D., Sinoway, A.N., and Sinoway, L.I. (2004). Muscle pressor reflex: potential role of vanilloid type 1 receptor and acid-sensing ion channel. J Appl Physiol (1985) *97*, 1709-1714.
Li, L., Rutlin, M., Abraira, V.E., Cassidy, C., Kus, L., Gong, S., Jankowski, M.P., Luo, W., Heintz, N., Koerber, H.R.*, et al.* (2011). The functional organization of cutaneous low-threshold mechanosensory neurons. Cell *147*, 1615-1627.
Li, W., Kohara, H., Uchida, Y., James, J.M., Soneji, K., Cronshaw, D.G., Zou, Y.R., Nagasawa, T., and Mukouyama, Y.S. (2013). Peripheral nerve-derived CXCL12 and VEGF-A regulate the patterning of arterial vessel branching in developing limb skin. Developmental cell *24*, 359-371.
Liu, Q., Vrontou, S., Rice, F.L., Zylka, M.J., Dong, X., and Anderson, D.J. (2007). Molecular genetic visualization of a rare subset of unmyelinated sensory neurons that may detect gentle touch. Nature neuroscience *10*, 946-948.
Liu, R., Heiss, E.H., Guo, D., Dirsch, V.M., and Atanasov, A.G. (2015). Capsaicin from chili (Capsicum spp.) inhibits vascular smooth muscle cell proliferation. F1000Res *4*, 26.

Liu, R., Heiss, E.H., Schachner, D., Jiang, B., Liu, W., Breuss, J.M., Dirsch, V.M., and Atanasov, A.G. (2017). Xanthohumol Blocks Proliferation and Migration of Vascular Smooth Muscle Cells in Vitro and Reduces Neointima Formation in Vivo. J Nat Prod *80*, 2146-2150.
Lloyd, G. (1975). Alcmaeon and the early history of dissection. Sudhoffs Archive, 113-147.
Lou, S., Duan, B., Vong, L., Lowell, B.B., and Ma, Q. (2013). Runx1 controls terminal morphology and mechanosensitivity of VGLUT3-expressing C-mechanoreceptors. The Journal of neuroscience : the official journal of the Society for Neuroscience *33*, 870-882.
Lu, K.T., Keen, H.L., Weatherford, E.T., Sequeira-Lopez, M.L., Gomez, R.A., and Sigmund, C.D. (2016). Estrogen Receptor alpha Is Required for Maintaining Baseline Renin Expression. Hypertension *67*, 992-999.
Lu, Y., Ma, X., Sabharwal, R., Snitsarev, V., Morgan, D., Rahmouni, K., Drummond, H.A., Whiteis, C.A., Costa, V., Price, M.*, et al.* (2009). The ion channel ASIC2 is required for baroreceptor and autonomic control of the circulation. Neuron *64*, 885-897.
Luo, X., Xiao, Y., Song, F., Yang, Y., Xia, M., and Ling, W. (2012). Increased plasma S-adenosyl-homocysteine levels induce the proliferation and migration of VSMCs through an oxidative stress-ERK1/2 pathway in apoE(-/-) mice. Cardiovascular research *95*, 241-250.
Ma, Q., Fode, C., Guillemot, F., and Anderson, D.J. (1999). Neurogenin1 and neurogenin2 control two distinct waves of neurogenesis in developing dorsal root ganglia. Genes Dev *13*, 1717-1728.
Majesky, M.W. (2007). Developmental basis of vascular smooth muscle diversity. Arterioscler Thromb Vasc Biol *27*, 1248-1258.
Martinez-Lemus, L.A., Hill, M.A., and Meininger, G.A. (2009). The plastic nature of the vascular wall: a continuum of remodeling events contributing to control of arteriolar diameter and structure. Physiology *24*, 45-57.
Matsukawa, K., Wall, P.T., Wilson, L.B., and Mitchell, J.H. (1994). Reflex stimulation of cardiac sympathetic nerve activity during static muscle contraction in cats. Am J Physiol *267*, H821-827.
Molinoff, P.B. (1984). Alpha- and beta-adrenergic receptor subtypes properties, distribution and regulation. Drugs *28 Suppl 2*, 1-15.
Molinoff, P.B., and Axelrod, J. (1971). Biochemistry of catecholamines. Annu Rev Biochem *40*, 465-500.
Moser, M., and Feig, P.U. (2009). Fifty years of thiazide diuretic therapy for hypertension. Arch Intern Med *169*, 1851-1856.
Mu, X., Silos-Santiago, I., Carroll, S.L., and Snider, W.D. (1993). Neurotrophin receptor genes are expressed in distinct patterns in developing dorsal root ganglia. The Journal of neuroscience : the official journal of the Society for Neuroscience *13*, 4029-4041.
Mukouyama, Y.S., Gerber, H.P., Ferrara, N., Gu, C., and Anderson, D.J. (2005). Peripheral nerve-derived VEGF promotes arterial differentiation via neuropilin 1-mediated positive feedback. Development *132*, 941-952.
Mukouyama, Y.S., Shin, D., Britsch, S., Taniguchi, M., and Anderson, D.J. (2002). Sensory nerves determine the pattern of arterial differentiation and blood vessel branching in the skin. Cell *109*, 693-705.
Nakamaru, M., Tabuchi, Y., Rakugi, H., Nagano, M., and Ogihara, T. (1989). Actions of endothelin on adrenergic neuroeffector junction. J Hypertens Suppl *7*, S132-133.
Navar, L.G. (2014). Physiology: hemodynamics, endothelial function, renin-angiotensin-aldosterone system, sympathetic nervous system. J Am Soc Hypertens *8*, 519-524.
Nehls, V., Denzer, K., and Drenckhahn, D. (1992). Pericyte involvement in capillary sprouting during angiogenesis in situ. Cell Tissue Res *270*, 469-474.
Nelson, M.T., Huang, Y., Brayden, J.E., Hescheler, J., and Standen, N.B. (1990). Arterial dilations in response to calcitonin gene-related peptide involve activation of K+ channels. Nature *344*, 770-773.
Nonomura, K., Woo, S.H., Chang, R.B., Gillich, A., Qiu, Z., Francisco, A.G., Ranade, S.S., Liberles, S.D., and Patapoutian, A. (2016). Piezo2 senses airway stretch and mediates lung inflation-induced apnoea. Nature.

O'Donnell, S.R., and Wanstall, J.C. (1984). Beta-1 and beta-2 adrenoceptor-mediated responses in preparations of pulmonary artery and aorta from young and aged rats. J Pharmacol Exp Ther *228*, 733-738.
Okubo, M., Fujita, A., Saito, Y., Komaki, H., Ishiyama, A., Takeshita, E., Kojima, E., Koichihara, R., Saito, T., Nakagawa, E.*, et al.* (2015). A family of distal arthrogryposis type 5 due to a novel PIEZO2 mutation. Am J Med Genet A *167A*, 1100-1106.
Oppenheim, R.W. (1991). Cell death during development of the nervous system. Annu Rev Neurosci *14*, 453-501.
Page, A.J., Brierley, S.M., Martin, C.M., Price, M.P., Symonds, E., Butler, R., Wemmie, J.A., and Blackshaw, L.A. (2005). Different contributions of ASIC channels 1a, 2, and 3 in gastrointestinal mechanosensory function. Gut *54*, 1408-1415.
Patapoutian, A., and Reichardt, L.F. (2001). Trk receptors: mediators of neurotrophin action. Curr Opin Neurobiol *11*, 272-280.
Pathak, M.M., Nourse, J.L., Tran, T., Hwe, J., Arulmoli, J., Le, D.T., Bernardis, E., Flanagan, L.A., and Tombola, F. (2014). Stretch-activated ion channel Piezo1 directs lineage choice in human neural stem cells. Proceedings of the National Academy of Sciences of the United States of America *111*, 16148-16153.
Peach, M.J., and Dostal, D.E. (1990). The angiotensin II receptor and the actions of angiotensin II. J Cardiovasc Pharmacol *16 Suppl 4*, S25-30.
Price, M.P., Lewin, G.R., McIlwrath, S.L., Cheng, C., Xie, J., Heppenstall, P.A., Stucky, C.L., Mannsfeldt, A.G., Brennan, T.J., Drummond, H.A.*, et al.* (2000). The mammalian sodium channel BNC1 is required for normal touch sensation. Nature *407*, 1007-1011.
Qamar, M.I., and Read, A.E. (1987). Effects of exercise on mesenteric blood flow in man. Gut *28*, 583-587.
Ramsey, A.J., and Fitzpatrick, P.F. (1998). Effects of phosphorylation of serine 40 of tyrosine hydroxylase on binding of catecholamines: evidence for a novel regulatory mechanism. Biochemistry *37*, 8980-8986.
Ranade, S.S., Qiu, Z., Woo, S.H., Hur, S.S., Murthy, S.E., Cahalan, S.M., Xu, J., Mathur, J., Bandell, M., Coste, B.*, et al.* (2014a). Piezo1, a mechanically activated ion channel, is required for vascular development in mice. Proceedings of the National Academy of Sciences of the United States of America *111*, 10347-10352.
Ranade, S.S., Woo, S.H., Dubin, A.E., Moshourab, R.A., Wetzel, C., Petrus, M., Mathur, J., Begay, V., Coste, B., Mainquist, J.*, et al.* (2014b). Piezo2 is the major transducer of mechanical forces for touch sensation in mice. Nature *516*, 121-125.
Retailleau, K., Duprat, F., Arhatte, M., Ranade, S.S., Peyronnet, R., Martins, J.R., Jodar, M., Moro, C., Offermanns, S., Feng, Y.*, et al.* (2015). Piezo1 in Smooth Muscle Cells Is Involved in Hypertension-Dependent Arterial Remodeling. Cell reports *13*, 1161-1171.
Rode, B., Shi, J., Endesh, N., Drinkhill, M.J., Webster, P.J., Lotteau, S.J., Bailey, M.A., Yuldasheva, N.Y., Ludlow, M.J., Cubbon, R.M.*, et al.* (2017). Piezo1 channels sense whole body physical activity to reset cardiovascular homeostasis and enhance performance. Nature communications *8*, 350.
Rodriguez-Linares, L., Lado, M.J., Vila, X.A., Mendez, A.J., and Cuesta, P. (2014). gHRV: Heart rate variability analysis made easy. Comput Methods Programs Biomed *116*, 26-38.
Ross, R. (1993). The pathogenesis of atherosclerosis: a perspective for the 1990s. Nature *362*, 801-809.
Rummery, N.M., Brock, J.A., Pakdeechote, P., Ralevic, V., and Dunn, W.R. (2007). ATP is the predominant sympathetic neurotransmitter in rat mesenteric arteries at high pressure. The Journal of physiology *582*, 745-754.
Ruocco, I., Cuello, A.C., Parent, A., and Ribeiro-da-Silva, A. (2002). Skin blood vessels are simultaneously innervated by sensory, sympathetic, and parasympathetic fibers. The Journal of comparative neurology *448*, 323-336.
Salmon, M., Gomez, D., Greene, E., Shankman, L., and Owens, G.K. (2012). Cooperative binding of KLF4, pELK-1, and HDAC2 to a G/C repressor element in the SM22alpha promoter mediates transcriptional silencing during SMC phenotypic switching in vivo. Circ Res *111*, 685-696.

Sands, J.M., and Layton, H.E. (2009). The physiology of urinary concentration: an update. Semin Nephrol *29*, 178-195.
Saraf, A., Oberg, E.A., and Strack, S. (2010). Molecular determinants for PP2A substrate specificity: charged residues mediate dephosphorylation of tyrosine hydroxylase by the PP2A/B' regulatory subunit. Biochemistry *49*, 986-995.
Shields, S.D., Cavanaugh, D.J., Lee, H., Anderson, D.J., and Basbaum, A.I. (2010). Pain behavior in the formalin test persists after ablation of the great majority of C-fiber nociceptors. Pain *151*, 422-429.
Smyth, L.C.D., Rustenhoven, J., Scotter, E.L., Schweder, P., Faull, R.L.M., Park, T.I.H., and Dragunow, M. (2018). Markers for human brain pericytes and smooth muscle cells. J Chem Neuroanat *92*, 48-60.
Spier, I., Kerick, M., Drichel, D., Horpaopan, S., Altmuller, J., Laner, A., Holzapfel, S., Peters, S., Adam, R., Zhao, B.*, et al.* (2016). Exome sequencing identifies potential novel candidate genes in patients with unexplained colorectal adenomatous polyposis. Fam Cancer *15*, 281-288.
Staden, H. (1989). The art of medecine in early Alexandria. Cambridge University Press *44*.
Standen, N.B., Quayle, J.M., Davies, N.W., Brayden, J.E., Huang, Y., and Nelson, M.T. (1989). Hyperpolarizing vasodilators activate ATP-sensitive K+ channels in arterial smooth muscle. Science *245*, 177-180.
Stantcheva, K.K., Iovino, L., Dhandapani, R., Martinez, C., Castaldi, L., Nocchi, L., Perlas, E., Portulano, C., Pesaresi, M., Shirlekar, K.S.*, et al.* (2016). A subpopulation of itch-sensing neurons marked by Ret and somatostatin expression. EMBO Rep.
Steen, K.H., Steen, A.E., and Reeh, P.W. (1995). A dominant role of acid pH in inflammatory excitation and sensitization of nociceptors in rat skin, in vitro. The Journal of neuroscience : the official journal of the Society for Neuroscience *15*, 3982-3989.
Sun, H., Li, D.P., Chen, S.R., Hittelman, W.N., and Pan, H.L. (2009). Sensing of blood pressure increase by transient receptor potential vanilloid 1 receptors on baroreceptors. J Pharmacol Exp Ther *331*, 851-859.
Syeda, R., Florendo, M.N., Cox, C.D., Kefauver, J.M., Santos, J.S., Martinac, B., and Patapoutian, A. (2016). Piezo1 Channels Are Inherently Mechanosensitive. Cell reports *17*, 1739-1746.
Tabuchi, Y., Nakamaru, M., Rakugi, H., Nagano, M., Higashimori, K., Mikami, H., and Ogihara, T. (1990). Effects of endothelin on neuroeffector junction in mesenteric arteries of hypertensive rats. Hypertension *15*, 739-743.
Tamargo, J., and Ruilope, L.M. (2016). Investigational calcium channel blockers for the treatment of hypertension. Expert Opin Investig Drugs *25*, 1295-1309.
Tesfamariam, B., and Cohen, R.A. (1988). Inhibition of adrenergic vasoconstriction by endothelial cell shear stress. Circ Res *63*, 720-725.
Tesfamariam, B., Weisbrod, R.M., and Cohen, R.A. (1992). Cyclic GMP modulators on vascular adrenergic neurotransmission. Journal of vascular research *29*, 396-404.
Tessarollo, L., Vogel, K.S., Palko, M.E., Reid, S.W., and Parada, L.F. (1994). Targeted mutation in the neurotrophin-3 gene results in loss of muscle sensory neurons. Proceedings of the National Academy of Sciences of the United States of America *91*, 11844-11848.
Thayer, J.F., Hansen, A.L., Saus-Rose, E., and Johnsen, B.H. (2009). Heart rate variability, prefrontal neural function, and cognitive performance: the neurovisceral integration perspective on self-regulation, adaptation, and health. Ann Behav Med *37*, 141-153.
Thorin, E., and Atkinson, J. (1994). Modulation by the endothelium of sympathetic vasoconstriction in an in vitro preparation of the rat tail artery. Br J Pharmacol *111*, 351-357.
Thyberg, J. (1998). Phenotypic modulation of smooth muscle cells during formation of neointimal thickenings following vascular injury. Histology and histopathology *13*, 871-891.
Tian, X., Hu, T., Zhang, H., He, L., Huang, X., Liu, Q., Yu, W., He, L., Yang, Z., Yan, Y.*, et al.* (2014). Vessel formation. De novo formation of a distinct coronary vascular population in neonatal heart. Science *345*, 90-94.

Tibes, U. (1977). Reflex inputs to the cardiovascular and respiratory centers from dynamically working canine muscles. Some evidence for involvement of group III or IV nerve fibers. Circ Res *41*, 332-341.
Usoskin, D., Furlan, A., Islam, S., Abdo, H., Lonnerberg, P., Lou, D., Hjerling-Leffler, J., Haeggstrom, J., Kharchenko, O., Kharchenko, P.V.*, et al.* (2015). Unbiased classification of sensory neuron types by large-scale single-cell RNA sequencing. Nature neuroscience *18*, 145-153.
van Zwieten, P.A., Hendriks, M.G., Pfaffendorf, M., Bruning, T.A., and Chang, P.C. (1995). The parasympathetic system and its muscarinic receptors in hypertensive disease. J Hypertens *13*, 1079-1090.
Vanhoutte, P.M., and Miller, V.M. (1989). Alpha 2-adrenoceptors and endothelium-derived relaxing factor. Am J Med *87*, 1S-5S.
Verdecchia, P., Angeli, F., Mazzotta, G., Gentile, G., and Reboldi, G. (2008). The renin angiotensin system in the development of cardiovascular disease: role of aliskiren in risk reduction. Vasc Health Risk Manag *4*, 971-981.
vonEuler, U. (1946). A specific sympathetic ergone in adrenergic nerve fibres (sympathin) and its relation to adrenaline and noradrenaline. Acta Physiol Scand *12*, 73-97.
Vrontou, S., Wong, A.M., Rau, K.K., Koerber, H.R., and Anderson, D.J. (2013). Genetic identification of C fibres that detect massage-like stroking of hairy skin in vivo. Nature *493*, 669-673.
Wang, S., Chennupati, R., Kaur, H., Iring, A., Wettschureck, N., and Offermanns, S. (2016). Endothelial cation channel PIEZO1 controls blood pressure by mediating flow-induced ATP release. J Clin Invest *126*, 4527-4536.
Wasteson, P., Johansson, B.R., Jukkola, T., Breuer, S., Akyurek, L.M., Partanen, J., and Lindahl, P. (2008). Developmental origin of smooth muscle cells in the descending aorta in mice. Development *135*, 1823-1832.
Wehrwein, E.A., and Joyner, M.J. (2013). Regulation of blood pressure by the arterial baroreflex and autonomic nervous system. Handb Clin Neurol *117*, 89-102.
Werner, P., Paluru, P., Simpson, A.M., Latney, B., Iyer, R., Brodeur, G.M., and Goldmuntz, E. (2014). Mutations in NTRK3 suggest a novel signaling pathway in human congenital heart disease. Human mutation *35*, 1459-1468.
Woo, S.H., Lukacs, V., de Nooij, J.C., Zaytseva, D., Criddle, C.R., Francisco, A., Jessell, T.M., Wilkinson, K.A., and Patapoutian, A. (2015). Piezo2 is the principal mechanotransduction channel for proprioception. Nature neuroscience *18*, 1756-1762.
Woo, S.H., Ranade, S., Weyer, A.D., Dubin, A.E., Baba, Y., Qiu, Z., Petrus, M., Miyamoto, T., Reddy, K., Lumpkin, E.A.*, et al.* (2014). Piezo2 is required for Merkel-cell mechanotransduction. Nature *509*, 622-626.
Wright, D.E., Zhou, L., Kucera, J., and Snider, W.D. (1997). Introduction of a neurotrophin-3 transgene into muscle selectively rescues proprioceptive neurons in mice lacking endogenous neurotrophin-3. Neuron *19*, 503-517.
Xie, W.B., Li, Z., Shi, N., Guo, X., Tang, J., Ju, W., Han, J., Liu, T., Bottinger, E.P., Chai, Y.*, et al.* (2013). Smad2 and myocardin-related transcription factor B cooperatively regulate vascular smooth muscle differentiation from neural crest cells. Circ Res *113*, e76-86.
Xing, J., Sinoway, L., and Li, J. (2008). Differential responses of sensory neurones innervating glycolytic and oxidative muscle to protons and capsaicin. The Journal of physiology *586*, 3245-3252.
Yamazaki, T., Li, W., Yang, L., Li, P., Cao, H., Motegi, S.I., Udey, M.C., Bernhard, E., Nakamura, T., and Mukouyama, Y.S. (2018). Whole-Mount Adult Ear Skin Imaging Reveals Defective Neuro-Vascular Branching Morphogenesis in Obese and Type 2 Diabetic Mouse Models. Scientific reports *8*, 430.
Yatabe, J., Yoneda, M., Yatabe, M.S., Watanabe, T., Felder, R.A., Jose, P.A., and Sanada, H. (2011). Angiotensin III stimulates aldosterone secretion from adrenal gland partially via angiotensin II type 2 receptor but not angiotensin II type 1 receptor. Endocrinology *152*, 1582-1588.

Yoshida, T., Kaestner, K.H., and Owens, G.K. (2008). Conditional deletion of Kruppel-like factor 4 delays downregulation of smooth muscle cell differentiation markers but accelerates neointimal formation following vascular injury. Circ Res *102*, 1548-1557.
Zeisel, A., Hochgerner, H., Lonnerberg, P., Johnsson, A., Memic, F., van der Zwan, J., Haring, M., Braun, E., Borm, L.E., La Manno, G.*, et al.* (2018). Molecular Architecture of the Mouse Nervous System. Cell *174*, 999-1014 e1022.
Zeng, W.Z., Marshall, K.L., Min, S., Daou, I., Chapleau, M.W., Abboud, F.M., Liberles, S.D., and Patapoutian, A. (2018). PIEZOs mediate neuronal sensing of blood pressure and the baroreceptor reflex. Science *362*, 464-467.
Zhao, Q., Wu, K., Geng, J., Chi, S., Wang, Y., Zhi, P., Zhang, M., and Xiao, B. (2016). Ion Permeation and Mechanotransduction Mechanisms of Mechanosensitive Piezo Channels. Neuron *89*, 1248-1263.

7. Supplementary figures

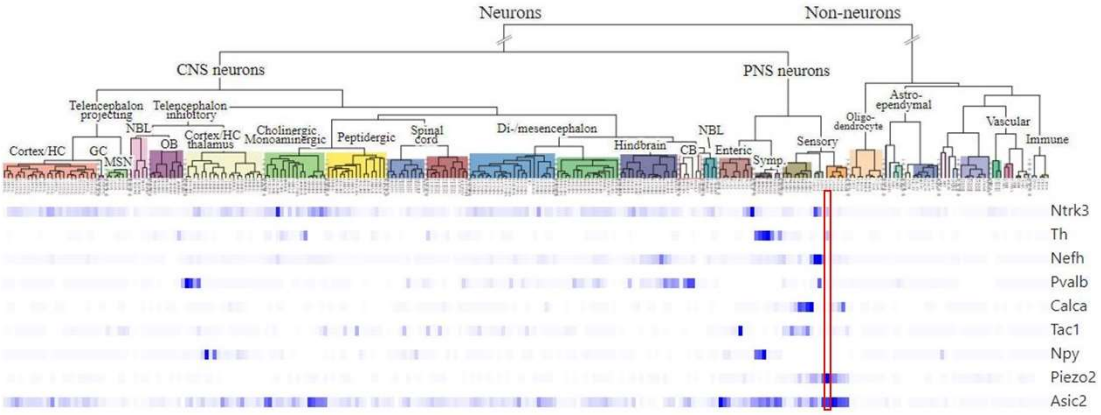

	Gene	Ntrk3	TH	Nefh	Pvalb	Calca	Tac1	Npy	Piezo2	Asic2
	Protein product	TrkC	TH	NF200	PV	CGRP	SP	NPY	Piezo2	Asic2
198	PSPEP8 Peptidergic (TrpM8), DRG	0.678	0.788	5.07	1.15	0.394	7.22	0.00	0.143	0.321
199	PSPEP7 Peptidergic (TrpM8), DRG	0.578	0.189	1.00	0.0302	0.320	6.99	0.00	0.0326	0.0630
200	PSPEP6 Peptidergic (TrpM8), DRG	0.501	0.182	0.706	0.0604	4.04	28.4	0.00	0.0937	0.0739
201	PSPEP5 Peptidergic (PEP1.2), DRG	0.0345	0.431	0.231	0.0302	11.3	10.8	0.00	0.265	0.467
202	PSPEP2 Peptidergic (PEP1.3), DRG	0.0766	0.330	3.20	0.00	43.4	8.24	0.00	1.62	1.16
203	PSPEP4 Peptidergic (PEP1.1), DRG	0.00766	0.00	0.407	0.0302	37.3	15.1	0.00	0.351	0.411
204	PSPEP3 Peptidergic (PEP1..4), DRG	0.0345	0.00	0.557	0.00	52.3	29.0	0.00	0.913	0.490
205	PSPEP1 Peptidergicv (PEP2), DRG	0.563	0.202	11.9	0.181	61.6	3.56	0.00	2.64	1.49
206	PSNF3 Neurofilament (NF2/3), DRG	6.71	0.0337	33.0	0.352	0.641	0.00	0.00	2.84	1.10
207	PSNF2 Neurofilament (NF4/5), DRG	3.33	0.00	34.0	15.3	0.0739	0.589	0.00	1.39	0.404
208	PSNF1 Neurofilament (NF1), DRG	0.528	0.0269	15.0	0.0302	0.0739	<=0.0256	0.00	5.76	2.32
209	PSNP1 Non-peptidergic (TH), DRG	1.76	3.44	0.665	<=0.0101	0.172	0.589	0.00	10.2	2.29
210	PSNP2 Non-peptidergic (NP1.1), DRG	0.111	0.108	1.25	<=0.0101	6.38	1.54	0.00	5.01	3.03
211	PSNP3 Non-peptidergic (NP1.2), DRG	0.0574	0.0269	1.15	0.0302	3.23	1.69	0.00	4.46	2.76
212	PSNP4 Non-peptidergic (NP2.1), DRG	0.402	0.00	1.64	0.0201	11.1	0.512	0.00	2.20	2.07
213	PSNP5 Non-peptidergic (NP2.2), DRG	0.0804	0.0135	0.570	<=0.0101	34.5	0.358	0.00	1.81	1.97
214	PSNP6 Non-peptidergic (NP3), DRG	0.0459	0.0269	0.747	0.0201	0.739	4.92	0.00	1.12	1.80

Supplementary figure 1. Gene expression analysis of TrkC$^+$ TH$^+$ neurons.
This analysis is based on the dataset produced by single cell RNAseq in Linnarsson's group (Zeisel et al., 2018). The upper panel shows a dendrogram made of 265 clusters identifying the different cellular populations. Using the online resource made available on http://mousebrain.org/, we checked the expression of genes of interest in all the 265 clusters. We identified only one population of DRG neurons expressing TrkC and TH (highlighted in red). As shown in the lower panel, this population, apart from TrkC and TH, expresses Piezo2 and Asic2. Extremely low or no expression of NF200, PV, CGRP, substance P or neuropeptide Y was detected.

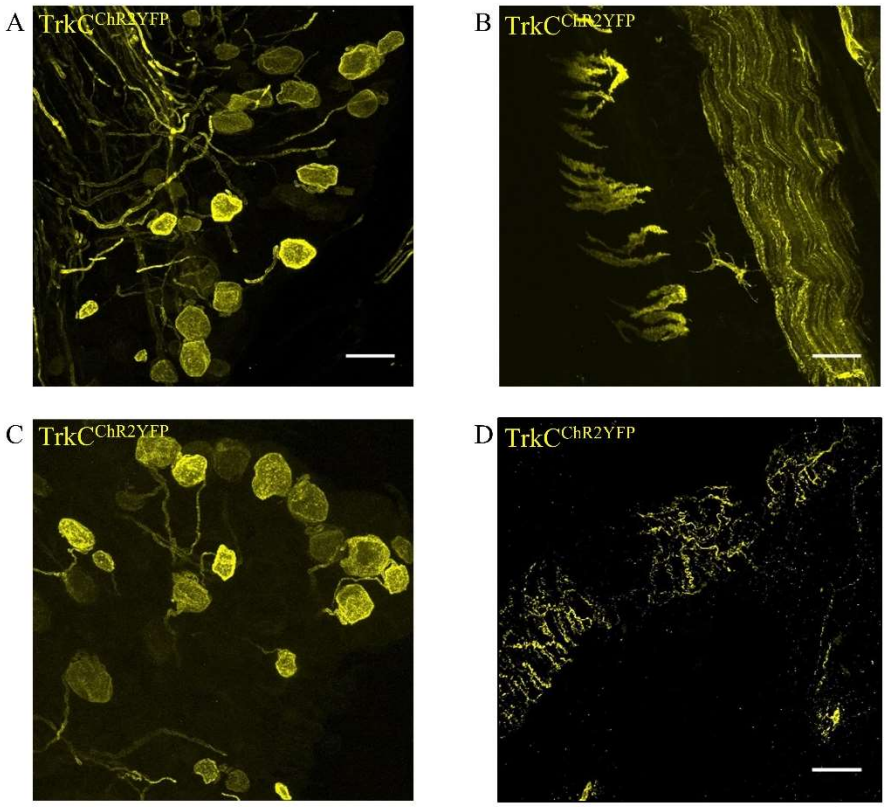

Supplementary figure 2. Differential expression of YFP reporter in TrkC^{CreERT2}::Rosa26$^{ChR2\text{-}YFP}$ mice following tamoxifen administration i.p. or i.v.

Systemic administration of tamoxifen via intraperitoneal (i.p.) injection results in YFP expression in DRG **(A)**, vSMCs and perivascular nerves **(B)**. Intrathecal injection of 4-OH tamoxifen causes Cre-driven recombination and YFP expression only in DRG neurons **(C)**. At the level of blood vessels only perivascular nerves are YFP$^+$, while vSMCs do not express the reporter **(D)**. Scale bar 50 μm.

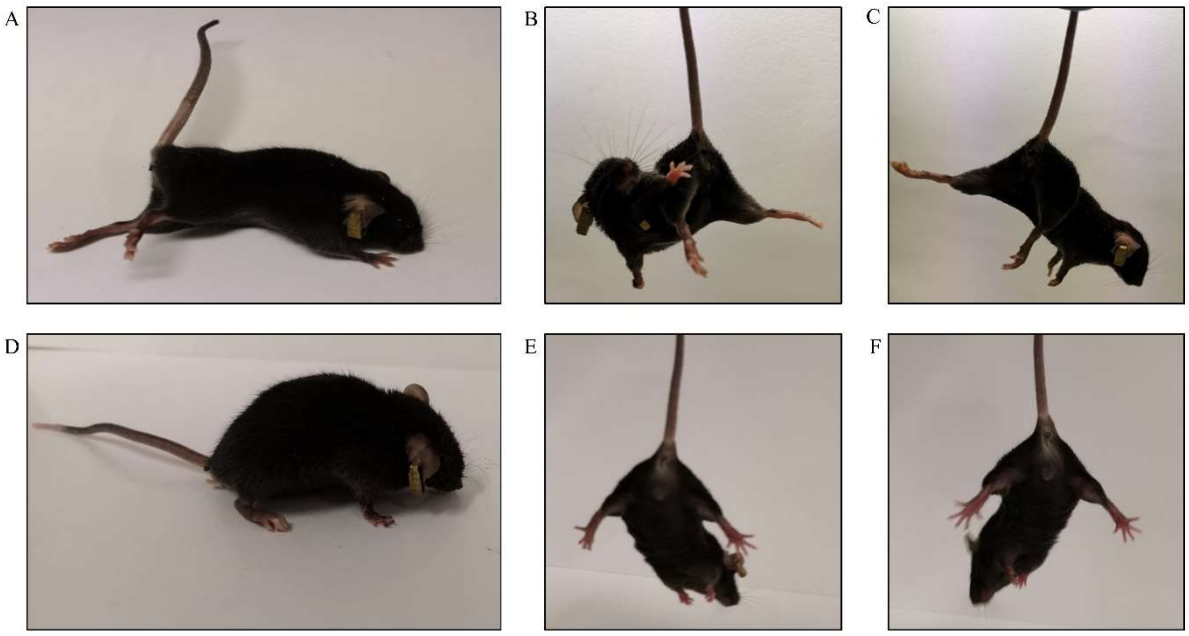

Supplementary figure 3. Ablated mice display severe locomotor problems.
Representative images showing TrkC^{CreERT2}::Avil^{iDTR} **(A-C)** and control mice **(D-F)** treated with DTX. TrkC^{CreERT2}::Avil^{iDTR} mice display locomotor problems with lack of coordination and unnatural limb positions due to loss of proprioceptors **(A-C)**. Control mice are not affected by DTX **(D-F)**.

8. Appendix

In parallel with the characterization of TrkC$^+$ sensory neurons, during my PhD I have also worked, together with Dr. Mariano Maffei, on the development of a new technology to selectively target specific cell populations to deliver enzymes, nucleic acids or small chemical compounds.

Below you can find a draft of the manuscript that we are about to submit, written by Dr. Mariano Maffei and Dr. Paul Heppenstall, where I will be a co-first author.

I have mainly contributed to the assessment of the system both *in vitro* and *in vivo* using Cre as an effector (Fig. 2 and Fig. 3) and to *in vivo* experiments with Cas9 (Fig. 6).

A ligand-based system for delivery of proteins in the skin

Mariano Maffei‡, Chiara Morelli‡, Ellie Graham, Stefano Patriarca, Laura Donzelli, Balint Doleschall, Fernanda de Castro Reis, Linda Nocchi, Cora Hallie Chadick, Luc Reymond, Ivan Correa, Kai Johnsson, Jamie Hackett & Paul A. Heppenstall
‡*Co-authors*

INTRODUCTION

Intracellular delivery of material is of fundamental importance for many research and clinical applications. The direct access to the interior of a cell enables, among others, gene editing (Zuris et al., 2015), modulation of gene expression (Dong et al., 2018) or ex-vivo therapies (Rosenberg and Restifo, 2015). Realization of those applications is commonly achieved by delivery of exogenous nucleic acids or virus-based methods. Despite their great use, those techniques often present many technical and safety drawbacks such as immunogenicity, risk of permanent integration (genotoxicity) or off-target effects. Moreover, viral vectors have limitations in cargo size narrowing their efficacy. In contrast, protein-based approaches substantially reduce those risks. During the last three decades, proteins have emerged as a new class of therapeutic drugs (Baumer et al., 2016; Leader et al., 2008; Mullen et al., 2014; Owens, 2017). There are two major obstacles for direct protein delivery: cellular internalization and the ability to reach the cytosol of the cell. To overcome these hurdles, proteins can be delivered via physical (e.g. electroporation, microinjection)

and biochemical modalities (e.g. pore-forming agents, cell-penetrating peptides) (Du et al., 2018). However, those methodologies are often restricted to *in-vitro* applications or can expose the cell to harsh treatments that are toxic. Most importantly, they lack selectivity, a critical parameter for specific targeting of cells, especially in clinical applications. Thus, efficient intracellular delivery of functional, intact proteins still remains a major challenge, reason why there is an urgent need of developing alternative methods. Recent studies have employed a ligand-mediated approach for targeted delivery of large cargoes in-vitro. In a first study Chen and collaborators conjugated the human transferrin to a zinc-finger nuclease to perform cell-type specific genome editing (Chen et al., 2013b). Similarly, an engineered version of Cas9 fused to the asialoglycoprotein ligand was selectively delivered in liver cells trough a receptor-mediated internalization mechanism (Rouet et al., 2018). Both works highlighted the many advantages of using a ligand-based platform including strong selectivity, low cell-toxicity and better temporal control. However, the employment of this system in-vivo represents the next challenge.

Skin is a highly extended organ, which is mainly constituted by keratinocytes. These cells constantly cycle to maintain a functional barrier that protects us against invading pathogens such as virus or bacteria. Moreover, keratinocytes are extremely hard to target and are not amenable to most of the standard delivery methodologies, thus limiting the strategies for effective therapies towards skin-related diseases. In this perspective, a ligand-based system could represent the key to get access to those cells enabling novel therapeutic applications.

We previously reported that a SNAP-tagged non-signaling version of the cytokine interleukin-31 (IL-31) is able to bind primary keratinocytes via its natural heterodimeric receptors composed of IL31 Receptor A (IL31RA) and Oncostatin M Receptor (OSMR) (Nocchi et al., 2018), which are both highly expressed on keratinocytes surface (Dillon et al., 2004; Diveu et al., 2004). Intriguingly, this ligand was used for targeted delivery of a small benzylguanine-derivatized photosensitizer in the skin enabling itch control for the treatment of inflammatory skin diseases (Nocchi et al., 2018).

Here we demonstrate that IL-31^{SNAP} is translocated to the nucleus of primary murine keratinocytes upon internalization. We further identify a second ligand (Nerve growth factor; NGF) able to bind keratinocytes and be internalized through a receptor-mediated process. Because both SNAP-ligands migrate to the nucleus, we reasoned that conjugation of large functional cargoes to IL-31 or NGF might allow for their intracellular uptake in primary

keratinocytes. Since production of large chimeric proteins failed, we decided to use a chemistry-based conjugation approach to link ligand with cargoes of interest.

In our strategy, we generate a recombinant version of the CRE recombinase fused to a CLIP-tag, which would allow for its chemical modification with benzylcytosine derivatives (Gautier et al., 2008). CLIP-tagged CRE is conjugated to SNAP-tagged ligands via a chemical cross-linking reaction. We show that cross-linked complexes are selectively delivered in primary keratinocytes both in-vitro and in-vivo. Similarly, we expand our approach to Cas9 nuclease achieving cell-type specific gene editing including homology-directed repair in-vivo.

RESULTS AND DISCUSSION

Nuclear translocation of IL31^{SNAP} and NGF^{SNAP} mutants in keratinocytes

A critical step for the delivery of functional proteins is the ability to get access to the interior of a cell upon uptake. Based on previous observations (Nocchi et al., 2018), we aimed to characterize IL-31 binding and internalization process in primary keratinocytes cultures. A recombinant IL-31$_{K138A}$SNAP (IL-31^{SNAP}) was in-vitro labelled with a BG-derivative fluorophore (BG-Surface^{549}) (Figure S1A) and applied in-vitro to primary keratinocytes isolated from a C57BL/6J WT mouse. Intriguingly, nuclear translocation was observed after 2 hours incubation by live cell imaging (Figure 1A and C). Similarly, we decided to expand our binding studies to a second ligand, NGF, previously reported to selectively bind its natural receptor Tyrosine-Receptor Kinase A (TrkA) which is also highly expressed in murine adult keratinocytes (Botchkarev et al., 2006),(Dechant, 2001). A pain-less recombinant version of NGF (Shaikh et al., 2018) (NGF$_{R121W}$SNAP; NGF^{SNAP}) was efficiently labeled with a BG-Surface^{549} (Figure S1B) and applied to primary mouse keratinocytes in culture at an increasing range of concentrations (Figure 1A and B). After extended incubation, a fluorescent signal was visible inside the cells suggesting that NGF$_{R121W}$SNAP was internalized upon binding to its natural TrkA receptor. Similar to IL-31$_{K138A}$SNAP uptake, nuclear staining was also detected for NGF$_{R121W}$SNAP (Figure 1D). In contrast, no cellular labeling was observed when cells were treated with labelled SNAP-tag alone or with BG-Surface^{549} (Figure 1B and Figure S1C and S1D). Internalization of SNAP-ligands was further assessed by Western blotting (Figure S1E). Thus, we demonstrated that IL-31$_{K138A}$SNAP and NGF$_{R121W}$SNAP ligands bind to primary keratinocytes and are successively translocated to the nucleus, enabling intracellular access.

Chemical cross-linking of SNAP-ligands to CLIP-Cre

We reasoned that SNAP-ligands might allow targeted delivery and nuclear translocation of proteins of interest (cargoes) in primary keratinocytes. To that end, we first aimed to use large chimeric proteins (ligands fused to CRE recombinase). Unfortunately, production fell into several technical problems including extremely low yields, precipitation issues and failure to recover active intact proteins (data not shown). We therefore asked whether selective cross-linking (S-CROSS) (Gautier et al., 2009) could be employed to bind molecules of interest. S-CROSS is based on self-labeling tags (SNAP and CLIP), which covalently bind synthetic probes. S-CROSS has been already used to detect protein-protein interactions in living cells (Gautier et al., 2009)·(Lemercier et al., 2007). A recombinant version of the CRE recombinase fused to an N-terminal CLIP-tag (CLIP-Cre) was produced in *E. Coli*. CLIP activity was successfully confirmed by selective labelling with a BC-derivative fluorophore (Figure S1F). S-CROSS was next assessed in-vitro by mixing CLIP-Cre with SNAP-ligands together with cross-linker molecules carrying both BG and BC moieties on their ends (Figure 1E). We first screened several cross-linker candidates in order to identify the synthetic probe that allowed the highest yield of S-CROSS (Table S1 and Figure S1G). We determined that long linkers (> 25 Å; linker #2, #3, #5, #6) were more effective for S-CROSS most likely because they reduce steric hindrance thus allowing the reactive groups (BG and BC) to be better accessible to the SNAP and CLIP tags. Particularly, linker #5 (Table S1) was shown to display the highest rate of S-CROSS. Finally, optimization of the cross-linking process was achieved through a two-step reaction (Figure 1F): CLIP-tagged cargo was firstly saturated with the cross-linker (linker #5) and, after elimination of the unbound compound, it was reacted with the SNAP-ligands. Up to 60% of cross-linked proteins were obtained with no excess of free SNAP-ligand present in the final product (Figure 1G and H).

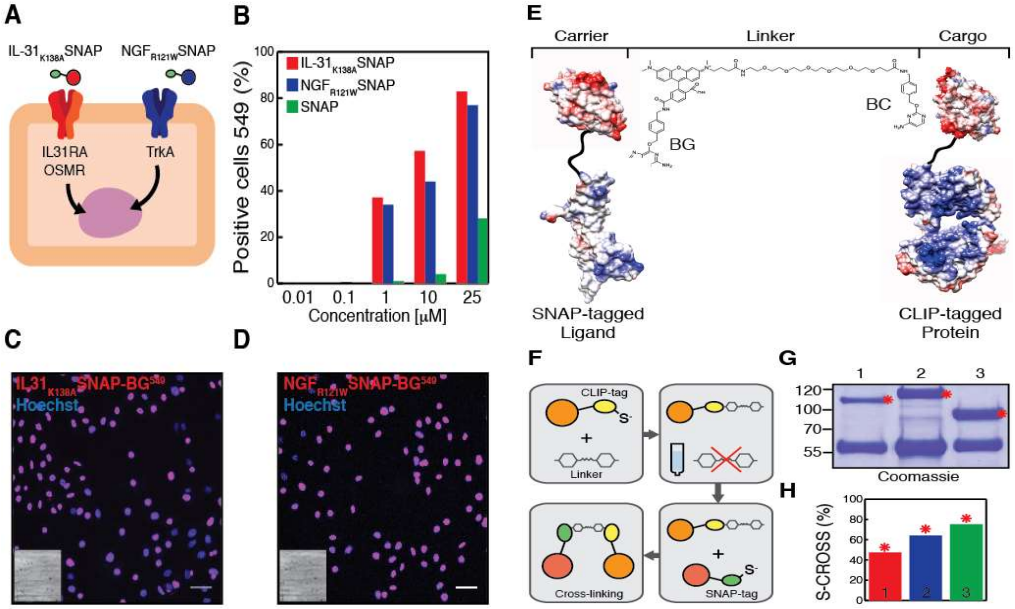

Figure 1. Binding of SNAP-tagged ligands to keratinocytes and selective cross-linking to CLIP-tagged enzymes. (A) Schematic representation of keratinocytes expressing receptors of interest and ligands used. **(B)** Quantification of labeled IL-31_{K138A}SNAP-BG^{549} **(C)** and NGF_{R121W}SNAP-BG^{549} **(D)** binding to primary keratinocytes. Nuclear localization was observed after 2 hours treatment. The nuclei were stained with Hoechst. Scale bars, 20 μm. The insets represent corresponding brightfield images. **(E)** 3D structures showing selective cross-linking of NGF-SNAP and CLIP-Cre through a BG-TMR-PEG_6-BC linker (PDB ID codes: 1BET, 1KBU, 3KZY). **(F)** Schematic representation of S-CROSS optimized chemical reaction. **(G)** Representative Coomassie gel showing cross-linking complexes (red asterisks). First lane (#1) is IL-$31^{SNAP::CLIP}$CRE, second lane (#2) is $NGF^{SNAP::CLIP}$CRE and third lane (#3) is $SNAP^{::CLIP}$CRE. **(H)** Quantification of cross-linking from Coomassie gel **(G)**.

Ligand-mediated selective delivery of CLIP-Cre in-vitro

To assess whether targeted delivery of cross-linked CLIP-Cre to ligands of interest was functional, we applied S-CROSS complexes to primary adult murine keratinocytes cultured from a $Rosa26^{LSL\text{-}ChR2\text{-}YFP}$ reporter mice. CLIP-Cre, cross-linked in-vitro to either IL-31_{K138A}SNAP (IL-$31^{SNAP::CLIP}$CRE; linker #5) or NGF_{R121W}SNAP ($NGF^{SNAP::CLIP}$CRE; linker #5) was applied to keratinocytes and after 5 days YFP expression was assessed (Figure 2A). Upon a single in-vitro treatment, we observed 26.5% ± 4.9 expression of reporter YFP for IL-$31^{SNAP::CLIP}$CRE complex and 20.0% ± 2.6 when cells were treated with $NGF^{SNAP::CLIP}$CRE S-CROSS (Figure 2B). Of note, the percentage of targeted cells was similar to the number of keratinocytes labelled with free SNAP-ligands (Figure 1C, 1 μM condition). Importantly, negligible YFP expression (0-3%) was detected upon incubation with a cross-linked binary complex lacking ligands of interest ($SNAP^{::CLIP}$CRE; linker #5) or when CLIP-Cre alone was applied to keratinocytes (Figure 2B) suggesting that S-CROSS internalization is primarily driven by ligands. To confirm the selectivity of our system, we

sought to use a reporter mouse model lacking the Interleukin 31 receptor alpha subunit (IL31RA$^{-/-}$ Knock-out) (Nocchi et al., 2018). Rosa26$^{LSL\text{-}ChR2\text{-}YFP}$ mice were crossed with IL31RA$^{-/-}$ mice and primary keratinocytes were *in-vitro* cultured. Next, S-CROSS (IL-31$^{SNAP::CLIP}$CRE or NGF$^{SNAP::CLIP}$CRE; linker #5) was applied to keratinocytes and YFP expression was assessed. Strikingly, no YFP activation was detected on cells treated with the cross-linking complex carrying the IL-31 ligand, while NGF S-CROSS displayed a similar YFP activation as for wild-type Rosa26$^{LSL\text{-}ChR2\text{-}YFP}$ keratinocytes (15.2% ± 0.8) (Figure 2C). Thus, SNAP-tagged ligands mediate selective intracellular delivery of CLIP-Cre in-vitro.

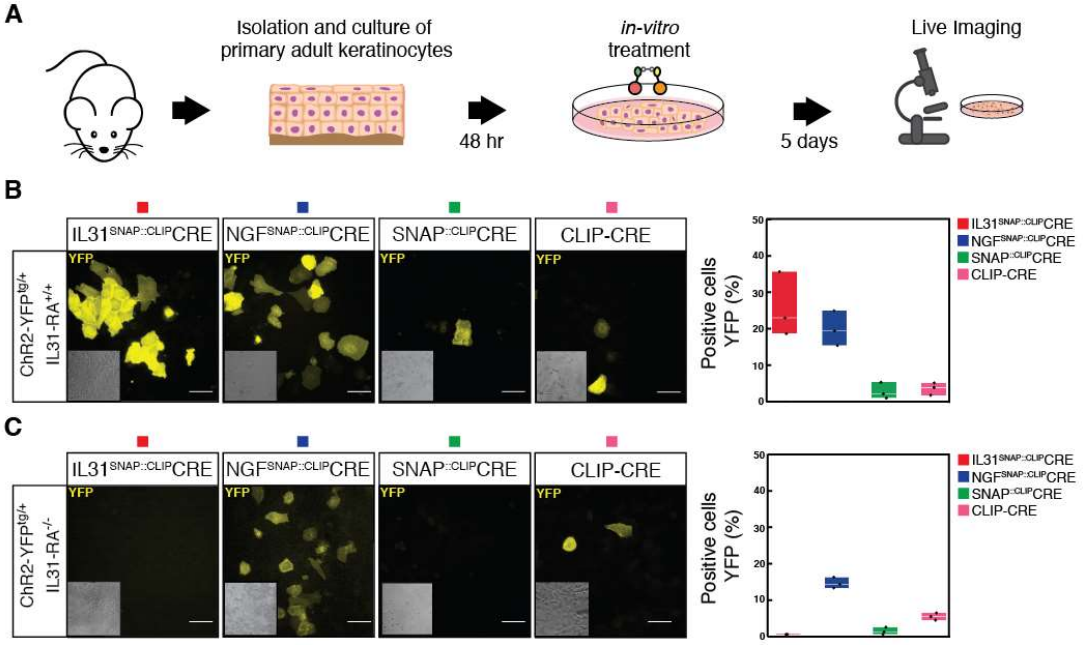

Figure 2. Ligand-mediated delivery of cross-linked CLIP-Cre. (A) Schematic of in-vitro keratinocytes treatment with cross-linked complexes. **(B)** Images and quantification (% of cells) of YFP positive primary keratinocytes from Rosa26$^{LSL\text{-}ChR2\text{-}YFP}$ mice 5 days after treatment with 2 µM of cross-linked complexes or CLIP-Cre alone. Scale bars, 20 µm. The insets represent corresponding brightfield images. Representative data from *n=3* independent experiments. **(C)** Representative images and quantification of YFP positive primary keratinocytes from double transgenic Rosa26$^{LSL\text{-}ChR2\text{-}YFP::IL31RA\text{-}/\text{-}}$ mice 5 days after treatment with 2 µM of cross-linked complexes or CLIP-Cre alone. Scale bars, 20 µm. The insets represent corresponding brightfield images. Representative data from *n=3* independent experiments.

Ligand-mediated selective delivery of CLIP-Cre in-vivo

We next investigated whether IL-31$_{K138A}$SNAP or NGF$_{R121W}$SNAP ligands can drive intracellular delivery of CLIP-Cre in-vivo in mice. S-CROSS reactions (IL-31$^{SNAP::CLIP}$CRE or NGF$^{SNAP::CLIP}$CRE; linker #5) were injected subcutaneously into the ear of Rosa26$^{LSL\text{-}ChR2\text{-}YFP}$ reporter mice and after 3 weeks YFP expression was assessed by confocal microscopy on whole mount samples (Figure 3A). Upon a single treatment, broad YFP

expression was detected in keratinocytes both in mice injected with IL-31$^{SNAP::CLIP}$CRE and NGF$^{SNAP::CLIP}$CRE (Figure 3B and C). Of note, no YFP signal was observed after injection with SNAP$^{::CLIP}$CRE complex or CLIP-Cre alone (Figure 3B and C and Figure S2A). Importantly, subcutaneous injection of a recombinant cell-permeant peptide fusion CRE-recombinase protein (Peitz et al., 2002)·(Nolden et al., 2006) led to a non-cell specific YFP expression and displayed lower efficiency compared with ligand-driven delivery (Figure 3B and C). We further validated cell-type specific delivery by injecting S-CROSS into the ear of double transgenic *IL31RA* knockout/reporter mice (Rosa26$^{LSL\text{-}ChR2\text{-}YFP::IL31RA\text{-}/\text{-}}$). No YFP signal was observed upon injection with IL-31$^{SNAP::CLIP}$CRE complex whereas reporter activation was maintained for NGF-mediated delivery of CLIP-Cre (Figure 3C and D). These results demonstrate that ligand-mediated delivery is functional and selective also *in-vivo*.

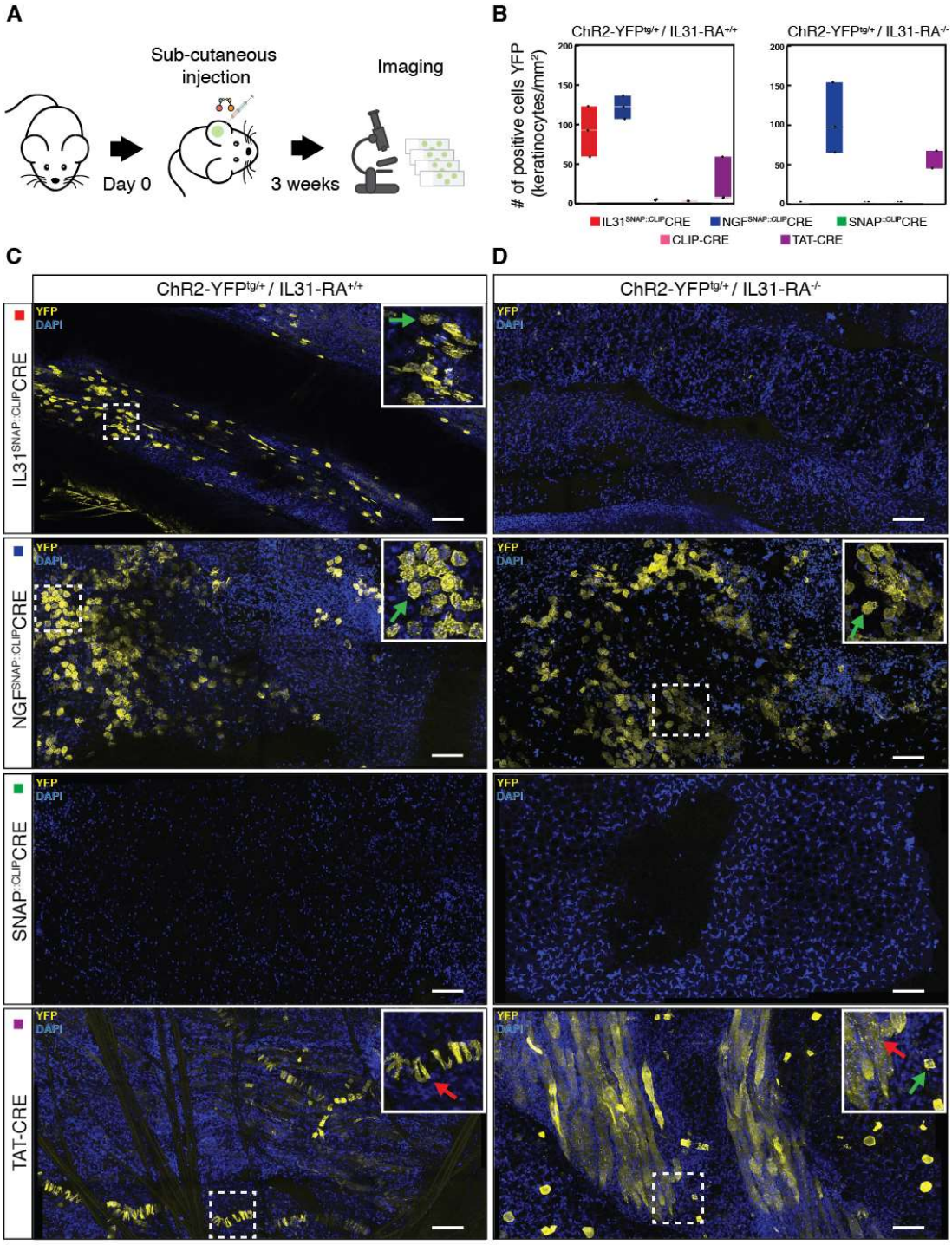

Figure 3. Selective delivery of cross-linked CLIP-CRE in-vivo. (A) Schematic of in-vivo treatment with cross-linked complexes. **(B)** Quantification (number of cells per mm^2) of YFP^+ keratinocytes from $Rosa26^{LSL\text{-}ChR2\text{-}YFP}$ mice **(C)** and from double transgenic $Rosa26^{LSL\text{-}ChR2\text{-}YFP::IL31RA\text{-}/\text{-}}$ mice **(D)** 3 weeks after subcutaneous injection with 5 µM of cross-linked complexes or TAT-Cre. The nuclei were stained with DAPI. Scale bars, 40 µm. The insets show the zoom of representative areas. Green arrows indicate YFP^+ keratinocytes. Red arrows indicate non-selective YFP expression. Data from *n=3* independent experiments.

Chemical cross-linking of functional CLIP-Cas9

We next expanded cross-linking approach to Cas9 nuclease. Similar to CLIP-Cre, a recombinant version of the Cas9 nuclease fused to an N-terminal CLIP-tag (CLIP-Cas9) was produced in *E. Coli*. Efficient labeling with a BC derivative fluorophore was observed indicating that the CLIP-tag was active (Figure S3A). Preliminary *in-vitro* digestion assay (IDA) (Aida et al., 2015) using *Atat1* PCR product and chemically synthesized dual RNAs (*Atat1* crRNA and trRNA) showed that CLIP-tagged Cas9 nuclease was functional (Figure S3E). We further confirmed recombinant CLIP-Cas9 nuclease activity in-cell by direct electroporation of preassembled CLIP-Cas9::sgRNA (*Atat1* crRNA and trRNA) ribonucleoprotein (RNP) complexes in primary keratinocytes isolated from C57BL/6J WT adult mice (Figure 4A). Gene editing was observed by tracking of indels by decomposition analysis (TIDE) (Brinkman et al., 2014) of the PCR amplicons from the *Atat1* genomic locus and supported by T7 endonuclease 1 (T7E1) assay (Figure 4B and Figure S3B). Of note, CLIP-Cas9 gene editing efficiency (45.2%) was comparable to native Cas9 activity (60.2%) when the latter was electroporated together with sgRNA (Cas9::sgRNA) in keratinocytes (Figure S3C). We finally assessed selective cross-linking of ligands with recombinant CLIP-Cas9. Similar to CLIP-Cre S-CROSS, we obtained up to 35% of cross-linked CLIP-Cas9 to IL-31$_{K138A}$SNAP (IL-31$^{SNAP::CLIP}$Cas9, linker #5) and about 55% to NGF$_{R121W}$SNAP (NGF$^{SNAP::CLIP}$Cas9, linker #5) (Figure S3D). Thus, validation assays showed that CLIP-Cas9 was functional and efficiently conjugated to ligands of interest.

Internalization of ligand cross-linked CLIP-Cas9 complexes

Large protein complexes can suffer of poor cellular internalization. To determine whether Cas9 S-CROSS could be internalized in keratinocytes, CLIP-Cas9 was cross-linked *in-vitro* to either IL-31$_{K138A}$SNAP (IL-31$^{SNAP::CLIP}$Cas9) or NGF$_{R121W}$SNAP (NGF$^{SNAP::CLIP}$Cas9) using a linker carrying a TMR fluorophore (linker #6; Table S1) in order to monitor internalization (Figure S4A). IL-31$^{SNAP::CLIP}$Cas9 or NGF$^{SNAP::CLIP}$Cas9 were applied to cultured murine WT keratinocytes and after 2 hours of incubation, S-CROSS uptake was assessed via live cell imaging. Red fluorescence was observed inside the cells, mostly localized in the nuclei suggesting that the protein complex was internalized (Figure 4C and D, condition #1). We next investigated whether ribonucleoprotein complexes (IL-31$^{SNAP::CLIP}$Cas9 or NGF$^{SNAP::CLIP}$Cas9 bound to sgRNA) were taken up by keratinocytes. Ligand cross-linked CLIP-Cas9 complexes were first incubated in-vitro with sgRNA (*Atat1*

crRNA and trRNA; IL-31$^{SNAP::CLIP}$Cas9::sgRNA or NGF$^{SNAP::CLIP}$Cas9::sgRNA) and successively applied to cultured cells. Internalization was imaged live after 2 hours. Compared to ligand-Cas9 complexes alone, a strong reduction of the fluorescent intracellular signal was observed for both complexes (Figure 4C and D, condition #2), suggesting that addition of sgRNA affects cellular internalization. Decrease of S-CROSS internalization in the presence of sgRNA was further confirmed by Western blotting analysis (Figure S4B). To circumvent this, we thought to test two candidate peptides that could promote RNP internalization: Protamine and ppTG21.

Protamine is a small positively charged peptide which binds with high affinity to nucleic acids and it has been previously employed for small and long RNA delivery (Baumer et al., 2016)·(Kauffman et al., 2016) (Figure S4C). ppTG21 is an endosomolytic peptide showed to enhance endosomal escape of Cas9 RNP complexes whilst maintaining selectivity (Rouet et al., 2018). Preassembled IL-31$^{SNAP::CLIP}$Cas9::sgRNA or NGF$^{SNAP::CLIP}$Cas9::sgRNA were incubated *in-vitro* with an excess of Protamine and then applied to cultured cells. After 2 hours of treatment, an increase of fluorescent signal was observed in the nuclei of live cells suggesting that co-incubation with protamine can favor cellular internalization of RNP complexes (Figure 4C and D, condition #3). We then examined S-CROSS::sgRNA complex internalization in the presence of ppTG21. Preassembled IL-31$^{SNAP::CLIP}$Cas9::sgRNA or NGF$^{SNAP::CLIP}$Cas9::sgRNA were co-incubated in-vitro with 30 molar equivalent of ppTG21 peptide. Next, cultured cells were treated for 2 hours and imaged live. Compared to protamine, ppTG21 did not improve RNP internalization (Figure 4C and D condition #4). Importantly, negligible internalization was observed in the absence of ligand when TMR-labelled CLIP-Cas9 (CLIP-Cas9 + linker #6) was incubated with cultured cells with or without sgRNA and in presence of Protamine or ppTG21 (Figure S4D and S4E, conditions #1-4).

Finally, we assessed in-cell gene editing (*Atat1* locus) using ligand-Cas9 complexes delivered under the conditions described above. No detectable gene editing was observed for both ligand cross-linked CLIP-Cas9 RNP complexes supporting the observation that the presence of sgRNA can interfere with internalization mechanisms (Figure S4F). Although co-incubation with Protamine suggested favoring internalization, no gene editing was detected. We therefore hypothesized that Protamine sequesters the sgRNA making RNP complexes unable to edit the target gene.

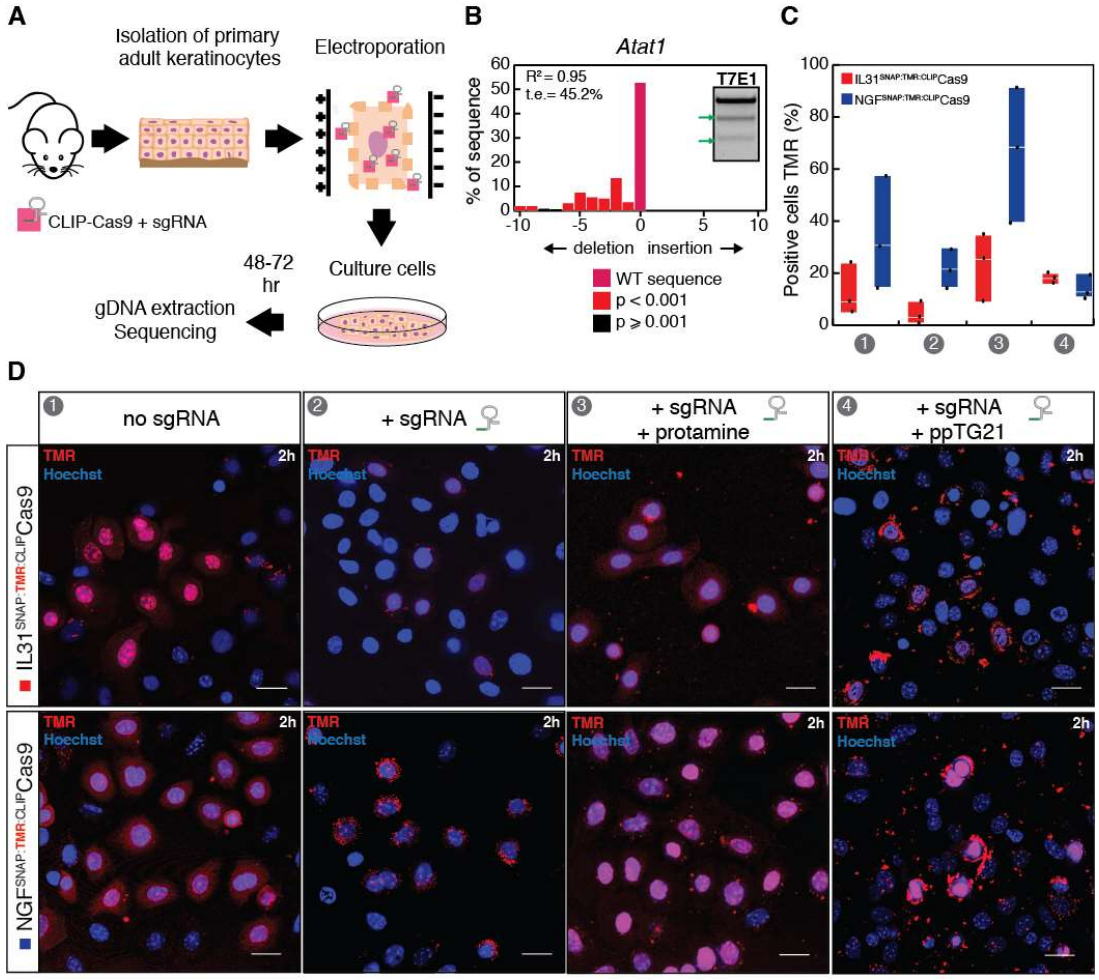

Figure 4. CLIP-Cas9 activity and internalization in keratinocytes. (A) Schematic of CLIP-Cas9::sgRNA electroporation strategy. **(B)** Indel spectrum determined by TIDE of primary keratinocytes electroporated with CLIP-Cas9::sgRNA targeting the *Atat1* gene. The inset show T7 endonuclease 1 assay performed on genomic DNA from electroporated keratinocytes. *t.e.*= total efficiency. **(C)** Quantification (% cells) and representative images **(D)** of TMR positive cells upon 2 hours treatment with 2 µM of ligand cross-linked Cas9 (#1 no sgRNA; #2 with sgRNA; #3 with sgRNA + Protamine; #4 with sgRNA + ppTG21). Nuclei were stained with Hoechst. Scale bars, 20 µm.

Ligand-mediated delivery of CLIP-Cas9 in-vitro

We have shown that single guide RNA affects internalization thus limiting efficacy. However, ligands efficiently delivered CLIP-Cas9 in cells when the guide was absent (Figure 4C and D, condition #1). We therefore investigate whether ligand cross-linked CLIP-Cas9 could allow for cell-targeted gene editing in keratinocytes already expressing the sgRNA of interest. To achieve this, adult primary keratinocytes were isolated from a C57BL/6J WT mouse and, prior to culturing, electroporated with a plasmid encoding for a Blue Fluorescent Protein (BFP) and an enhanced single guide RNA driven by U6 promoter (U6-sgRNA) (Chen et al., 2013a) targeting the *Atat1* locus (Figure 5A). After 36 hour, BFP

expression was assessed by live imaging. Electroporation efficiency was further verified by fluorescence activated cell sorting (FACS) indicating that 10% of the cells expressed the BFP reporter. Next, CLIP-Cas9 was cross-linked to either IL-31$_{K138A}$SNAP (IL-31$^{SNAP::CLIP}$Cas9) or NGF$_{R121W}$SNAP (NGF$^{SNAP::CLIP}$Cas9) *in-vitro* and applied to transfected keratinocytes. S-CROSS was carried out using 3 different cross-linkers (linker #3, #5 and #6, Table S1). In parallel, electroporated cells were also treated with IL-31$^{SNAP::CLIP}$Cas9 or NGF$^{SNAP::CLIP}$Cas9 cross-linking (linker #3, #5 and #6, Table S1) in the presence of 30 molar equivalent of ppTG21 peptide. Indeed, live imaging showed that co-incubation with ppTG21 enhanced ligand cross-linked Cas9 internalization in the absence of sgRNA while no uptake was observed for TMR-labelled CLIP-Cas9 (Linker #6) in the presence of the endosomolytic peptide. After treatment, BFP positive keratinocytes were sorted by flow cytometry and genomic DNA was extracted to assess genome editing of target of interest (*Atat1*) (Figure 5A). Gene editing was observed with comparable efficiency across ligands at significantly greater levels than under control conditions (6.2% ± 0.5 indels for IL-31$^{SNAP::CLIP}$Cas9; 6.6% ± 2.4 indels for NGF$^{SNAP::CLIP}$Cas9; 1.9% ± 0.2 indels for control conditions; Figure 5B). No substantial gene editing improvement was detected in presence of ppTG21 peptide (6.6% ± 3.0 indels for IL-31$^{SNAP::CLIP}$Cas9; 11.8% ± 4.9 indels for NGF$^{SNAP::CLIP}$Cas9) except for NGF$^{SNAP::CLIP}$Cas9 with linker #5 (19.8% indels) (Figure 5B).

Ligand-mediated selective delivery of CLIP-Cas9 allows for HDR *in-vitro*

We next investigated whether ligand-mediated delivery of CLIP-Cas9 could also be employed for precise sequence replacement through homology-directed repair (HDR) (Sander and Joung, 2014) mechanism. HDR needs the employment of a guide RNA and a donor DNA template that must be present together with Cas9 inside the target cell. To achieve this, we decided to use a previously described strategy employing an adeno-associated virus (AAV) containing a U6-sgRNA targeting the mouse *ß-Actin* gene and a donor template encoding for the monomeric Green Fluorescent Protein (mEGFP) (Nishiyama et al., 2017) (Figure 5C). This approach allows for inserting the mEGFP sequence into the *ß-Actin* gene, producing a recombinant fluorescent ß-Actin protein. Keratinocytes are resistant to viral infection (Orthwein et al., 2015; Saleh-Gohari and Helleday, 2004; Suzuki et al., 2016). We therefore decided to test HDR-mediated gene editing by delivering ligand cross-linked Cas9 in Neuro-2a (N2a) cells, a murine neuroblastoma cellular line (McMorris and Ruddle, 1974) expressing NGF receptors. As

expected, we observed labeled NGF_{R121W}SNAP binding to N2a cells by live imaging upon 2 hours treatment (Figure S5A). To assess HDR *in-vitro*, cultured N2a were infected with AAV, packaged with a chimera serotype 1/2 capsid (AAV1/2::HDR) 1/2::HDR, and successively treated with NGF cross-linked CLIP-Cas9 ($NGF^{SNAP::CLIP}$Cas9) (Figure 5C). Again, efficiency was compared across 3 different cross-linkers (linker #3, #5 and #6, Table S1) and by co-incubation with the ppTG21 peptide. Cells were imaged 72-96 hours post-treatment and the percentage of mEGFP expressing cells was evaluated. A mEGFP fluorescent signal was observed upon a single treatment with NGF cross-linked CLIP-Cas9 suggesting that the donor sequence was correctly inserted into the genome (Figure 5E). We observed 3.9% ± 0.7 of mEGFP positive cells with no effective improvement when complexes were co-incubated with the ppTG21 peptide (3.4% ± 0.6, Figure 5F). Importantly, no mEGFP signal was detected in cells transduced only with AAV1/2::HDR (0.1% ± 0.1) or treated with CLIP-Cas9 alone (Figure 5D and 5E and Figure S5B).

TrkA overexpression enhanced HDR-mediated gene editing in N2a cells

We reasoned that over-expression of TrkA receptor could promote higher internalization of NGF cross-linked complexes. Indeed, N2a cells binding by labeled NGF_{R121W}SNAP was enhanced when TrkA over-expression occurred (Figure S5C). To assess HDR, NGF cross-linked CLIP-Cas9 (linker #3, #5 and #6, Table S1) was applied to AAV1/2::HDR transduced N2a cells previously transfected with a plasmid encoding for the NGF receptor, TrkA (Figure 5G). Remarkably, the proportion of targeted N2a cells expressing mEGFP-ß-Actin was higher compared to non-transfected cells. The percentage of green-fluorescent positive cells after a single treatment with $NGF^{SNAP::CLIP}$Cas9 was 8.9% ± 2.1 (Figure 5H). Cross-linked complex carrying linker #3 (Table S1) displayed the highest efficiency (~15%) while S-CROSS (linker #5) and S-CROSS (linker #6) were shown to be less effective (~5-7%) (Figure 5H). Importantly, no significative effect was observed when ppTG21 co-incubation occurred (10.2% ± 1.5), except for $NGF^{SNAP::CLIP}$Cas9 with linker #5. Again, no mEGFP positive cells were found upon infection only with AAV1/2::HDR (0.7% ± 0.1).

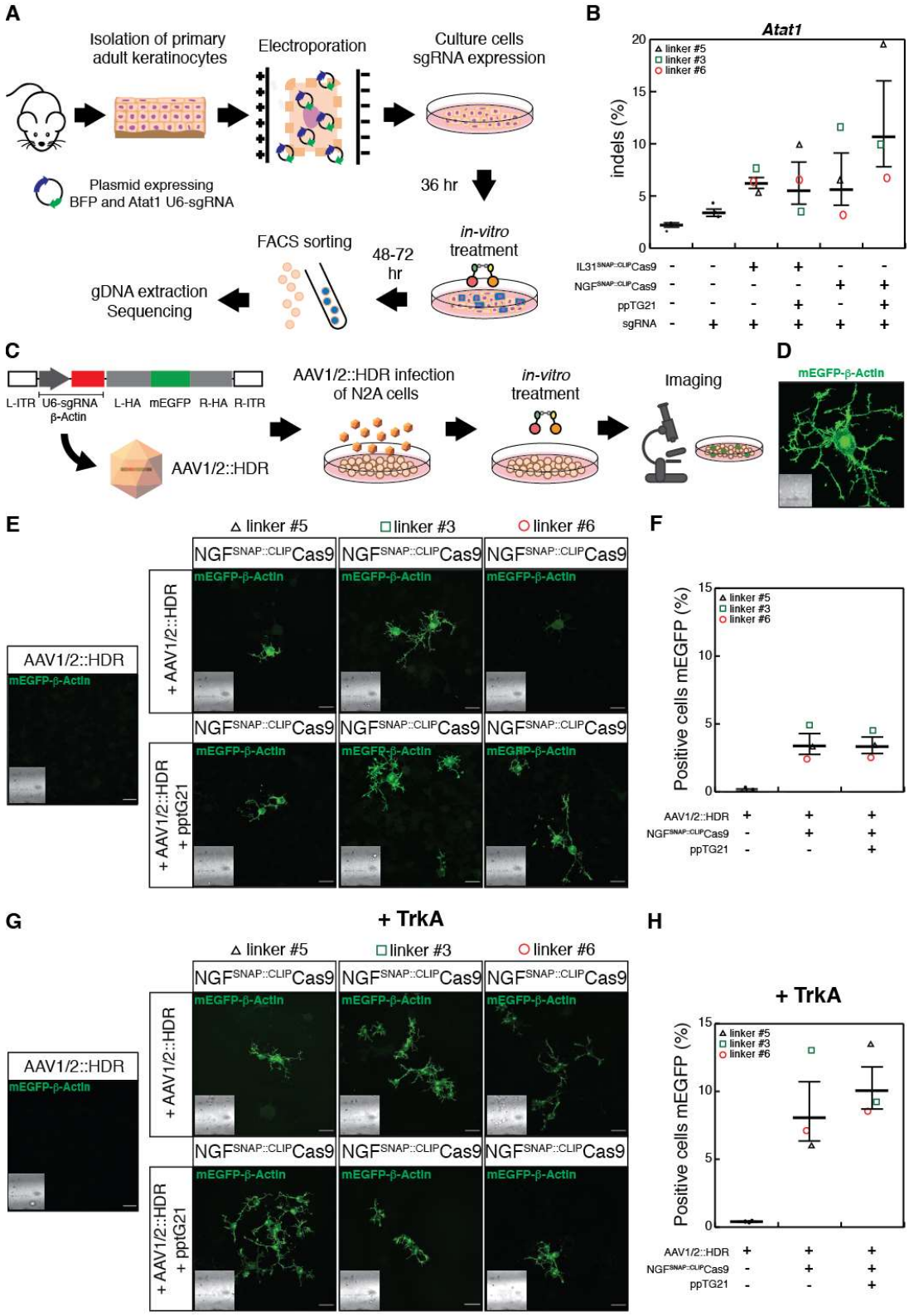

Figure 5. Ligand-mediated delivery of cross-linked CLIP-Cas9 in-vitro. (A) Schematic of plasmid electroporation strategy in primary keratinocytes. **(B)** % of indels detected from DNA sequencing of BFP-sorted keratinocytes expressing Atat1 U6-sgRNA treated with: cross-linked complex IL-31$^{SNAP::CLIP}$Cas9 (3rd column from left), NGF$^{SNAP::CLIP}$Cas9 (5th column from left) and in presence of ppTG21 peptide (IL-31$^{SNAP::CLIP}$Cas9 + ppTG21; 4th column from left) (NGF$^{SNAP::CLIP}$Cas9 + ppTG21 peptide; 6th column from left). Untreated controls and untreated BFP-sorted keratinocytes are shown in column 1 and 2,

respectively. **(C)** Graphical representation of AAV1/2::HDR and N2a cells experimental strategy. **(D)** Zoom of mEGFP-ß-Actin N2a positive cell. The inset represents corresponding brightfield images. **(E)** Confocal images of AAV1/2::HDR transduced N2a WT cells or overexpressing TrkA receptor **(G)** treated with $NGF^{SNAP::CLIP}$Cas9 alone (upper panels) or in presence of ppTG21 peptide (lower panels). First images on the left show control N2a cells infected only with AAV1/2::HDR. Scale bars, 40 μm. The insets represent corresponding brightfield images. **(F)** and **(H)** Quantification (% cells) of mEGFP positive cells from **(E)** and **(G)**, respectively. The horizontal black lines mark the geometric mean and the error bars mark the standard error. Black triangles: cross-linking complexes carrying linker #5 (Table S1); green squares: cross-linking complexes carrying linker #3 (Table S1); red circles: cross-linking complexes carrying linker #6 (Table S1).

Ligand-mediated selective delivery of CLIP-Cas9 allows for HDR *in-vivo*

We finally investigated whether CLIP-Cas9 S-CROSS could also allow for Homology-directed repair in the skin using the previously described approach. Although keratinocytes are highly resistant to viral infection, AAV serotype 1 was shown to mediate viral transduction of those cells (Ellis et al., 2013). Indeed, co-infection of primary keratinocytes isolated from a C57BL/6J WT mouse with AAV1/2::HDR and AAV1/2::Cas9 induced mEGFP knock-in *in-vitro*, albeit with scarce efficiency (<5%) (Figure S5D). To assess HDR-mediated gene editing *in-vivo*, $IL\text{-}31^{SNAP::CLIP}$Cas9 or $NGF^{SNAP::CLIP}$Cas9 (linker #5, #3, #6) were subcutaneously injected together with AAV1/2::HDR into the ear of C57BL/6J WT mice (Figure 6A). 2-3 weeks post-treatment, we evaluated mEGFP-ß-Actin expression by confocal microscopy on whole mount samples (Figure 6A). Remarkably, mEGFP positive keratinocytes were observed in mice injected with ligand cross-linked complexes suggesting that HDR occurred *in-vivo* (Figure 6B). Clusters of mEGFP positive cells were detected around the injection site, probably sprang from a targeted progenitor (Figure S6). S-CROSS with linker #3 showed the highest efficiency especially for NGF-mediated delivery (Figure 6B, green square). HDR was also observed, at lower frequency, in samples injected with cross-linked complexes carrying linker #6 (Figure 6B, red circle) while no HDR event was detected for S-CROSS linker #5 (Figure 6B, black triangle). We finally benchmarked our ligand-based system against viral delivery of Cas9. AAV1/2::HDR and a second AAV carrying the Cas9 sequence under the control of an EFS short promoter (AAV1/2::Cas9) (Nishiyama et al., 2017) were subcutaneously injected into the ear of WT mice. Of note, no mEGFP-ß-Actin expression was detected after 2-3 weeks from the initial treatment (Figure 6B).

Although observed HDR events mediated by ligand cross-linked Cas9 occurred sparsely, our system showed better efficiency than Cas9 viral delivery and, importantly, its feasibility *in-vivo*.

Further improvements and targeted studies for its therapeutic applications are still required, but the use of ligands as carriers to deliver Cas9 or other gene-editing enzymes could represent a potential tool for future gene therapies in the skin.

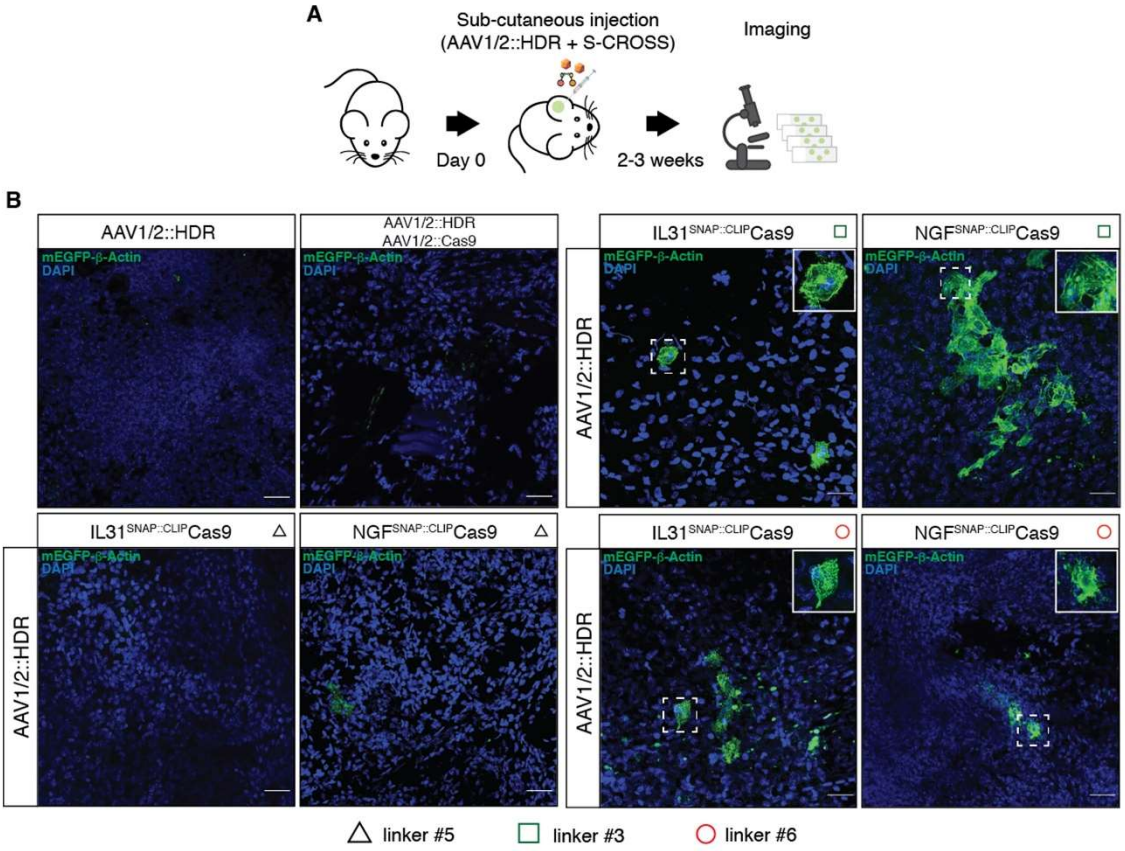

Figure 6. Ligand-mediated delivery of cross-linked CLIP-Cas9 in-vivo. (A) Schematic of subcutaneous injection of cross-linked CLIP-Cas9 and AAV1/2::HDR. **(B)** Confocal images of mEGFP positive keratinocytes 2-3 weeks after subcutaneous injection with CLIP-Cas9 cross-linked to IL-31 (left) or NGF (right). First upper images show control samples injected only with AAV1/2::HDR (left frame) or with dual AAV system AAV1/2::HDR + AAV1/2::Cas9 (right frame). The nuclei were stained with DAPI. Scale bars, 40 μm. The insets show enlarged representative areas with mEGFP-ß-Actin positive cells. Black triangles: cross-linking complexes carrying linker #5 (Table S1); green squares: cross-linking complexes carrying linker #3 (Table S1); red circles: cross-linking complexes carrying linker #6 (Table S1).

CONCLUSIONS

Here we present an efficient method for non-viral cell-type selective delivery of large cargoes based on natural ligands. We have identified two ligands able to selectively target keratinocytes: IL-31 and Nerve growth factor. We have exploited the ability of those molecules to be translocated to the nucleus upon a receptor-based internalization, to deliver 2 different types of cargo proteins: CRE recombinase and Cas9 nuclease. We covalently cross-linked ligands to proteins of interest by the employment of self-modifying and

biologically inert small enzymes together with long bio-orthogonal linkers that were shown to reduce steric hindrance effects. The main advantage of this approach is versatility, allowing combinations of "protein building blocks" by using a two-step simple chemical reaction and avoiding issues related to the production of large fusion proteins. We demonstrated that this ligand-based system is efficient and, most importantly, selective, a feature that is crucial for cell-specific delivery. Moreover, it enabled access to keratinocytes, which constitute the major cellular component of the skin and the first barrier from the external environment. Keratinocytes have been shown to be highly resistant to viral infection or to standard established delivery methods (e.g. lipid-based reagents), making them a challenging target. To that end, our system is a viable and powerful tool to target the skin. The most promising application is the intracellular delivery of Cas9 nuclease, which allows for cell-specific gene editing *in-vivo*. Many keratinocyte-associated genetic disorders have been described (Duchatelet et al., 2014; Hu et al., 2012; Lin et al., 2010) with no effective therapies available on the market. In this perspective, the technology we describe here could represent a promising platform for treating those diseases. Furthermore, the direct delivery of Cas9 as a protein has the main advantage to minimize the risk of potential integration into genomic DNA that are normally related to other delivery methods (viral vectors or plasmid-based technologies), making it a safer alternative. Future developments will focus on improving delivery efficiency and on expanding the types of cargoes (siRNA, therapeutic proteins) for broader biological and clinical applications. We also expect that the employment of other ligands could allow for selective targeting of distinct cellular populations offering new options to current methodologies.

REFERENCES

(1996). Heart rate variability. Standards of measurement, physiological interpretation, and clinical use. Task Force of the European Society of Cardiology and the North American Society of Pacing and Electrophysiology. Eur Heart J *17*, 354-381.

Aida, T., Chiyo, K., Usami, T., Ishikubo, H., Imahashi, R., Wada, Y., Tanaka, K.F., Sakuma, T., Yamamoto, T., and Tanaka, K. (2015). Cloning-free CRISPR/Cas system facilitates functional cassette knock-in in mice. Genome Biol *16*, 87.

Akbarian, S., Bates, B., Liu, R.J., Skirboll, S.L., Pejchal, T., Coppola, V., Sun, L.D., Fan, G., Kucera, J., Wilson, M.A.*, et al.* (2001). Neurotrophin-3 modulates noradrenergic neuron function and opiate withdrawal. Mol Psychiatry *6*, 593-604.

Alam, M., and Smirk, F.H. (1937). Observations in man upon a blood pressure raising reflex arising from the voluntary muscles. The Journal of physiology *89*, 372-383.

Allahverdian, S., Pannu, P.S., and Francis, G.A. (2012). Contribution of monocyte-derived macrophages and smooth muscle cells to arterial foam cell formation. Cardiovascular research *95*, 165-172.

Armulik, A., Genove, G., and Betsholtz, C. (2011). Pericytes: developmental, physiological, and pathological perspectives, problems, and promises. Developmental cell *21*, 193-215.
Bai, L., Lehnert, B.P., Liu, J., Neubarth, N.L., Dickendesher, T.L., Nwe, P.H., Cassidy, C., Woodbury, C.J., and Ginty, D.D. (2015). Genetic Identification of an Expansive Mechanoreceptor Sensitive to Skin Stroking. Cell *163*, 1783-1795.
Bakker, E.N., Buus, C.L., Spaan, J.A., Perree, J., Ganga, A., Rolf, T.M., Sorop, O., Bramsen, L.H., Mulvany, M.J., and Vanbavel, E. (2005). Small artery remodeling depends on tissue-type transglutaminase. Circ Res *96*, 119-126.
Baumer, N., Appel, N., Terheyden, L., Buchholz, F., Rossig, C., Muller-Tidow, C., Berdel, W.E., and Baumer, S. (2016). Antibody-coupled siRNA as an efficient method for in vivo mRNA knockdown. Nature protocols *11*, 22-36.
Bauters, C., and Isner, J.M. (1997). The biology of restenosis. Prog Cardiovasc Dis *40*, 107-116.
Bayliss, W.M. (1902). On the local reactions of the arterial wall to changes of internal pressure. The Journal of physiology *28*, 220-231.
Birklein, F., Weber, M., Ernst, M., Riedl, B., Neundorfer, B., and Handwerker, H.O. (2000a). Experimental tissue acidosis leads to increased pain in complex regional pain syndrome (CRPS). Pain *87*, 227-234.
Birklein, F., Weber, M., and Neundorfer, B. (2000b). Increased skin lactate in complex regional pain syndrome: evidence for tissue hypoxia? Neurology *55*, 1213-1215.
Bobrovskaya, L., Dunkley, P.R., and Dickson, P.W. (2004). Phosphorylation of Ser19 increases both Ser40 phosphorylation and enzyme activity of tyrosine hydroxylase in intact cells. J Neurochem *90*, 857-864.
Bolton, T.B., and Clapp, L.H. (1986). Endothelial-dependent relaxant actions of carbachol and substance P in arterial smooth muscle. Br J Pharmacol *87*, 713-723.
Bolton, T.B., and Lim, S.P. (1991). Action of acetylcholine on smooth muscle. Z Kardiol *80 Suppl 7*, 73-77.
Botchkarev, V.A., Yaar, M., Peters, E.M., Raychaudhuri, S.P., Botchkareva, N.V., Marconi, A., Raychaudhuri, S.K., Paus, R., and Pincelli, C. (2006). Neurotrophins in skin biology and pathology. J Invest Dermatol *126*, 1719-1727.
Brain, S.D. (1997). Sensory neuropeptides: their role in inflammation and wound healing. Immunopharmacology *37*, 133-152.
Briers, J.D., and Webster, S. (1996). Laser speckle contrast analysis (LASCA): a nonscanning, full-field technique for monitoring capillary blood flow. J Biomed Opt *1*, 174-179.
Brinkman, E.K., Chen, T., Amendola, M., and van Steensel, B. (2014). Easy quantitative assessment of genome editing by sequence trace decomposition. Nucleic Acids Res *42*, e168.
Burnstock, G., and Kennedy, C. (1986). A dual function for adenosine 5'-triphosphate in the regulation of vascular tone. Excitatory cotransmitter with noradrenaline from perivascular nerves and locally released inhibitory intravascular agent. Circ Res *58*, 319-330.
Cahalan, S.M., Lukacs, V., Ranade, S.S., Chien, S., Bandell, M., and Patapoutian, A. (2015). Piezo1 links mechanical forces to red blood cell volume. eLife *4*.
Cao, X., Peterson, J.R., Wang, G., Anrather, J., Young, C.N., Guruju, M.R., Burmeister, M.A., Iadecola, C., and Davisson, R.L. (2012). Angiotensin II-dependent hypertension requires cyclooxygenase 1-derived prostaglandin E2 and EP1 receptor signaling in the subfornical organ of the brain. Hypertension *59*, 869-876.
Caspary, T., and Anderson, K.V. (2003). Patterning cell types in the dorsal spinal cord: what the mouse mutants say. Nature reviews. Neuroscience *4*, 289-297.
Chaplan, S.R., Bach, F.W., Pogrel, J.W., Chung, J.M., and Yaksh, T.L. (1994). Quantitative assessment of tactile allodynia in the rat paw. Journal of neuroscience methods *53*, 55-63.
Chen, B., Gilbert, L.A., Cimini, B.A., Schnitzbauer, J., Zhang, W., Li, G.W., Park, J., Blackburn, E.H., Weissman, J.S., Qi, L.S.*, et al.* (2013a). Dynamic imaging of genomic loci in living human cells by an optimized CRISPR/Cas system. Cell *155*, 1479-1491.
Chen, Z., Jaafar, L., Agyekum, D.G., Xiao, H., Wade, M.F., Kumaran, R.I., Spector, D.L., Bao, G., Porteus, M.H., Dynan, W.S.*, et al.* (2013b). Receptor-mediated delivery of engineered nucleases for genome modification. Nucleic Acids Res *41*, e182.
Colucci, W.S., and Alexander, R.W. (1986). Norepinephrine-induced alteration in the coupling of alpha 1-adrenergic receptor occupancy to calcium efflux in rabbit aortic smooth muscle cells. Proceedings of the National Academy of Sciences of the United States of America *83*, 1743-1746.
Colucci, W.S., Brock, T.A., Gimbrone, M.A., Jr., and Alexander, R.W. (1984). Regulation of alpha 1-adrenergic receptor-coupled calcium flux in cultured vascular smooth muscle cells. Hypertension *6*, I19-24.
Coote, J.H., Hilton, S.M., and Perez-Gonzalez, J.F. (1971). The reflex nature of the pressor response to muscular exercise. The Journal of physiology *215*, 789-804.
Coste, B., Houge, G., Murray, M.F., Stitziel, N., Bandell, M., Giovanni, M.A., Philippakis, A., Hoischen, A., Riemer, G., Steen, U.*, et al.* (2013). Gain-of-function mutations in the mechanically activated ion channel

PIEZO2 cause a subtype of Distal Arthrogryposis. Proceedings of the National Academy of Sciences of the United States of America *110*, 4667-4672.
Cousins, D.A., Butts, K., and Young, A.H. (2009). The role of dopamine in bipolar disorder. Bipolar Disord *11*, 787-806.
Crisan, D., and Carr, J. (2000). Angiotensin I-converting enzyme: genotype and disease associations. J Mol Diagn *2*, 105-115.
Critchley, H.D., and Harrison, N.A. (2013). Visceral influences on brain and behavior. Neuron *77*, 624-638.
Cruickshank, J.M. (2017). The Role of Beta-Blockers in the Treatment of Hypertension. Advances in experimental medicine and biology *956*, 149-166.
Davis, M.J. (1993). Myogenic response gradient in an arteriolar network. Am J Physiol *264*, H2168-2179.
Dechant, G. (2001). Molecular interactions between neurotrophin receptors. Cell Tissue Res *305*, 229-238.
Dhandapani, R., Arokiaraj, C.M., Taberner, F.J., Pacifico, P., Raja, S., Nocchi, L., Portulano, C., Franciosa, F., Maffei, M., Hussain, A.F.*, et al.* (2018). Control of mechanical pain hypersensitivity in mice through ligand-targeted photoablation of TrkB-positive sensory neurons. Nature communications *9*, 1640.
Dierssen, M., Gratacos, M., Sahun, I., Martin, M., Gallego, X., Amador-Arjona, A., Martinez de Lagran, M., Murtra, P., Marti, E., Pujana, M.A.*, et al.* (2006). Transgenic mice overexpressing the full-length neurotrophin receptor TrkC exhibit increased catecholaminergic neuron density in specific brain areas and increased anxiety-like behavior and panic reaction. Neurobiology of disease *24*, 403-418.
Dillon, S.R., Sprecher, C., Hammond, A., Bilsborough, J., Rosenfeld-Franklin, M., Presnell, S.R., Haugen, H.S., Maurer, M., Harder, B., Johnston, J.*, et al.* (2004). Interleukin 31, a cytokine produced by activated T cells, induces dermatitis in mice. Nature immunology *5*, 752-760.
Diveu, C., Lak-Hal, A.H., Froger, J., Ravon, E., Grimaud, L., Barbier, F., Hermann, J., Gascan, H., and Chevalier, S. (2004). Predominant expression of the long isoform of GP130-like (GPL) receptor is required for interleukin-31 signaling. Eur Cytokine Netw *15*, 291-302.
Dong, Y., Yu, T., Ding, L., Laurini, E., Huang, Y., Zhang, M., Weng, Y., Lin, S., Chen, P., Marson, D.*, et al.* (2018). A Dual Targeting Dendrimer-Mediated siRNA Delivery System for Effective Gene Silencing in Cancer Therapy. J Am Chem Soc *140*, 16264-16274.
Donovan, M.J., Hahn, R., Tessarollo, L., and Hempstead, B.L. (1996). Identification of an essential nonneuronal function of neurotrophin 3 in mammalian cardiac development. Nature genetics *14*, 210-213.
Doskeland, A.P., and Flatmark, T. (2002). Ubiquitination of soluble and membrane-bound tyrosine hydroxylase and degradation of the soluble form. Eur J Biochem *269*, 1561-1569.
Draid, M., Shiina, T., El-Mahmoudy, A., Boudaka, A., Shimizu, Y., and Takewaki, T. (2005). Neurally released ATP mediates endothelium-dependent hyperpolarization in the circular smooth muscle cells of chicken anterior mesenteric artery. Br J Pharmacol *146*, 983-989.
Drenjancevic-Peric, I., Jelakovic, B., Lombard, J.H., Kunert, M.P., Kibel, A., and Gros, M. (2011). High-salt diet and hypertension: focus on the renin-angiotensin system. Kidney Blood Press Res *34*, 1-11.
Drummond, H.A., Price, M.P., Welsh, M.J., and Abboud, F.M. (1998). A molecular component of the arterial baroreceptor mechanotransducer. Neuron *21*, 1435-1441.
Drummond, P.D., Finch, P.M., Skipworth, S., and Blockey, P. (2001). Pain increases during sympathetic arousal in patients with complex regional pain syndrome. Neurology *57*, 1296-1303.
Du, S., Liew, S.S., Li, L., and Yao, S.Q. (2018). Bypassing Endocytosis: Direct Cytosolic Delivery of Proteins. J Am Chem Soc *140*, 15986-15996.
Duan, B., Cheng, L., Bourane, S., Britz, O., Padilla, C., Garcia-Campmany, L., Krashes, M., Knowlton, W., Velasquez, T., Ren, X.*, et al.* (2014). Identification of spinal circuits transmitting and gating mechanical pain. Cell *159*, 1417-1432.
Duchatelet, S., Pruvost, S., de Veer, S., Fraitag, S., Nitschke, P., Bole-Feysot, C., Bodemer, C., and Hovnanian, A. (2014). A new TRPV3 missense mutation in a patient with Olmsted syndrome and erythromelalgia. JAMA Dermatol *150*, 303-306.
Dunkley, P.R., Bobrovskaya, L., Graham, M.E., von Nagy-Felsobuki, E.I., and Dickson, P.W. (2004). Tyrosine hydroxylase phosphorylation: regulation and consequences. J Neurochem *91*, 1025-1043.
Duschek, S., Hadjamu, M., and Schandry, R. (2007). Dissociation between cortical activation and cognitive performance under pharmacological blood pressure elevation in chronic hypotension. Biol Psychol *75*, 277-285.
Duschek, S., Heiss, H., Werner, N., and Reyes del Paso, G.A. (2009). Modulations of autonomic cardiovascular control following acute alpha-adrenergic treatment in chronic hypotension. Hypertension research : official journal of the Japanese Society of Hypertension *32*, 938-943.
Dusing, R., Waeber, B., Destro, M., Santos Maia, C., and Brunel, P. (2017). Triple-combination therapy in the treatment of hypertension: a review of the evidence. J Hum Hypertens *31*, 501-510.

Edvinsson, L. (1985). Characterization of the contractile effect of neuropeptide Y in feline cerebral arteries. Acta Physiol Scand *125*, 33-41.
Eisenhoffer, G.T., Loftus, P.D., Yoshigi, M., Otsuna, H., Chien, C.B., Morcos, P.A., and Rosenblatt, J. (2012). Crowding induces live cell extrusion to maintain homeostatic cell numbers in epithelia. Nature *484*, 546-549.
Ekblad, E., Edvinsson, L., Wahlestedt, C., Uddman, R., Hakanson, R., and Sundler, F. (1984). Neuropeptide Y co-exists and co-operates with noradrenaline in perivascular nerve fibers. Regul Pept *8*, 225-235.
Ellis, B.L., Hirsch, M.L., Barker, J.C., Connelly, J.P., Steininger, R.J., 3rd, and Porteus, M.H. (2013). A survey of ex vivo/in vitro transduction efficiency of mammalian primary cells and cell lines with Nine natural adeno-associated virus (AAV1-9) and one engineered adeno-associated virus serotype. Virol J *10*, 74.
Epstein, M. (2007). Resistant hypertension: prevalence and evolving concepts. J Clin Hypertens (Greenwich) *9*, 2-6.
Ernfors, P., Lee, K.F., Kucera, J., and Jaenisch, R. (1994). Lack of neurotrophin-3 leads to deficiencies in the peripheral nervous system and loss of limb proprioceptive afferents. Cell *77*, 503-512.
Ernsberger, U. (2009). Role of neurotrophin signalling in the differentiation of neurons from dorsal root ganglia and sympathetic ganglia. Cell Tissue Res *336*, 349-384.
Feener, E.P., Northrup, J.M., Aiello, L.P., and King, G.L. (1995). Angiotensin II induces plasminogen activator inhibitor-1 and -2 expression in vascular endothelial and smooth muscle cells. J Clin Invest *95*, 1353-1362.
Florez-Paz, D., Bali, K.K., Kuner, R., and Gomis, A. (2016). A critical role for Piezo2 channels in the mechanotransduction of mouse proprioceptive neurons. Scientific reports *6*, 25923.
Funfschilling, U., Ng, Y.G., Zang, K., Miyazaki, J., Reichardt, L.F., and Rice, F.L. (2004). TrkC kinase expression in distinct subsets of cutaneous trigeminal innervation and nonneuronal cells. The Journal of comparative neurology *480*, 392-414.
Furchgott, R.F. (1959). The receptors for epinephrine and norepinephrine (adrenergic receptors). Pharmacological reviews *11*, 429-441; discussion 441-422.
Garcia-Anoveros, J., Samad, T.A., Zuvela-Jelaska, L., Woolf, C.J., and Corey, D.P. (2001). Transport and localization of the DEG/ENaC ion channel BNaC1alpha to peripheral mechanosensory terminals of dorsal root ganglia neurons. The Journal of neuroscience : the official journal of the Society for Neuroscience *21*, 2678-2686.
Garland, C.J., Bagher, P., Powell, C., Ye, X., Lemmey, H.A.L., Borysova, L., and Dora, K.A. (2017). Voltage-dependent Ca2+ entry into smooth muscle during contraction promotes endothelium-mediated feedback vasodilation in arterioles. Science signaling *10*.
Gautier, A., Juillerat, A., Heinis, C., Correa, I.R., Jr., Kindermann, M., Beaufils, F., and Johnsson, K. (2008). An engineered protein tag for multiprotein labeling in living cells. Chem Biol *15*, 128-136.
Gautier, A., Nakata, E., Lukinavicius, G., Tan, K.T., and Johnsson, K. (2009). Selective cross-linking of interacting proteins using self-labeling tags. J Am Chem Soc *131*, 17954-17962.
Ge, J., Li, W., Zhao, Q., Li, N., Chen, M., Zhi, P., Li, R., Gao, N., Xiao, B., and Yang, M. (2015). Architecture of the mammalian mechanosensitive Piezo1 channel. Nature *527*, 64-69.
Genc, B., Ozdinler, P.H., Mendoza, A.E., and Erzurumlu, R.S. (2004). A chemoattractant role for NT-3 in proprioceptive axon guidance. PLoS Biol *2*, e403.
Glazebrook, P.A., Schilling, W.P., and Kunze, D.L. (2005). TRPC channels as signal transducers. Pflugers Archiv : European journal of physiology *451*, 125-130.
Glebova, N.O., and Ginty, D.D. (2005). Growth and survival signals controlling sympathetic nervous system development. Annu Rev Neurosci *28*, 191-222.
Gnanasambandam, R., Bae, C., Gottlieb, P.A., and Sachs, F. (2015). Ionic Selectivity and Permeation Properties of Human PIEZO1 Channels. PLoS One *10*, e0125503.
Gordon, S.L., Quinsey, N.S., Dunkley, P.R., and Dickson, P.W. (2008). Tyrosine hydroxylase activity is regulated by two distinct dopamine-binding sites. J Neurochem *106*, 1614-1623.
Gordon, S.L., Webb, J.K., Shehadeh, J., Dunkley, P.R., and Dickson, P.W. (2009). The low affinity dopamine binding site on tyrosine hydroxylase: the role of the N-terminus and in situ regulation of enzyme activity. Neurochem Res *34*, 1830-1837.
Grasby, D.J., Morris, J.L., and Segal, S.S. (1999). Heterogeneity of vascular innervation in hamster cheek pouch and retractor muscle. Journal of vascular research *36*, 465-476.
Grobecker H, J.S., R McCarty VK Weise, IJ Kopin (1978). Role of noradrenergic nerves
and adrenal medulla during the development of genetic and experimental hypertension in rats. In Catecholamines: Basic and clinical frontiers (New York: Pergamon Press), pp. 906-908.
Guan, H., Zhu, L., Fu, M., Yang, D., Tian, S., Guo, Y., Cui, C., Wang, L., and Jiang, H. (2012). 3,3'Diindolylmethane suppresses vascular smooth muscle cell phenotypic modulation and inhibits neointima formation after carotid injury. PLoS One *7*, e34957.

Gudipaty, S.A., Lindblom, J., Loftus, P.D., Redd, M.J., Edes, K., Davey, C.F., Krishnegowda, V., and Rosenblatt, J. (2017). Mechanical stretch triggers rapid epithelial cell division through Piezo1. Nature *543*, 118-121.
Hagner, S., Haberberger, R., Kummer, W., Springer, J., Fischer, A., Bohm, S., Goke, B., and McGregor, G.P. (2001). Immunohistochemical detection of calcitonin gene-related peptide receptor (CGRPR)-1 in the endothelium of human coronary artery and bronchial blood vessels. Neuropeptides *35*, 58-64.
Hakanson, R., Wahlestedt, C., Ekblad, E., Edvinsson, L., and Sundler, F. (1986). Neuropeptide Y: coexistence with noradrenaline. Functional implications. Prog Brain Res *68*, 279-287.
Han, J.H., Kim, Y., Jung, S.H., Lee, J.J., Park, H.S., Song, G.Y., Cuong, N.M., Kim, Y.H., and Myung, C.S. (2015). Murrayafoline A Induces a G0/G1-Phase Arrest in Platelet-Derived Growth Factor-Stimulated Vascular Smooth Muscle Cells. Korean J Physiol Pharmacol *19*, 421-426.
Hanna, R.L., and Kaufman, M.P. (2003). Role played by purinergic receptors on muscle afferents in evoking the exercise pressor reflex. J Appl Physiol (1985) *94*, 1437-1445.
Hasegawa, H., and Wang, F. (2008). Visualizing mechanosensory endings of TrkC-expressing neurons in HS3ST-2-hPLAP mice. The Journal of comparative neurology *511*, 543-556.
Hayward, I.P., Bridle, K.R., Campbell, G.R., Underwood, P.A., and Campbell, J.H. (1995). Effect of extracellular matrix proteins on vascular smooth muscle cell phenotype. Cell Biol Int *19*, 839-846.
He, F.J., and MacGregor, G.A. (2003). Cost of poor blood pressure control in the UK: 62,000 unnecessary deaths per year. J Hum Hypertens *17*, 455-457.
Hill, J.M., Adreani, C.M., and Kaufman, M.P. (1996). Muscle reflex stimulates sympathetic postganglionic efferents innervating triceps surae muscles of cats. Am J Physiol *271*, H38-43.
Hill, M.A., Sun, Z., Martinez-Lemus, L., and Meininger, G.A. (2007). New technologies for dissecting the arteriolar myogenic response. Trends in pharmacological sciences *28*, 308-315.
Hill, R.A., Tong, L., Yuan, P., Murikinati, S., Gupta, S., and Grutzendler, J. (2015). Regional Blood Flow in the Normal and Ischemic Brain Is Controlled by Arteriolar Smooth Muscle Cell Contractility and Not by Capillary Pericytes. Neuron *87*, 95-110.
Hu, Z., Xiong, Z., Xu, X., Li, F., Lu, L., Li, W., Su, J., Liu, Y., Liu, D., Xie, Z*., et al.* (2012). Loss-of-function mutations in filaggrin gene associate with psoriasis vulgaris in Chinese population. Hum Genet *131*, 1269-1274.
Huang, E.J., Wilkinson, G.A., Farinas, I., Backus, C., Zang, K., Wong, S.L., and Reichardt, L.F. (1999). Expression of Trk receptors in the developing mouse trigeminal ganglion: in vivo evidence for NT-3 activation of TrkA and TrkB in addition to TrkC. Development *126*, 2191-2203.
Inoue, K., Ozaki, S., Shiga, T., Ito, K., Masuda, T., Okado, N., Iseda, T., Kawaguchi, S., Ogawa, M., Bae, S.C*., et al.* (2002). Runx3 controls the axonal projection of proprioceptive dorsal root ganglion neurons. Nature neuroscience *5*, 946-954.
Insel, P.A. (1996). Seminars in medicine of the Beth Israel Hospital, Boston. Adrenergic receptors--evolving concepts and clinical implications. N Engl J Med *334*, 580-585.
Investigators, S., Yusuf, S., Pitt, B., Davis, C.E., Hood, W.B., and Cohn, J.N. (1991). Effect of enalapril on survival in patients with reduced left ventricular ejection fractions and congestive heart failure. N Engl J Med *325*, 293-302.
Iwamoto, G.A., and Botterman, B.R. (1985). Peripheral factors influencing expression of pressor reflex evoked by muscular contraction. J Appl Physiol (1985) *58*, 1676-1682.
Jiang, X., Rowitch, D.H., Soriano, P., McMahon, A.P., and Sucov, H.M. (2000). Fate of the mammalian cardiac neural crest. Development *127*, 1607-1616.
Joyner, M.J., and Casey, D.P. (2015). Regulation of increased blood flow (hyperemia) to muscles during exercise: a hierarchy of competing physiological needs. Physiol Rev *95*, 549-601.
Kauffman, K.J., Webber, M.J., and Anderson, D.G. (2016). Materials for non-viral intracellular delivery of messenger RNA therapeutics. J Control Release *240*, 227-234.
Kaufman, M.P. (2012). The exercise pressor reflex in animals. Exp Physiol *97*, 51-58.
Kaufman, M.P., Iwamoto, G.A., Ashton, J.H., and Cassidy, S.S. (1982). Responses to inflation of vagal afferents with endings in the lung of dogs. Circ Res *51*, 525-531.
Kaufman, M.P., Longhurst, J.C., Rybicki, K.J., Wallach, J.H., and Mitchell, J.H. (1983). Effects of static muscular contraction on impulse activity of groups III and IV afferents in cats. J Appl Physiol Respir Environ Exerc Physiol *55*, 105-112.
Kawasaki, H., Takasaki, K., Saito, A., and Goto, K. (1988). Calcitonin gene-related peptide acts as a novel vasodilator neurotransmitter in mesenteric resistance vessels of the rat. Nature *335*, 164-167.
Kearney, P.M., Whelton, M., Reynolds, K., Whelton, P.K., and He, J. (2004). Worldwide prevalence of hypertension: a systematic review. J Hypertens *22*, 11-19.
Kirchheim, H.R. (1976). Systemic arterial baroreceptor reflexes. Physiol Rev *56*, 100-177.

Klein, R., Silos-Santiago, I., Smeyne, R.J., Lira, S.A., Brambilla, R., Bryant, S., Zhang, L., Snider, W.D., and Barbacid, M. (1994). Disruption of the neurotrophin-3 receptor gene trkC eliminates la muscle afferents and results in abnormal movements. Nature *368*, 249-251.
Knot, H.J., and Nelson, M.T. (1998). Regulation of arterial diameter and wall [Ca2+] in cerebral arteries of rat by membrane potential and intravascular pressure. The Journal of physiology *508 (Pt 1)*, 199-209.
Koban, M., Leis, S., Schultze-Mosgau, S., and Birklein, F. (2003). Tissue hypoxia in complex regional pain syndrome. Pain *104*, 149-157.
Kobori, H., Hayashi, M., and Saruta, T. (2001). Thyroid Hormone Stimulates Renin Gene Expression Through the Thyroid Hormone Response Element. Hypertension *37*, 99-104.
Koob, G.F., and Volkow, N.D. (2010). Neurocircuitry of addiction. Neuropsychopharmacology *35*, 217-238.
Kopp, U.C., and DiBona, G.F. (1993). Neural regulation of renin secretion. Semin Nephrol *13*, 543-551.
Lau, O.C., Shen, B., Wong, C.O., Tjong, Y.W., Lo, C.Y., Wang, H.C., Huang, Y., Yung, W.H., Chen, Y.C., Fung, M.L.*, et al.* (2016). TRPC5 channels participate in pressure-sensing in aortic baroreceptors. Nature communications *7*, 11947.
Leader, B., Baca, Q.J., and Golan, D.E. (2008). Protein therapeutics: a summary and pharmacological classification. Nat Rev Drug Discov *7*, 21-39.
Lemercier, G., Gendreizig, S., Kindermann, M., and Johnsson, K. (2007). Inducing and sensing protein--protein interactions in living cells by selective cross-linking. Angew Chem Int Ed Engl *46*, 4281-4284.
Levanon, D., Bettoun, D., Harris-Cerruti, C., Woolf, E., Negreanu, V., Eilam, R., Bernstein, Y., Goldenberg, D., Xiao, C., Fliegauf, M.*, et al.* (2002). The Runx3 transcription factor regulates development and survival of TrkC dorsal root ganglia neurons. The EMBO journal *21*, 3454-3463.
Levi-Montalcini, R. (1987). The nerve growth factor 35 years later. Science *237*, 1154-1162.
Li, J., Hou, B., Tumova, S., Muraki, K., Bruns, A., Ludlow, M.J., Sedo, A., Hyman, A.J., McKeown, L., Young, R.S.*, et al.* (2014). Piezo1 integration of vascular architecture with physiological force. Nature *515*, 279-282.
Li, J., Maile, M.D., Sinoway, A.N., and Sinoway, L.I. (2004). Muscle pressor reflex: potential role of vanilloid type 1 receptor and acid-sensing ion channel. J Appl Physiol (1985) *97*, 1709-1714.
Li, L., Rutlin, M., Abraira, V.E., Cassidy, C., Kus, L., Gong, S., Jankowski, M.P., Luo, W., Heintz, N., Koerber, H.R.*, et al.* (2011). The functional organization of cutaneous low-threshold mechanosensory neurons. Cell *147*, 1615-1627.
Li, W., Kohara, H., Uchida, Y., James, J.M., Soneji, K., Cronshaw, D.G., Zou, Y.R., Nagasawa, T., and Mukouyama, Y.S. (2013). Peripheral nerve-derived CXCL12 and VEGF-A regulate the patterning of arterial vessel branching in developing limb skin. Developmental cell *24*, 359-371.
Lin, M.W., Lee, D.D., Liu, T.T., Lin, Y.F., Chen, S.Y., Huang, C.C., Weng, H.Y., Liu, Y.F., Tanaka, A., Arita, K.*, et al.* (2010). Novel IL31RA gene mutation and ancestral OSMR mutant allele in familial primary cutaneous amyloidosis. Eur J Hum Genet *18*, 26-32.
Liu, Q., Vrontou, S., Rice, F.L., Zylka, M.J., Dong, X., and Anderson, D.J. (2007). Molecular genetic visualization of a rare subset of unmyelinated sensory neurons that may detect gentle touch. Nature neuroscience *10*, 946-948.
Liu, R., Heiss, E.H., Guo, D., Dirsch, V.M., and Atanasov, A.G. (2015). Capsaicin from chili (Capsicum spp.) inhibits vascular smooth muscle cell proliferation. F1000Res *4*, 26.
Liu, R., Heiss, E.H., Schachner, D., Jiang, B., Liu, W., Breuss, J.M., Dirsch, V.M., and Atanasov, A.G. (2017). Xanthohumol Blocks Proliferation and Migration of Vascular Smooth Muscle Cells in Vitro and Reduces Neointima Formation in Vivo. J Nat Prod *80*, 2146-2150.
Lloyd, G. (1975). Alcmaeon and the early history of dissection. Sudhoffs Archive, 113-147.
Lou, S., Duan, B., Vong, L., Lowell, B.B., and Ma, Q. (2013). Runx1 controls terminal morphology and mechanosensitivity of VGLUT3-expressing C-mechanoreceptors. The Journal of neuroscience : the official journal of the Society for Neuroscience *33*, 870-882.
Lu, K.T., Keen, H.L., Weatherford, E.T., Sequeira-Lopez, M.L., Gomez, R.A., and Sigmund, C.D. (2016). Estrogen Receptor alpha Is Required for Maintaining Baseline Renin Expression. Hypertension *67*, 992-999.
Lu, Y., Ma, X., Sabharwal, R., Snitsarev, V., Morgan, D., Rahmouni, K., Drummond, H.A., Whiteis, C.A., Costa, V., Price, M.*, et al.* (2009). The ion channel ASIC2 is required for baroreceptor and autonomic control of the circulation. Neuron *64*, 885-897.
Luo, X., Xiao, Y., Song, F., Yang, Y., Xia, M., and Ling, W. (2012). Increased plasma S-adenosyl-homocysteine levels induce the proliferation and migration of VSMCs through an oxidative stress-ERK1/2 pathway in apoE(-/-) mice. Cardiovascular research *95*, 241-250.
Ma, Q., Fode, C., Guillemot, F., and Anderson, D.J. (1999). Neurogenin1 and neurogenin2 control two distinct waves of neurogenesis in developing dorsal root ganglia. Genes Dev *13*, 1717-1728.

Majesky, M.W. (2007). Developmental basis of vascular smooth muscle diversity. Arterioscler Thromb Vasc Biol *27*, 1248-1258.
Martinez-Lemus, L.A., Hill, M.A., and Meininger, G.A. (2009). The plastic nature of the vascular wall: a continuum of remodeling events contributing to control of arteriolar diameter and structure. Physiology *24*, 45-57.
Matsukawa, K., Wall, P.T., Wilson, L.B., and Mitchell, J.H. (1994). Reflex stimulation of cardiac sympathetic nerve activity during static muscle contraction in cats. Am J Physiol *267*, H821-827.
McMorris, F.A., and Ruddle, F.H. (1974). Expression of neuronal phenotypes in neuroblastoma cell hybrids. Dev Biol *39*, 226-246.
Molinoff, P.B. (1984). Alpha- and beta-adrenergic receptor subtypes properties, distribution and regulation. Drugs *28 Suppl 2*, 1-15.
Molinoff, P.B., and Axelrod, J. (1971). Biochemistry of catecholamines. Annu Rev Biochem *40*, 465-500.
Moser, M., and Feig, P.U. (2009). Fifty years of thiazide diuretic therapy for hypertension. Arch Intern Med *169*, 1851-1856.
Mu, X., Silos-Santiago, I., Carroll, S.L., and Snider, W.D. (1993). Neurotrophin receptor genes are expressed in distinct patterns in developing dorsal root ganglia. The Journal of neuroscience : the official journal of the Society for Neuroscience *13*, 4029-4041.
Mukouyama, Y.S., Gerber, H.P., Ferrara, N., Gu, C., and Anderson, D.J. (2005). Peripheral nerve-derived VEGF promotes arterial differentiation via neuropilin 1-mediated positive feedback. Development *132*, 941-952.
Mukouyama, Y.S., Shin, D., Britsch, S., Taniguchi, M., and Anderson, D.J. (2002). Sensory nerves determine the pattern of arterial differentiation and blood vessel branching in the skin. Cell *109*, 693-705.
Mullen, L., Adams, G., Layward, L., Vessillier, S., Annenkov, A., Mittal, G., Rigby, A., Sclanders, M., Baker, D., Gould, D.*, et al.* (2014). Latent cytokines for targeted therapy of inflammatory disorders. Expert Opin Drug Deliv *11*, 101-110.
Nakamaru, M., Tabuchi, Y., Rakugi, H., Nagano, M., and Ogihara, T. (1989). Actions of endothelin on adrenergic neuroeffector junction. J Hypertens Suppl *7*, S132-133.
Navar, L.G. (2014). Physiology: hemodynamics, endothelial function, renin-angiotensin-aldosterone system, sympathetic nervous system. J Am Soc Hypertens *8*, 519-524.
Nehls, V., Denzer, K., and Drenckhahn, D. (1992). Pericyte involvement in capillary sprouting during angiogenesis in situ. Cell Tissue Res *270*, 469-474.
Nelson, M.T., Huang, Y., Brayden, J.E., Hescheler, J., and Standen, N.B. (1990). Arterial dilations in response to calcitonin gene-related peptide involve activation of K+ channels. Nature *344*, 770-773.
Nishiyama, J., Mikuni, T., and Yasuda, R. (2017). Virus-Mediated Genome Editing via Homology-Directed Repair in Mitotic and Postmitotic Cells in Mammalian Brain. Neuron *96*, 755-768 e755.
Nocchi, L., Roy, N., D'Attilia, M., Dhandapani, R., Maffei, M., Traista, A., Castaldi, L., Perlas, E., Chadick, C.H., and Heppenstall, P.A. (2018). Interleukin-31-mediated photoablation of pruritogenic epidermal neurons reduces itch-associated behaviours in mice. Nature Biomedical Engineering.
Nolden, L., Edenhofer, F., Haupt, S., Koch, P., Wunderlich, F.T., Siemen, H., and Brustle, O. (2006). Site-specific recombination in human embryonic stem cells induced by cell-permeant Cre recombinase. Nat Methods *3*, 461-467.
Nonomura, K., Woo, S.H., Chang, R.B., Gillich, A., Qiu, Z., Francisco, A.G., Ranade, S.S., Liberles, S.D., and Patapoutian, A. (2016). Piezo2 senses airway stretch and mediates lung inflation-induced apnoea. Nature.
O'Donnell, S.R., and Wanstall, J.C. (1984). Beta-1 and beta-2 adrenoceptor-mediated responses in preparations of pulmonary artery and aorta from young and aged rats. J Pharmacol Exp Ther *228*, 733-738.
Okubo, M., Fujita, A., Saito, Y., Komaki, H., Ishiyama, A., Takeshita, E., Kojima, E., Koichihara, R., Saito, T., Nakagawa, E.*, et al.* (2015). A family of distal arthrogryposis type 5 due to a novel PIEZO2 mutation. Am J Med Genet A *167A*, 1100-1106.
Oppenheim, R.W. (1991). Cell death during development of the nervous system. Annu Rev Neurosci *14*, 453-501.
Orthwein, A., Noordermeer, S.M., Wilson, M.D., Landry, S., Enchev, R.I., Sherker, A., Munro, M., Pinder, J., Salsman, J., Dellaire, G.*, et al.* (2015). A mechanism for the suppression of homologous recombination in G1 cells. Nature *528*, 422-426.
Owens, B. (2017). Faster, deeper, smaller-the rise of antibody-like scaffolds. Nat Biotechnol *35*, 602-603.
Page, A.J., Brierley, S.M., Martin, C.M., Price, M.P., Symonds, E., Butler, R., Wemmie, J.A., and Blackshaw, L.A. (2005). Different contributions of ASIC channels 1a, 2, and 3 in gastrointestinal mechanosensory function. Gut *54*, 1408-1415.
Patapoutian, A., and Reichardt, L.F. (2001). Trk receptors: mediators of neurotrophin action. Curr Opin Neurobiol *11*, 272-280.

Pathak, M.M., Nourse, J.L., Tran, T., Hwe, J., Arulmoli, J., Le, D.T., Bernardis, E., Flanagan, L.A., and Tombola, F. (2014). Stretch-activated ion channel Piezo1 directs lineage choice in human neural stem cells. Proceedings of the National Academy of Sciences of the United States of America *111*, 16148-16153.
Peach, M.J., and Dostal, D.E. (1990). The angiotensin II receptor and the actions of angiotensin II. J Cardiovasc Pharmacol *16 Suppl 4*, S25-30.
Peitz, M., Pfannkuche, K., Rajewsky, K., and Edenhofer, F. (2002). Ability of the hydrophobic FGF and basic TAT peptides to promote cellular uptake of recombinant Cre recombinase: a tool for efficient genetic engineering of mammalian genomes. Proc Natl Acad Sci U S A *99*, 4489-4494.
Price, M.P., Lewin, G.R., McIlwrath, S.L., Cheng, C., Xie, J., Heppenstall, P.A., Stucky, C.L., Mannsfeldt, A.G., Brennan, T.J., Drummond, H.A*., et al.* (2000). The mammalian sodium channel BNC1 is required for normal touch sensation. Nature *407*, 1007-1011.
Qamar, M.I., and Read, A.E. (1987). Effects of exercise on mesenteric blood flow in man. Gut *28*, 583-587.
Ramsey, A.J., and Fitzpatrick, P.F. (1998). Effects of phosphorylation of serine 40 of tyrosine hydroxylase on binding of catecholamines: evidence for a novel regulatory mechanism. Biochemistry *37*, 8980-8986.
Ranade, S.S., Qiu, Z., Woo, S.H., Hur, S.S., Murthy, S.E., Cahalan, S.M., Xu, J., Mathur, J., Bandell, M., Coste, B*., et al.* (2014a). Piezo1, a mechanically activated ion channel, is required for vascular development in mice. Proceedings of the National Academy of Sciences of the United States of America *111*, 10347-10352.
Ranade, S.S., Woo, S.H., Dubin, A.E., Moshourab, R.A., Wetzel, C., Petrus, M., Mathur, J., Begay, V., Coste, B., Mainquist, J*., et al.* (2014b). Piezo2 is the major transducer of mechanical forces for touch sensation in mice. Nature *516*, 121-125.
Retailleau, K., Duprat, F., Arhatte, M., Ranade, S.S., Peyronnet, R., Martins, J.R., Jodar, M., Moro, C., Offermanns, S., Feng, Y*., et al.* (2015). Piezo1 in Smooth Muscle Cells Is Involved in Hypertension-Dependent Arterial Remodeling. Cell reports *13*, 1161-1171.
Rode, B., Shi, J., Endesh, N., Drinkhill, M.J., Webster, P.J., Lotteau, S.J., Bailey, M.A., Yuldasheva, N.Y., Ludlow, M.J., Cubbon, R.M*., et al.* (2017). Piezo1 channels sense whole body physical activity to reset cardiovascular homeostasis and enhance performance. Nature communications *8*, 350.
Rodriguez-Linares, L., Lado, M.J., Vila, X.A., Mendez, A.J., and Cuesta, P. (2014). gHRV: Heart rate variability analysis made easy. Comput Methods Programs Biomed *116*, 26-38.
Rosenberg, S.A., and Restifo, N.P. (2015). Adoptive cell transfer as personalized immunotherapy for human cancer. Science *348*, 62-68.
Ross, R. (1993). The pathogenesis of atherosclerosis: a perspective for the 1990s. Nature *362*, 801-809.
Rouet, R., Thuma, B.A., Roy, M.D., Lintner, N.G., Rubitski, D.M., Finley, J.E., Wisniewska, H.M., Mendonsa, R., Hirsh, A., de Onate, L*., et al.* (2018). Receptor-Mediated Delivery of CRISPR-Cas9 Endonuclease for Cell-Type-Specific Gene Editing. J Am Chem Soc *140*, 6596-6603.
Rummery, N.M., Brock, J.A., Pakdeechote, P., Ralevic, V., and Dunn, W.R. (2007). ATP is the predominant sympathetic neurotransmitter in rat mesenteric arteries at high pressure. The Journal of physiology *582*, 745-754.
Ruocco, I., Cuello, A.C., Parent, A., and Ribeiro-da-Silva, A. (2002). Skin blood vessels are simultaneously innervated by sensory, sympathetic, and parasympathetic fibers. The Journal of comparative neurology *448*, 323-336.
Saleh-Gohari, N., and Helleday, T. (2004). Conservative homologous recombination preferentially repairs DNA double-strand breaks in the S phase of the cell cycle in human cells. Nucleic Acids Res *32*, 3683-3688.
Salmon, M., Gomez, D., Greene, E., Shankman, L., and Owens, G.K. (2012). Cooperative binding of KLF4, pELK-1, and HDAC2 to a G/C repressor element in the SM22alpha promoter mediates transcriptional silencing during SMC phenotypic switching in vivo. Circ Res *111*, 685-696.
Sander, J.D., and Joung, J.K. (2014). CRISPR-Cas systems for editing, regulating and targeting genomes. Nat Biotechnol *32*, 347-355.
Sands, J.M., and Layton, H.E. (2009). The physiology of urinary concentration: an update. Semin Nephrol *29*, 178-195.
Saraf, A., Oberg, E.A., and Strack, S. (2010). Molecular determinants for PP2A substrate specificity: charged residues mediate dephosphorylation of tyrosine hydroxylase by the PP2A/B' regulatory subunit. Biochemistry *49*, 986-995.
Shaikh, S.S., Nahorski, M.S., and Woods, C.G. (2018). A third HSAN5 mutation disrupts the nerve growth factor furin cleavage site. Mol Pain *14*, 1744806918809223.
Shields, S.D., Cavanaugh, D.J., Lee, H., Anderson, D.J., and Basbaum, A.I. (2010). Pain behavior in the formalin test persists after ablation of the great majority of C-fiber nociceptors. Pain *151*, 422-429.
Smyth, L.C.D., Rustenhoven, J., Scotter, E.L., Schweder, P., Faull, R.L.M., Park, T.I.H., and Dragunow, M. (2018). Markers for human brain pericytes and smooth muscle cells. J Chem Neuroanat *92*, 48-60.

Spier, I., Kerick, M., Drichel, D., Horpaopan, S., Altmuller, J., Laner, A., Holzapfel, S., Peters, S., Adam, R., Zhao, B., *et al.* (2016). Exome sequencing identifies potential novel candidate genes in patients with unexplained colorectal adenomatous polyposis. Fam Cancer *15*, 281-288.
Staden, H. (1989). The art of medecine in early Alexandria. Cambridge University Press *44*.
Standen, N.B., Quayle, J.M., Davies, N.W., Brayden, J.E., Huang, Y., and Nelson, M.T. (1989). Hyperpolarizing vasodilators activate ATP-sensitive K+ channels in arterial smooth muscle. Science *245*, 177-180.
Stantcheva, K.K., Iovino, L., Dhandapani, R., Martinez, C., Castaldi, L., Nocchi, L., Perlas, E., Portulano, C., Pesaresi, M., Shirlekar, K.S., *et al.* (2016). A subpopulation of itch-sensing neurons marked by Ret and somatostatin expression. EMBO Rep.
Steen, K.H., Steen, A.E., and Reeh, P.W. (1995). A dominant role of acid pH in inflammatory excitation and sensitization of nociceptors in rat skin, in vitro. The Journal of neuroscience : the official journal of the Society for Neuroscience *15*, 3982-3989.
Sun, H., Li, D.P., Chen, S.R., Hittelman, W.N., and Pan, H.L. (2009). Sensing of blood pressure increase by transient receptor potential vanilloid 1 receptors on baroreceptors. J Pharmacol Exp Ther *331*, 851-859.
Suzuki, K., Tsunekawa, Y., Hernandez-Benitez, R., Wu, J., Zhu, J., Kim, E.J., Hatanaka, F., Yamamoto, M., Araoka, T., Li, Z., *et al.* (2016). In vivo genome editing via CRISPR/Cas9 mediated homology-independent targeted integration. Nature *540*, 144-149.
Syeda, R., Florendo, M.N., Cox, C.D., Kefauver, J.M., Santos, J.S., Martinac, B., and Patapoutian, A. (2016). Piezo1 Channels Are Inherently Mechanosensitive. Cell reports *17*, 1739-1746.
Tabuchi, Y., Nakamaru, M., Rakugi, H., Nagano, M., Higashimori, K., Mikami, H., and Ogihara, T. (1990). Effects of endothelin on neuroeffector junction in mesenteric arteries of hypertensive rats. Hypertension *15*, 739-743.
Tamargo, J., and Ruilope, L.M. (2016). Investigational calcium channel blockers for the treatment of hypertension. Expert Opin Investig Drugs *25*, 1295-1309.
Tesfamariam, B., and Cohen, R.A. (1988). Inhibition of adrenergic vasoconstriction by endothelial cell shear stress. Circ Res *63*, 720-725.
Tesfamariam, B., Weisbrod, R.M., and Cohen, R.A. (1992). Cyclic GMP modulators on vascular adrenergic neurotransmission. Journal of vascular research *29*, 396-404.
Tessarollo, L., Vogel, K.S., Palko, M.E., Reid, S.W., and Parada, L.F. (1994). Targeted mutation in the neurotrophin-3 gene results in loss of muscle sensory neurons. Proceedings of the National Academy of Sciences of the United States of America *91*, 11844-11848.
Thayer, J.F., Hansen, A.L., Saus-Rose, E., and Johnsen, B.H. (2009). Heart rate variability, prefrontal neural function, and cognitive performance: the neurovisceral integration perspective on self-regulation, adaptation, and health. Ann Behav Med *37*, 141-153.
Thorin, E., and Atkinson, J. (1994). Modulation by the endothelium of sympathetic vasoconstriction in an in vitro preparation of the rat tail artery. Br J Pharmacol *111*, 351-357.
Thyberg, J. (1998). Phenotypic modulation of smooth muscle cells during formation of neointimal thickenings following vascular injury. Histology and histopathology *13*, 871-891.
Tian, X., Hu, T., Zhang, H., He, L., Huang, X., Liu, Q., Yu, W., He, L., Yang, Z., Yan, Y., *et al.* (2014). Vessel formation. De novo formation of a distinct coronary vascular population in neonatal heart. Science *345*, 90-94.
Tibes, U. (1977). Reflex inputs to the cardiovascular and respiratory centers from dynamically working canine muscles. Some evidence for involvement of group III or IV nerve fibers. Circ Res *41*, 332-341.
Usoskin, D., Furlan, A., Islam, S., Abdo, H., Lonnerberg, P., Lou, D., Hjerling-Leffler, J., Haeggstrom, J., Kharchenko, O., Kharchenko, P.V., *et al.* (2015). Unbiased classification of sensory neuron types by large-scale single-cell RNA sequencing. Nature neuroscience *18*, 145-153.
van Zwieten, P.A., Hendriks, M.G., Pfaffendorf, M., Bruning, T.A., and Chang, P.C. (1995). The parasympathetic system and its muscarinic receptors in hypertensive disease. J Hypertens *13*, 1079-1090.
Vanhoutte, P.M., and Miller, V.M. (1989). Alpha 2-adrenoceptors and endothelium-derived relaxing factor. Am J Med *87*, 1S-5S.
Verdecchia, P., Angeli, F., Mazzotta, G., Gentile, G., and Reboldi, G. (2008). The renin angiotensin system in the development of cardiovascular disease: role of aliskiren in risk reduction. Vasc Health Risk Manag *4*, 971-981.
vonEuler, U. (1946). A specific sympathetic ergone in adrenergic nerve fibres (sympathin) and its relation to adrenaline and noradrenaline. Acta Physiol Scand *12*, 73-97.
Vrontou, S., Wong, A.M., Rau, K.K., Koerber, H.R., and Anderson, D.J. (2013). Genetic identification of C fibres that detect massage-like stroking of hairy skin in vivo. Nature *493*, 669-673.

Wang, S., Chennupati, R., Kaur, H., Iring, A., Wettschureck, N., and Offermanns, S. (2016). Endothelial cation channel PIEZO1 controls blood pressure by mediating flow-induced ATP release. J Clin Invest *126*, 4527-4536.
Wasteson, P., Johansson, B.R., Jukkola, T., Breuer, S., Akyurek, L.M., Partanen, J., and Lindahl, P. (2008). Developmental origin of smooth muscle cells in the descending aorta in mice. Development *135*, 1823-1832.
Wehrwein, E.A., and Joyner, M.J. (2013). Regulation of blood pressure by the arterial baroreflex and autonomic nervous system. Handb Clin Neurol *117*, 89-102.
Werner, P., Paluru, P., Simpson, A.M., Latney, B., Iyer, R., Brodeur, G.M., and Goldmuntz, E. (2014). Mutations in NTRK3 suggest a novel signaling pathway in human congenital heart disease. Human mutation *35*, 1459-1468.
Woo, S.H., Lukacs, V., de Nooij, J.C., Zaytseva, D., Criddle, C.R., Francisco, A., Jessell, T.M., Wilkinson, K.A., and Patapoutian, A. (2015). Piezo2 is the principal mechanotransduction channel for proprioception. Nature neuroscience *18*, 1756-1762.
Woo, S.H., Ranade, S., Weyer, A.D., Dubin, A.E., Baba, Y., Qiu, Z., Petrus, M., Miyamoto, T., Reddy, K., Lumpkin, E.A*., et al.* (2014). Piezo2 is required for Merkel-cell mechanotransduction. Nature *509*, 622-626.
Wright, D.E., Zhou, L., Kucera, J., and Snider, W.D. (1997). Introduction of a neurotrophin-3 transgene into muscle selectively rescues proprioceptive neurons in mice lacking endogenous neurotrophin-3. Neuron *19*, 503-517.
Xie, W.B., Li, Z., Shi, N., Guo, X., Tang, J., Ju, W., Han, J., Liu, T., Bottinger, E.P., Chai, Y*., et al.* (2013). Smad2 and myocardin-related transcription factor B cooperatively regulate vascular smooth muscle differentiation from neural crest cells. Circ Res *113*, e76-86.
Xing, J., Sinoway, L., and Li, J. (2008). Differential responses of sensory neurones innervating glycolytic and oxidative muscle to protons and capsaicin. The Journal of physiology *586*, 3245-3252.
Yamazaki, T., Li, W., Yang, L., Li, P., Cao, H., Motegi, S.I., Udey, M.C., Bernhard, E., Nakamura, T., and Mukouyama, Y.S. (2018). Whole-Mount Adult Ear Skin Imaging Reveals Defective Neuro-Vascular Branching Morphogenesis in Obese and Type 2 Diabetic Mouse Models. Scientific reports *8*, 430.
Yatabe, J., Yoneda, M., Yatabe, M.S., Watanabe, T., Felder, R.A., Jose, P.A., and Sanada, H. (2011). Angiotensin III stimulates aldosterone secretion from adrenal gland partially via angiotensin II type 2 receptor but not angiotensin II type 1 receptor. Endocrinology *152*, 1582-1588.
Yoshida, T., Kaestner, K.H., and Owens, G.K. (2008). Conditional deletion of Kruppel-like factor 4 delays downregulation of smooth muscle cell differentiation markers but accelerates neointimal formation following vascular injury. Circ Res *102*, 1548-1557.
Zeisel, A., Hochgerner, H., Lonnerberg, P., Johnsson, A., Memic, F., van der Zwan, J., Haring, M., Braun, E., Borm, L.E., La Manno, G*., et al.* (2018). Molecular Architecture of the Mouse Nervous System. Cell *174*, 999-1014 e1022.
Zeng, W.Z., Marshall, K.L., Min, S., Daou, I., Chapleau, M.W., Abboud, F.M., Liberles, S.D., and Patapoutian, A. (2018). PIEZOs mediate neuronal sensing of blood pressure and the baroreceptor reflex. Science *362*, 464-467.
Zhao, Q., Wu, K., Geng, J., Chi, S., Wang, Y., Zhi, P., Zhang, M., and Xiao, B. (2016). Ion Permeation and Mechanotransduction Mechanisms of Mechanosensitive Piezo Channels. Neuron *89*, 1248-1263.
Zuris, J.A., Thompson, D.B., Shu, Y., Guilinger, J.P., Bessen, J.L., Hu, J.H., Maeder, M.L., Joung, J.K., Chen, Z.Y., and Liu, D.R. (2015). Cationic lipid-mediated delivery of proteins enables efficient protein-based genome editing in vitro and in vivo. Nature biotechnology *33*, 73-80.

SUPPLEMENTARY FIGURES

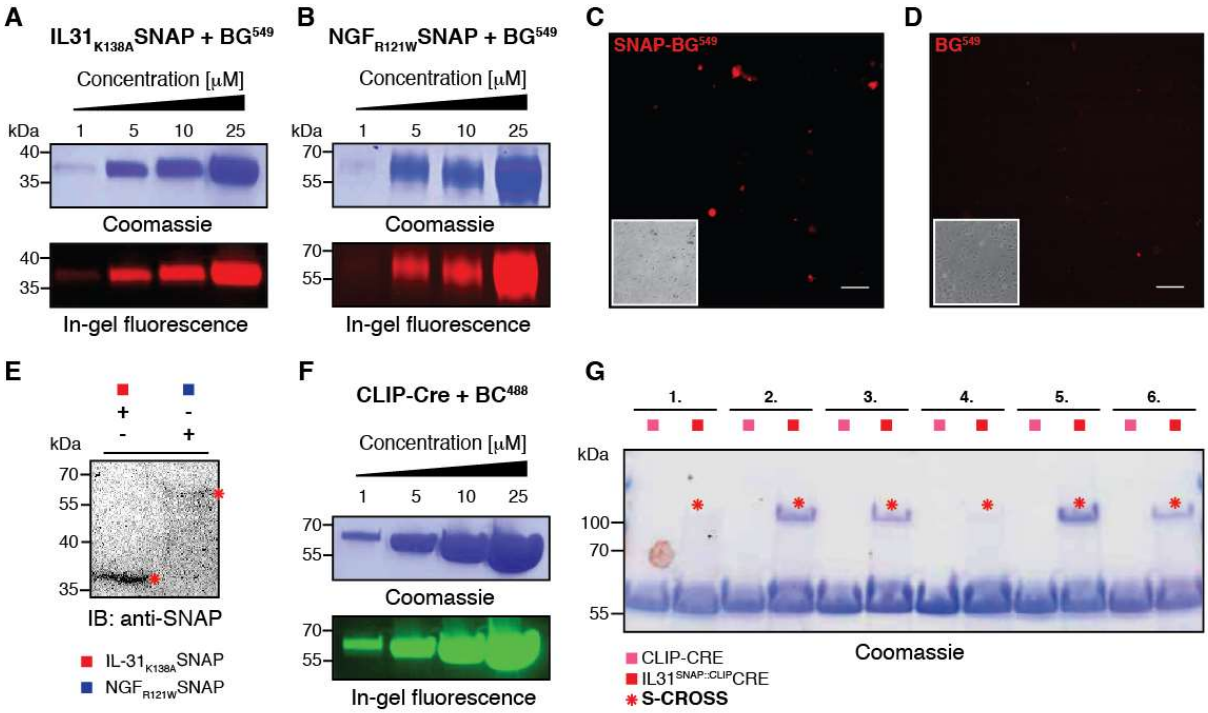

Supplementary Figure 1. Representative Coomassie and fluorescence gel showing IL31$_{K138A}$SNAP **(A)** and NGF$_{R121W}$SNAP **(B)** binding to a BG^{549} fluorophore at an increasing range of concentration. **(C)** Labelled SNAP-BG^{549} binding to primary keratinocytes. The inset represents the corresponding brightfield image. Scale bars, 20 μm. **(D)** BG^{549} incubation with primary keratinocytes. The inset represents the corresponding brightfield image. Scale bars, 20 μm. **(E)** Western blots showing IL31$_{K138A}$SNAP (lane #1) and NGF$_{R121W}$SNAP (lane #2) internalization in primary keratinocytes after 2 hours incubation with 2 μM of each ligand. **(F)** Representative Coomassie and fluorescence gel showing CLIP-Cre binding to a BC^{488} fluorophore at an increasing range of concentration. **(G)** Coomassie gel showing S-CROSS of IL31$_{K138A}$SNAP and CLIP-Cre. Red asterisks indicate cross-linking. Condition 1: linker #1 BG-BC; Condition 2: linker #2 BG$_{PEG}$-649-$_{PEG}$BC; Condition 3: linker #3 BG$_{PEG}$-(S-S$_{PEG}$BT)-$_{PEG}$BC; Condition 4: linker #4 BG-647-BC; Condition 5: linker #5 BG$_{PEG}$-biotin-$_{PEG}$BC; Condition 6: linker #6 BG-TMR-$_{PEG}$CP (Supplementary Table 1).

	Molecule synonym	Molecule	Distance (Å)
1.	BG-BC	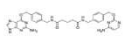	< 25
2.	BG$_{PEG}$-*649*-$_{PEG}$BC	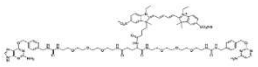	> 25
3.	BG$_{PEG}$-(*S*-S$_{PEG}$*BT*)-$_{PEG}$BC		> 25
4.	BG-*647*-BC	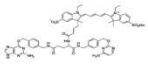	< 25
5.	BG$_{PEG}$-*biotin*-$_{PEG}$BC	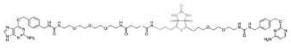	> 25
6.	BG-*TMR*-$_{PEG}$CP	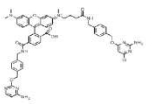	> 25

Supplementary Table 1. Table showing the cross-linker compounds tested for S-CROSS reactions. (I need the right structures).

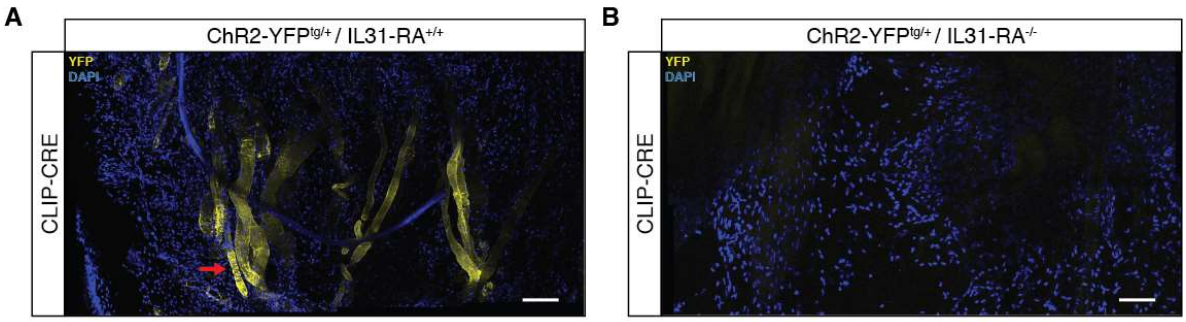

Supplementary Figure 2. YFP expression from Rosa26$^{LSL\text{-}ChR2\text{-}YFP}$ mice **(A)** and from double transgenic Rosa26$^{LSL\text{-}ChR2\text{-}YFP::IL31RA\text{-}/\text{-}}$ mice **(B)** 3 weeks after subcutaneous injection with 5 µM of CLIP-Cre. The nuclei were stained with DAPI. Scale bars, 40 µm. Red arrow indicates non-selective YFP expression.

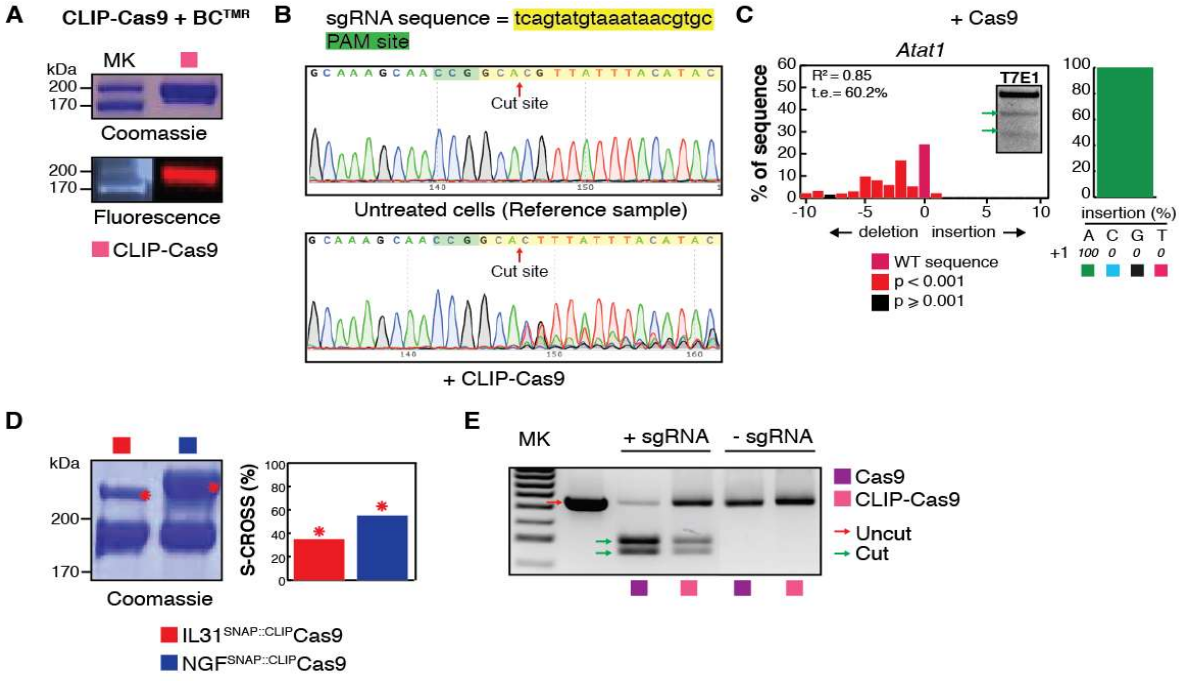

Supplementary Figure 3. (A) Representative Coomassie and fluorescence gel showing CLIP-Cas9 binding to a BC^{TMR} fluorophore. Lane #1 protein ladder. **(B)** Sequencing chromatograms showing the targeted *Atat1* locus. Control sample (upper chromatogram) and treated sample (+ CLIP-Cas9; lower chromatogram). **(C)** Indel spectrum determined by TIDE of primary keratinocytes electroporated with Cas9::sgRNA targeting the *Atat1* gene. The inset show T7 endonuclease 1 assay performed on genomic DNA from electroporated keratinocytes. *t.e.*= total efficiency. The estimated composition of the inserted base for the +1 insertion is also shown. **(D)** Representative Coomassie gel and quantification (% S-CROSS) showing cross-linking complexes (red asterisks). First lane (#1) is IL-31$^{SNAP::CLIP}$Cas9, second lane (#2) is NGF$^{SNAP::CLIP}$Cas9. **(E)** In-vitro digestion assay of the PCR products amplified from the *Atat1* locus and incubated with: Cas9::sgRNA (lane #2), CLIP-Cas9::sgRNA (lane #3), Cas9 (lane #4), CLIP-Cas9 (lane #5). *Atat1* undigested PCR product is shown in lane #1.

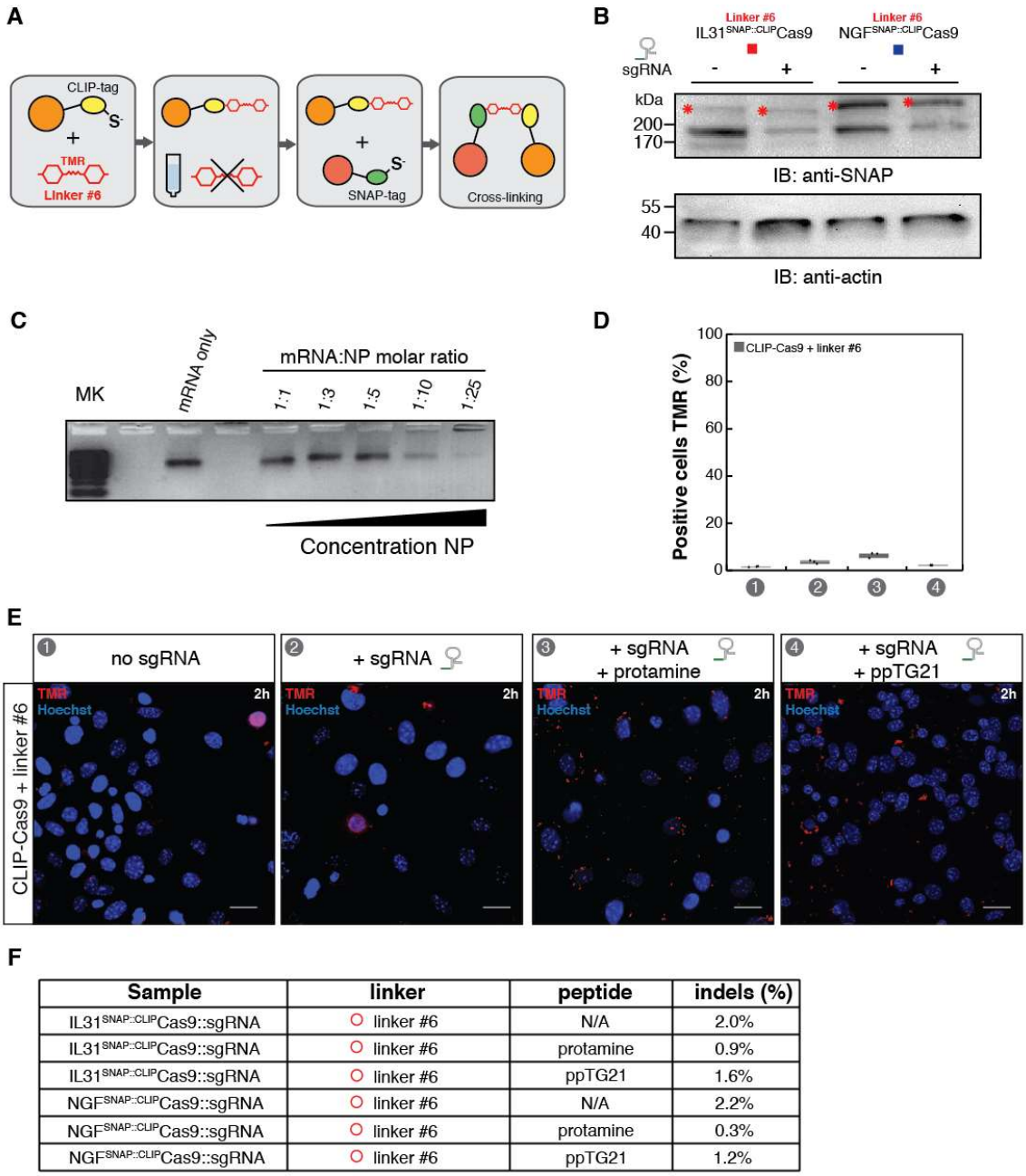

F

Sample	linker	peptide	indels (%)
IL31$^{SNAP::CLIP}$Cas9::sgRNA	linker #6	N/A	2.0%
IL31$^{SNAP::CLIP}$Cas9::sgRNA	linker #6	protamine	0.9%
IL31$^{SNAP::CLIP}$Cas9::sgRNA	linker #6	ppTG21	1.6%
NGF$^{SNAP::CLIP}$Cas9::sgRNA	linker #6	N/A	2.2%
NGF$^{SNAP::CLIP}$Cas9::sgRNA	linker #6	protamine	0.3%
NGF$^{SNAP::CLIP}$Cas9::sgRNA	linker #6	ppTG21	1.2%

Supplementary Figure 4. (A) Schematic representation of S-CROSS using linker #6. **(B)** Western blots showing IL-31$^{SNAP::CLIP}$Cas9 and NGF$^{SNAP::CLIP}$Cas9 internalization in primary keratinocytes in absence (lanes #1 and #3) and in presence (lanes #2 and #4) of *Atat1* dual sgRNA after 2 hours incubation with 2 µM of each ligand. **(C)** RNA gel shift assay in presence of increasing molar ratio (mRNA:NP) of native protamine. **(D)** Quantification of **(E)** TMR positive cells upon 2 hour treatment with 2 µM of CLIP-Cas9 (#1 no sgRNA; #2 with sgRNA; #3 with sgRNA + Protamine; #4 with sgRNA + ppTG21). The nuclei were stained with Hoechst. Scale bars, 20 µm. **(F)** Percentage of indels measured from genomic DNA sequencing.

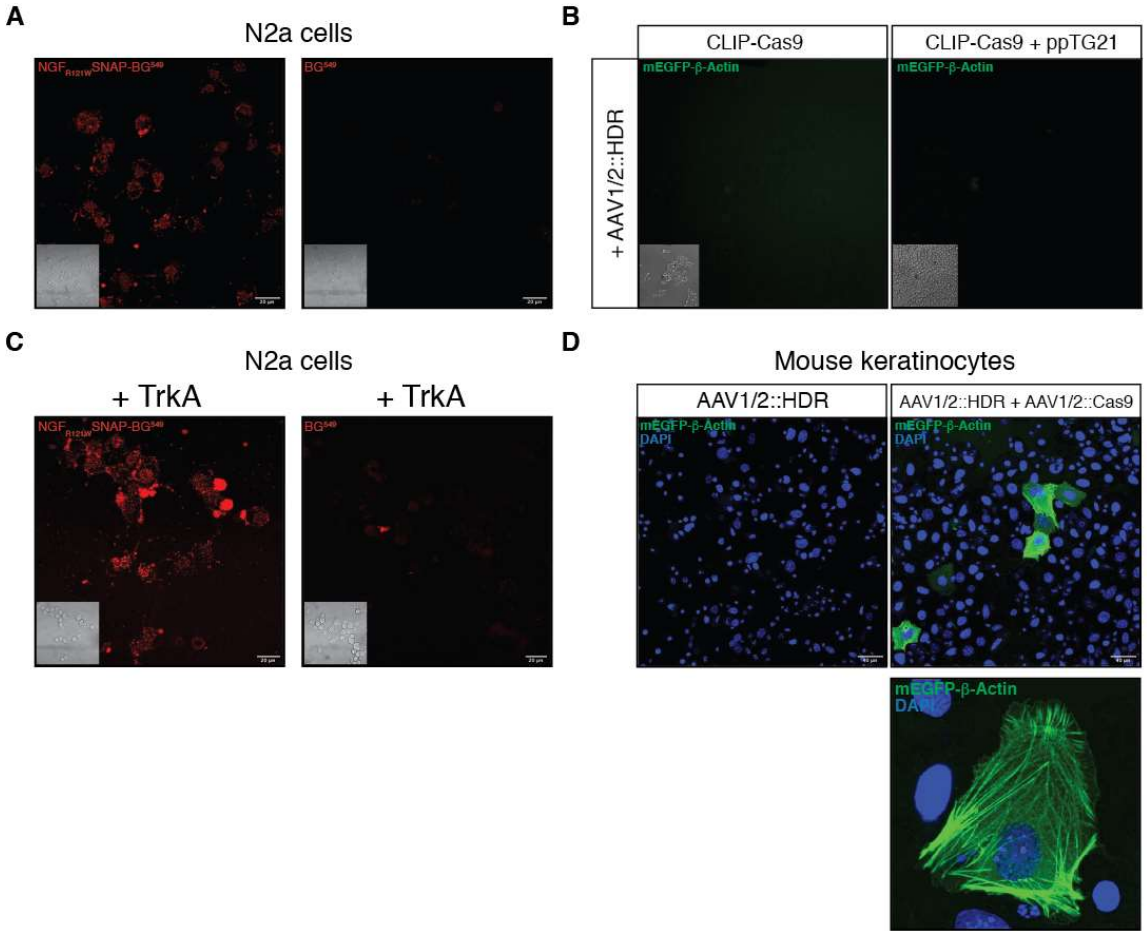

Supplementary Figure 5. (A) Labelled $NGF_{R121W}SNAP\text{-}BG^{549}$ binding (left frame) and only to BG^{549} N2a cells. The insets represent the corresponding brightfield image. Scale bars, 20 µm. **(B)** Representative images of AAV1/2::HDR transduced N2a cells treated only with CLIP-Cas9 (left frame) or in presence of ppTG21 peptide (right frame). The insets represent corresponding brightfield images. **(C)** Labelled $NGF_{R121W}SNAP\text{-}BG^{549}$ binding (left frame) and only to BG^{549} N2a cells over-expressing TrkA receptor. The insets represent the corresponding brightfield image. Scale bars, 20 µm. **(D)** Confocal images of AAV1/2::HDR transduced (left frame) and AAV1/2::HDR + AAV1/2::Cas9 double transduced (right frame) primary murine keratinocytes. Scale bars, 40 µm. The lower frame shows an enlarged imaged of mEGFP-ß-Actin positive keratinocyte.

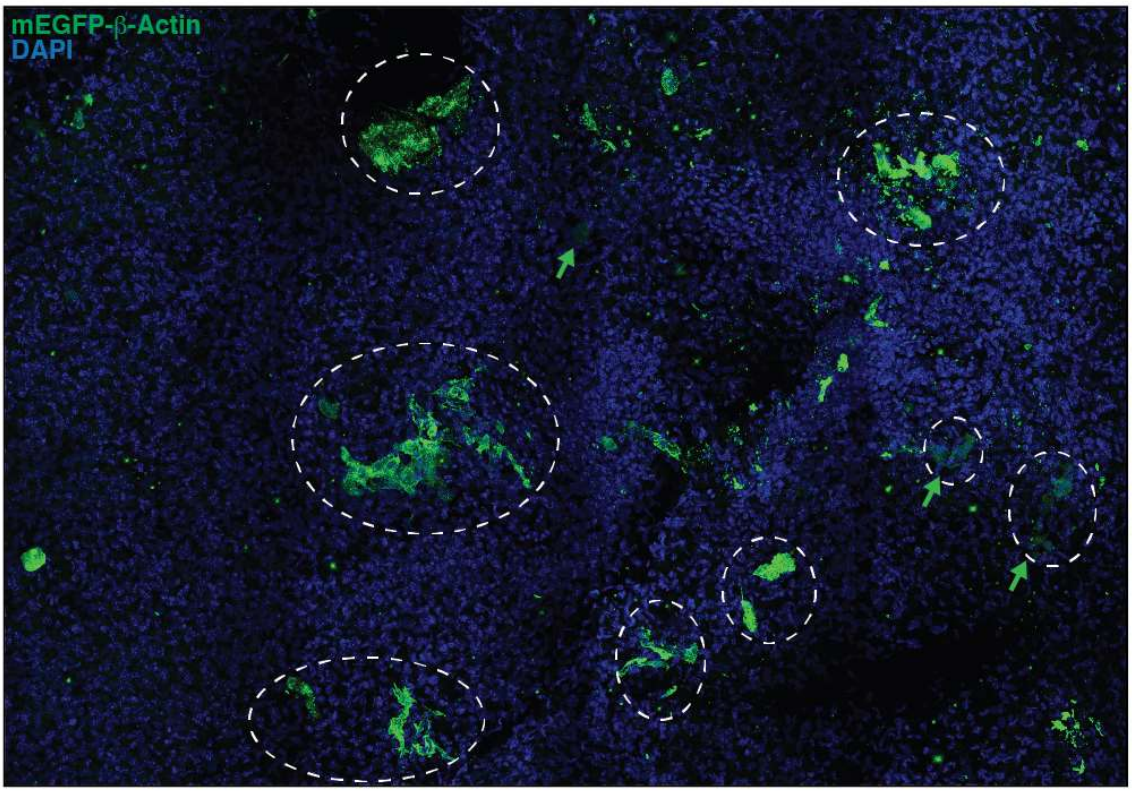

Supplementary Figure 6. Mosaic representation (1.07 mm x 1.43 mm) of mEGFP-ß-Actin positive cells from WT mice 2-3 weeks after subcutaneous injection with $NGF^{SNAP::CLIP}$Cas9 (linker #3). The nuclei were stained with DAPI. White dashed circles mark mEGFP positive targeted cell clusters. Green arrows indicate mEGFP positive cells starting to express mEGFP.